



پژوهش های خشکسالی و تغییر اقلیم



دوره دوم، شماره دوم، پیاپی ۶، تابستان ۱۴۰۳

- Evaluation of Drought in Gandaki River Basin, Nepal** 1
Aayush Bhattarai, Sachin Timilsina, Santosh Ayer, Gayatri Paudel, Menuka Maharjan
- A Biophysical Approach to Assess the Risks Associated with Climate Change for Spatial Analysis of Agricultural Drought Vulnerability** 27
Mohammadreza Farzaneh, Masoumeh Fakhri, Iman Fazeli-Farsani, Maryam Najafi-Biragani, Mohammad Abdolhosseini
- Assessment of Water, Food, and Energy Efficiency Indicators with a Nexus Approach and Sustainable Agricultural Management** 57
Seyyed Ali Moasheri, Saman Javadi, Mahmoud Mashal, Behzad Azadegan, Hamid Kardan Moghadam
- Monitoring Changes in Rice Cultivation Area Using Multi-Temporal Satellite Images (Case Study: Beiranshahr Region, Iran)** 77
Samad Abdi, Mohsen Ahmadede, Rabee Rustum, Anahid Salmanpour
- Measuring Discharge in a Shallow River in an Arid Area solely using an Unmanned Aerial Vehicle** 93
Farhad Akbarpour, Mohammad Adel Khorasani Nejad, Shervin Shahriari, Mostafa Rahmanshahi
- Spatial Analysis of Flood Risk in Tabas Watershed Using Satellite Images and Geographic Information System** 105
Mahdi Kaffash, Elham Yousefi, Mohsen Shariati
- Application of Time Series Method and Artificial Neural Networks in Drought Simulation (Case study: Bojnourd city)** 119
Mohtaram Mohamadyariyan, Ebrahim Amiri





Evaluation of Drought in Gandaki River Basin, Nepal

Aayush Bhattarai¹, Sachin Timilsina², Santosh Ayer³, Gayatri Paudel¹, Menuka Maharjan^{1, 4*}

1. Institute of Forestry, Hetauda Campus, Tribhuvan University, Makwanpur, Nepal.
2. Institute of Forestry, Pokhara Campus, Pokhara, Tribhuvan University, Pokhara, Nepal.
3. College of Natural Resource Management (CNRM), Agriculture and Forestry University, Katari, Nepal.
4. School of Forestry and Natural Resource Management, Institute of Forestry, Tribhuvan University, Kathmandu, Nepal.

*Corresponding Author: menuka.maharjan@iof.tu.edu.np

Keywords:

Climate change, NDVI, NDWI, NDDI, LST.

Abstract

Drought is often considered a silent disaster, leading to food and water shortages, displacement, and even conflict. Although evidence of ongoing climate change has been observed, limited research is carried out on drought conditions in the Gandaki River Basin of Nepal. This study analyzed four indices i.e., Normalized Difference Vegetation Index (NDVI), Normalized Difference Water Index (NDWI), Land Surface Temperature (LST) and Normalized Difference Drought Index (NDDI) for January and November between 1991 and 2021 by using Geographic Information System (GIS) and remote sensing data. NDVI showed that dense vegetation decreased by 93.26% and built-up area increased by 96.88% in January compared between 1991 and 2021. Compared between 1991 and 2021, NDWI showed that the high water stressed area increased by 49.5% in January. NDDI showed an increase in abnormally drought area in January (164.03%) compared between 1991 and 2021. Both climate change and human activities significantly contributes increasing trend of drought over the 30-year period in Gandaki River Basin. The study suggests exploring the potential of modern tools such as GIS and Remote Sensing for prediction of drought and monitoring its impact on ecosystems and human. This will be beneficial for policy makers for developing a strategy for combating drought and climate change.

Received:

13 October 2023

Revised:

05 November 2023

Accepted:

06 November 2023

How to cite this article:

Bhattarai, A., Timilsina, S., Ayer, S., Paudel, G., & Maharjan, M. (2024). Evaluation of drought in gandaki river basin, Nepal. *Journal of Drought and Climate change Research* (JDCR), 2(6), 1-26. [10.22077/jdcr.2023.6865.1046](https://doi.org/10.22077/jdcr.2023.6865.1046)



Introduction

Drought, although among the most intricate of natural disasters, remains one of the least comprehended, impacting a larger population than any other disaster (Hagman et al., 1984; Mehta & Yadav, 2023). The term “drought” commonly denotes an extended duration, spanning months or even years, during which a specific area experiences an inadequate supply of surface water or groundwater, leading to a disruption in its hydrological equilibrium (Hisdal et al., 2000; Jonathan & Suvarna Raju, 2017; Natarajan & Vasudevan, 2020). There are different types of droughts (meteorological, hydrological, ecological, agricultural, and socioeconomic) with their own unique characteristics and impacts (Khan et al., 2020; Liu et al., 2022). According to prior studies, insufficient rainfall is the main reason for drought (Chen et al., 2015; Haile, 1988; Liu et al., 2015; Natarajan et al., 2023; Zolotokrylin, 2010). However, severity and duration of drought recurrences are further exacerbated by human interferences such as deforestation (Vaglietti et al., 2022), unsustainable grazing (Jordaan et al., 2019), and over cultivation, increasing demands and consumption of water (Khan et al., 2020) and rising temperature trends and shifting weather patterns (Bernstein et al., 2008). Drought exerts a substantial influence on primary production (Ciais et al., 2005), the surface water flow (Lotfirad et al., 2022; Radmanesh et al., 2022), groundwater availability, hydropower production (Vliet et al., 2016), and heightened vulnerability to wildfires (Natarajan et al., 2023). Furthermore, droughts amplify water scarcity, which can have negative impacts on people’s health and overall productivity (Turrall et al., 2011).

Droughts have substantial, pervasive, and

frequently underestimated consequences for people, ecosystems, and economies, and only a fraction of the damage is officially documented (GAR, 2021; UNDRR, 2021). Each year, droughts are expected to directly affect 55 million people worldwide, making them the greatest threat to agricultural products (crops and livestock) in almost every region of the world (Eckstein et al., 2021). More than 10 million people have lost their lives as a consequence of significant drought occurrences over the past century, resulting in hundreds of billions of dollars in economic losses around the world, and the figures are rising (Guha-Sapir et al., 2017; Haitham et al., 2021). Every year, approximately 12 million hectares of land are lost due to the combined effects of drought and desertification, and there has been a more than two-fold increase in the proportion of plants suffering from drought damage over the past four decades (FAO, 2017). Drought-caused wildfires are threatening 84% of all terrestrial ecosystems and 14% of all wetlands crucial for migratory species are located in drought-prone areas (WWF, 2019). UNCCD (2022) has projected that as many as 700 million people might be compelled to leave their homes as a result of drought by 2030. Similarly, there will be between 4.8 and 5.7 billion people living in drought affected places by the year 2050, up from 3.6 billion at present (UN-Water, 2021). South Asia is regarded as a hotspot for hazards-prone regions, where the danger of climatic extremes like drought has increased due to a warming climate (IPCC, 2023). Future predictions indicate that climate change is expected to have significant impacts on South Asia including Nepal, India and Pakistan (Miyan, 2015) in the middle of the 21st century (Aadhar & Mishra, 2020). Nepal is vulnerable to

climate change impacts. It has experienced more pronounced warming in recent years compared to the global average (Ghimire, 2019; Mehta et al., 2012; MOHA, 2009). Nepal ranks among the top 10 most affected countries by climate change in 2020 as per the long-term Climate Risk Index (Eckstein et al., 2021). Nepal is also experiencing rising temperatures and a shortening of the monsoon season with high-intensity rains (Tripathi et al., 2020). Such circumstances have resulted in drought, particularly in the rain-dependent hill farming system, where people rely on rains for substantial agricultural production (Adhikari, 2018; Bista et al., 2021). The issue, however, had got worse due to a lack of research on an appropriate index, inconsistent precipitation and rainfall patterns, a lack of real-time monitoring systems, etc., and therefore calls for prompt assessment of drought occurrences for decision-making (Bista et al., 2021).

Remote sensing techniques and Geographic Information Systems (GIS) combined together is very useful for drought assessment as it can monitor drought conditions continuously and consistently and make spatial data available for regional and global drought analysis, especially in places where spatial data is few or non-existent (Tang et al., 2009), especially in mountainous countries like Nepal (Sharma et al., 2020). Drought severity is a quantitative measure of the intensity of the drought event and indices are used to provide quantitative assessment of the severity of the drought (WMO and GWP, 2016). There exists a wide array of indices used for assessing various aspects of drought, including the Palmer Drought Severity Index (PDSI) developed by Palmer (Palmer, 1968), the Normalized Difference Vegetation Index (NDVI) introduced by Rouse (Rouse et al., 1974), the Standard

Precipitation Evapo-transpiration Index (SPEI) by Vicente (Vicente-Serrano et al., 2010), the Standardized Precipitation Index (SPI) formulated by McKee et al., (1993), the Normalized Difference Water Index (NDWI) by Gao, (1996), and the Normalized Difference Drought Index (NDDI) proposed by Gu et al., (2007), etc., that can be used to assess drought severity. Due to the complex nature of drought, Diego et al., (2010) as well as Ndayiragije & Li (2022) suggested a cross-combination of various drought indices for more accurate assessment of drought. Therefore, in this study, the NDVI, NDDI and NDWI based on Land Surface Temperature (LST) were adopted among other indices for drought severity assessment because of their cost effectiveness (Gulácsi & Kovács, 2018), reliability, wide availability and easiness to use in remote sensing and GIS. These indices are also well-established in the scientific literature and have been used in numerous studies (Bashit et al., 2022; Gu et al., 2007; Nepal et al., 2021; Paniagua et al., 2020; Tavazohi & Nadoushan, 2018) to monitor and assess the impacts of drought. The Gandaki River Basin (GRB) of Nepal's climate has been changing (Sigdel et al., 2022), but there aren't enough researches available to analyze the drought in light of potential future climatic scenarios (Mallick et al., 2019; Shrestha et al., 2018). Furthermore, certain studies have noted instances of drought events occurring in Nepal, with variations observed both in terms of location and timing (Adhikari, 2018; Dahal et al., 2016; Hamal et al., 2020; Sigdel et al., 2010). In particular, available studies and research (Baidya et al., 2008; Bajracharya et al., 2011; Gautam & Regmi, 2013; Gurung & Bhandari, 2009; Chaulagain et al., 2006; Shrestha et al., 1999) in the GRB have primarily focused on temperature and

precipitation patterns. However, there is limited research on drought conditions in the GRB (Shrestha et al., 2020). Therefore, to fill this research gap, this study aimed at assessing drought in the GRB of Nepal using GIS and remotely sensed data.

Material and Methods

1. Study Area

GRB (Figure 1) is a cross-border basin spanning three distinct nations: China, Nepal, and India (Dandekhya et al., 2017). It is situated in the central region of Nepal, characterized by coordinates ranging from 25.6° to 29.4° N latitude and 82.8° to 85.82° E longitude (Panthi et al., 2015). It is the second-largest among Nepal's three major river basins (Panthi et al., 2015). Emerging from the southernmost point of the Tibetan Plateau, this basin meanders its way through Nepal and into India, ultimately merging with the Ganges River (Pant et al., 2018). The elevation within the basin varies significantly, ranging from 60 meters in the southern region to over 8000 meters north (Shrestha et al., 2011). GRB encompasses 46,300 square kilometers of catchment area, with a significant portion, approximately 35,000 square kilometers, situated in Nepal, covering all of its agro-ecological zones (Panthi et al., 2015). The prevailing climate in this region is predominantly influenced by the summer monsoon system of India, with roughly 80% of the annual rainfall occurring between June and September (Panthi et al., 2015; Zhang & Fang, 2020).

The GRB can be categorized into five distinct physiographic regions: Terai, Siwalik (Sub-Himalaya), Lesser Himalaya (Middle Mountains), Higher Himalaya, and Trans-Himalaya (Shrestha et al., 2011). Consequently, the GRB showcases a spectrum of topographical, climatic, ecological, and socio-economic variations

along Nepal's elevation gradient (Panthi et al., 2015). This basin is notably susceptible to water-related hazards, such as floods and landslides, during the monsoon season, as well as forest fires, often ignited by dry season winds (Dandekhya et al., 2017). In Nepal, the GRB spans 19 districts (Maharjan et al., 2020) and 12 of these districts are totally inside the river basin, while seven are partially within it (Regmi et al., 2016). The total population residing either partially or entirely within the basin is approximately 40 million people, with 5 million of them accounted for in Nepal according (CBS, 2011).

2. Data Collection

United States Geological Survey (USGS) archives (1991 and 2021) were used to obtain the Operational Land Imager (OLI), Thermal Infrared Sensor (TIRS) and LANDSAT-8 images. Images having cloud cover < 5% were selected. The images were collected for the post-monsoon (November) and winter season (January) for the year 1991 and 2021.

3. Data Analysis

3.1 Drought Severity Map

The drought severity map was created by classifying the Normalized Difference Drought Index (NDDI) map. The NDDI was computed from the LANDSAT-8, OLI/TIRS images using ArcGIS 10.8. Normalized Difference Vegetation Index (NDVI) was obtained using Equation 1 (Rouse et al., 1974).

$$NDVI = \frac{\rho_{NIR} - \rho_{Red}}{\rho_{NIR} + \rho_{Red}} \quad (1)$$

Where,

NIR is the reflectance corresponding to Near Infrared Reflectance band and Red is the reflectance corresponding to red band. The Normalized Difference Water Index

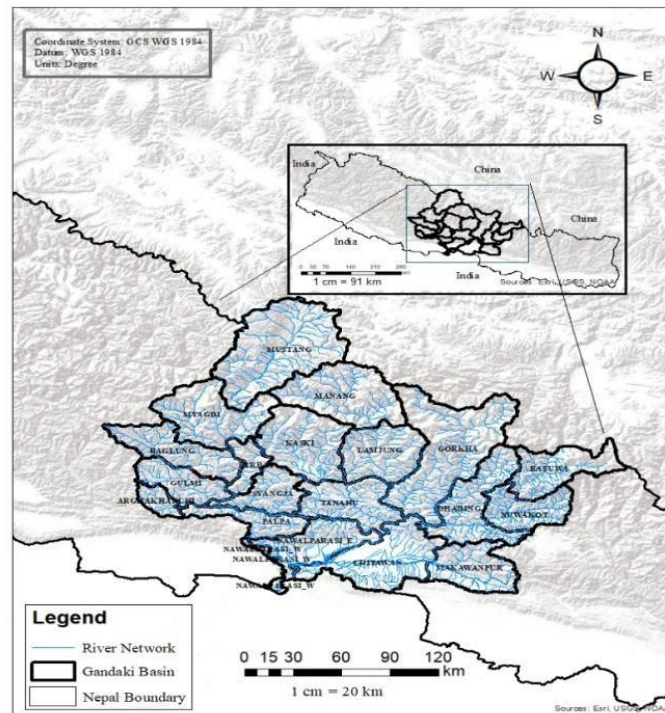


Fig 1. Study area showing Gandaki River Basin

(NDWI) results show a faster reaction to drought circumstances. It was calculated using Equation 2 (McFeeters, 1996).

$$NDWI = \frac{\rho_{Green} - \rho_{NIR}}{\rho_{Green} + \rho_{NIR}} \quad (2)$$

Where,

Green is reflectance corresponding to green band and Red is reflectance corresponding to red band.

The Land Surface Temperature (LST) is used as an indicator for evaluating vegetation water stress, evapotranspiration, and soil moisture. It was calculated using Equation 3 (Orimoloye et al., 2018).

$$LST = \frac{T_b}{1 + (\lambda * T_b(\rho) / \epsilon)} \quad (3)$$

Where,

T_b: Brightness Temperature,
 λ : wavelength of emitted radiance,
 ρ : $h \times c / \sigma$; h is Planck's constant ($6.26 \times$

10^{-34} J s); c is the velocity of light (2.998×10^8 m/s); σ is Stefan Boltzmann's constant (1.38×10^{-23} J K⁻¹)

ϵ : land surface emissivity.

Both the NDWI and NDVI data generated from LANDSAT bands were used for calculating the NDDI. It was estimated using Equation 4 (Gu et al., 2007).

$$NDDI = \frac{NDVI - NDWI}{NDVI + NDWI} \quad (4)$$

Discussion

1. Normalized Difference Vegetation Index (NDVI)

The NDVI classes were classified into five NDVI categories (ANNEX 1.1). Dense¹ vegetation decreased by 93.26% in January between the year 1991 and 2021 (Figure 2 and Table 1). However, dense vegetation increased by 222.37% in November when compared between the

1. The trees and other plants in a large densely wooded area

year 1991 and 2021. Sparse¹ vegetation decreased by 12.14% in January when compared between the year 1991 and 2021. However, the sparse vegetation area increased by 163.42% in November when compared between the year 1991 and 2021. The shrub and grassland were found to be increased by 49.45% and 14.5 % in January and November respectively when compared between the year 1991 and 2021. The barren land was observed to increase by 102.73% in January when compared between the year 1991 and

2021. Though, decline of barren land by 5.02% was observed in November when compared between the year 1991 and 2021. The built-up area increased by 96.88% in January when compared to the year 1991 and 2021. However, the built up area was decreased by 14.61% in November when compared to the year 1991 and 2021. The water body decreased by 56.15% and 14.61% in January and November respectively when compared between the year 1991 and 2021.

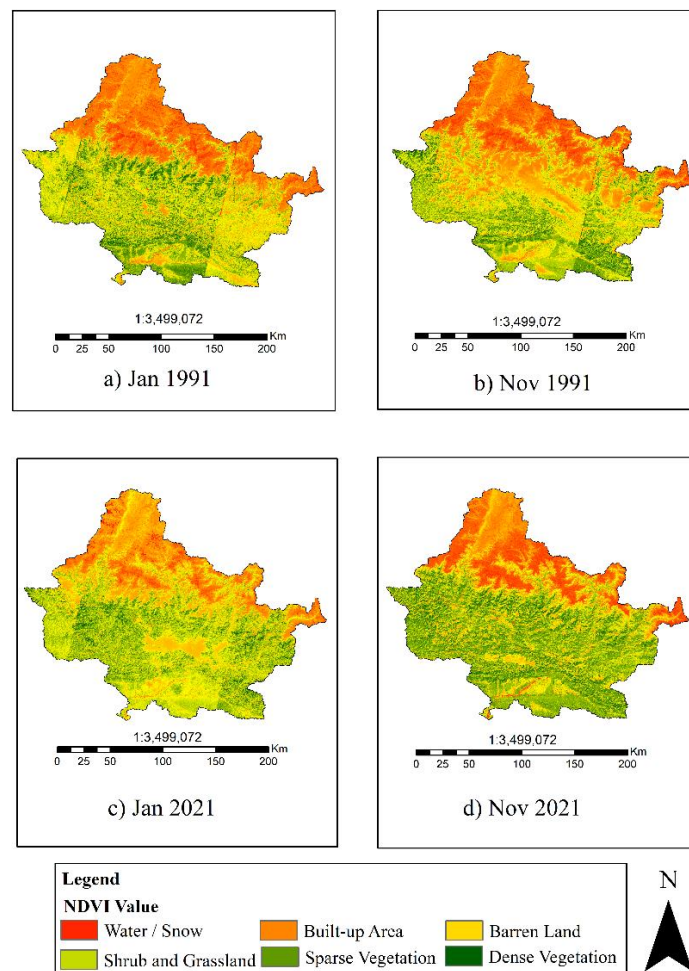


Fig 2. NDVI map of GRB

1. Limited or very little vegetation, as in things on the forest floor, due to lack of sun

Table 1. Area in percentage of different vegetation

Vegetation	Area in percentage			
	Jan 1991	Nov 1991	Jan 2021	Nov 2021
Water	34.3	39.5	15.0	16.1
Built-up Area	18.5	23.9	36.5	20.4
Barren Land	7.6	7.3	15.4	7.0
Shrub and Grassland	15.0	15.6	22.3	17.9
Sparse Vegetation	11.2	9.2	9.8	24.3
Dense Vegetation	13.5	4.5	0.9	14.4
Total	100	100	100	100

As NDVI serves as a robust indicator of drought-affected vegetation, it was computed and cartographically represented using ArcGIS (Joshi & Dongol, 2018). The study found a considerable increase in barren land and a decline in dense vegetation during January when compared between the year 1991 and 2021 (Table 1). The idea that drought-induced stress slows down photosynthesis (Hossain & Li, 2021), increases mortality, and reduces plant recruitment and seedling establishment is supported by the declining vegetation, which may possibly be a result of increased drought intensity and frequency (Das et al., 2023). Shrub and grassland areas, on the other hand, increased during January and November (Table 1), indicating a possible shifting cultivation and biotic pressure (Sangita & Dulal, 2021). The NDVI analysis unveiled a noteworthy reduction in the extent of water bodies, attributable to the influence of climate change and amplified human activities within the basin (Table 1) (Bajracharya et al., 2011; Mirza, 2003; Paudel et al., 2021). The study conducted in Bangladesh's northwest, found the increasing impact of drought on the country's existing waterways (such as rivers and canals) (Das et al., 2023; Seto, 2011). Furthermore, ecosystem functioning was also observed declining (Das et al., 2023; Sultana et al., 2021). Conversion of natural areas into built-up land is

another crucial factor in declining water bodies (Ramachandriah & Prasad, 2004). However, the number of emerging cities and megacities has increased in built-up areas (Nagendra et al., 2014). Our study's findings are comparable with several recent studies conducted in the northern part of Bangladesh (Ahmed et al., 2020; Das et al., 2023; Rai et al., 2017), which show a declining tendency of water bodies and a rising trend of settlement and built-up land. Overall, the NDVI experienced increasing trends which is parallel with the findings of several studies in Nepal (Baniya et al., 2018) and the Northern Hemisphere (Chen et al., 2014; Mishra & Mainali, 2017; Wang et al., 2017; Xu et al., 2014; Zhong et al., 2010). Research findings have shown a rise in NDVI levels in regions such as Russia, Europe, and northern China characterized by northern mid and high latitudes, as well as in equatorial regions like Africa and Southeastern Asia, with the exception of South America. This observation was documented in studies conducted by Kawabata et al., (2001) and Ichii et al., (2002). The increase in NDVI between November 1991 and 2021 in our study might be due to the afforestation program carried out in the degraded land and conservation initiatives led by the government which is comparative to the study in the North Western region of Bangladesh (Das et al., 2023; Kafy et al.,

2020). However, the NDVI had declined in the Southern Hemisphere i.e., Argentina, and Australia (Ichii et al., 2002; Kawabata et al., 2001). Furthermore, the study found a negative trend in the NDVI value due to the increase in drought events from 1990 to 2020 (Das et al., 2023; Isbell et al., 2015). This can be due to the combined effects of deforestation, climate change, and migration in the basin (Nepal et al., 2021; Regmi et al., 2016; Wassie, 2020; Yang et al., 2023). It might also be feasible to utilize NDVI projection methods based on rainfall patterns, as demonstrated in the work of (Brown et al., 2005), to offer advance alerts for early drought situations.

2. Normalized Difference Water Index (NDWI)

The NDWI classes were classified into six NDWI categories (ANNEX 1.2). The very high water stressed area decreased by 85.45% and 85.26% in January and November respectively when compared between the year 1991 and 2021 (Figure 3 and Table 2). The high water stressed area increased by 49.5% in January when compared between the year 1991 and 2021. However, the high water stressed area decreased by 21.27% in November when compared between the year 1991 and 2021. The less water stressed area increased by 94% and 1.77% in January and November respectively when compared between the year 1991 and 2021. The no effect area was increased by 205.97% and 67.41% in January and November respectively when compared between the year 1991 and 2021. The normal conditions increased by 93.67% and 244.73% in January and November respectively when compared between the year 1991 and 2021. The snow/glacier area decreased by 69.76 % and 30.43 % in January and November respectively when compared between the

year 1991 and 2021.

Nepal ranks 40th for overall water stress around the world and lies in the high water stress category (Hofste et al., 2019). In GRB, the very high water stressed area decreased from 1991 to 2021 (Table 2). Adaptation practices like modern agriculture practices, rain water harvesting, conservation ponds, etc., practiced in the basin may be the possible cause (Regmi et al., 2016). High water stressed area was increased in January between the year 1991 and 2021 (Table 2) due to more soil moisture loss, low precipitation, climate change, and increase in temperature than in November (Dhakal et al., 2010). The study in Bangladesh's northwest between 2004 and 2013 revealed a decrease in annual average precipitation, which also supports drought in the region (Das et al., 2023; Rahaman et al., 2016). Drip irrigation and water uplifting might have contributed in the increment of less water stress area and no effect area along with normal condition class (Dhakal et al., 2010). Snow, glaciers and mountains are the primary sources of water in the South Asian countries (Cui & Graf, 2009). They shifted greatly from 1991 to 2021, with reductions of areas in November (Figure 3 and Table 2) due to climate change and human action (Cui & Graf, 2009). The snow decreased due to an increase in temperature and changing precipitation pattern which is analogous with the record of Rebetz (1996) in six different locations of Switzerland. Rising temperatures have contributed to the melting of snow and glaciers across the world i.e., India (Mastny, 2000; Vohra, 1981), China (Mool et al., 2004; Tang et al., 2013), Bhutan (Ageta et al., 2003), and GRB in recent years (Rai et al., 2018). The stress in water availability has serious impact on climate change (Figure

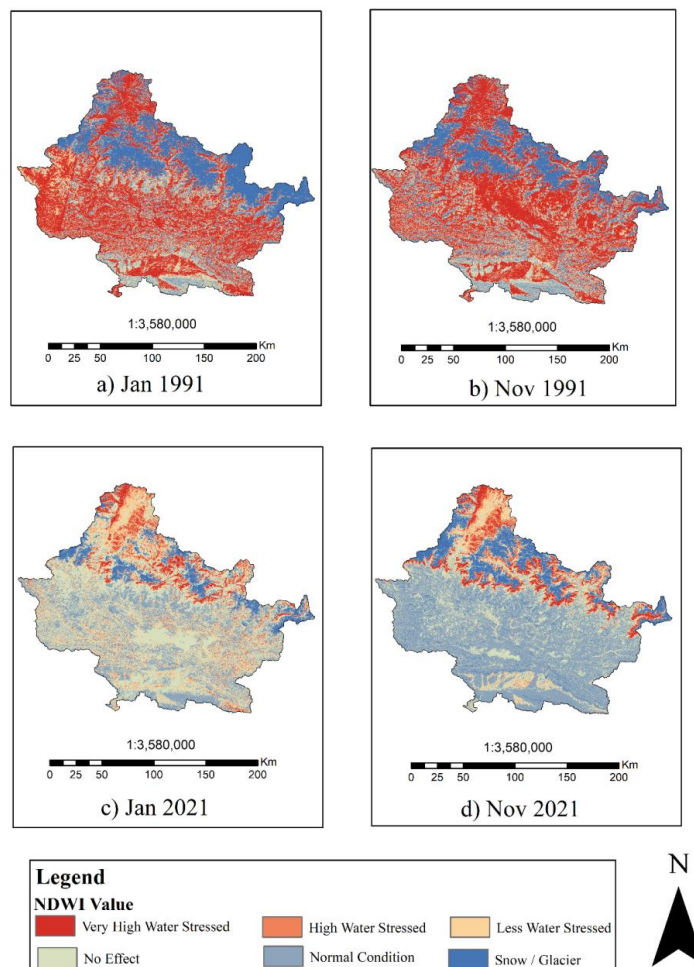


Fig 3. NDWI Map of GRB

Table 2. Area in percentage of different water stress level

Water Stress Level	Area in percentage			
	Jan 1991	Nov 1991	Jan 2021	Nov 2021
Very High Water Stressed	41.2	44.6	6.0	6.6
High Water Stressed	4.6	5.2	6.9	4.1
Less Water Stressed	7.8	7.2	15.1	7.3
No Effect	13.5	13.1	41.2	21.9
Normal Condition	12.7	14.3	24.7	49.2
Snow / Glacier	20.1	15.7	6.1	10.9
Total	100	100	100	100

3). A further sign of climate change is the decline in water supplies (groundwater recharge decreases) especially in downstream areas (Nagendra et al., 2013) which is correlate with the result of Park

et al., (2016) in the north-western areas of Bangladesh.

3. Land Surface Temperature (LST)

The LST classes were classified into five

categories based on temperature (i.e., $<10^{\circ}\text{C}$, $10^{\circ}\text{C} - 20^{\circ}\text{C}$, $20^{\circ}\text{C} - 30^{\circ}\text{C}$, $30^{\circ}\text{C} <$). Land area with temperature less than 0°C was decreased in both the months by 23.97% and 55.56 % in January and November when compared between the year 1991 and 2021 (Figure 4 and Table 3). Land area with temperature between $0-10^{\circ}\text{C}$ decreased by 7.59% in January, and 21.04 % in November when compared between the year 1991 and 2021. Land area with temperature between $10-20^{\circ}\text{C}$

increased by 12.78% in January and 36.23% in November when compared between the year 1991 and 2021. Land area with a temperature between $20-30^{\circ}\text{C}$ increased by 62.08% (3.56% to 5.78%) in January and 544.73% (0.16% to 6.19%) in November when compared between the year 1991 and 2021. Land area with temperature more than 30°C decreased by 44.32% in January however, it increased in November when compared between the year 1991 and 2021.

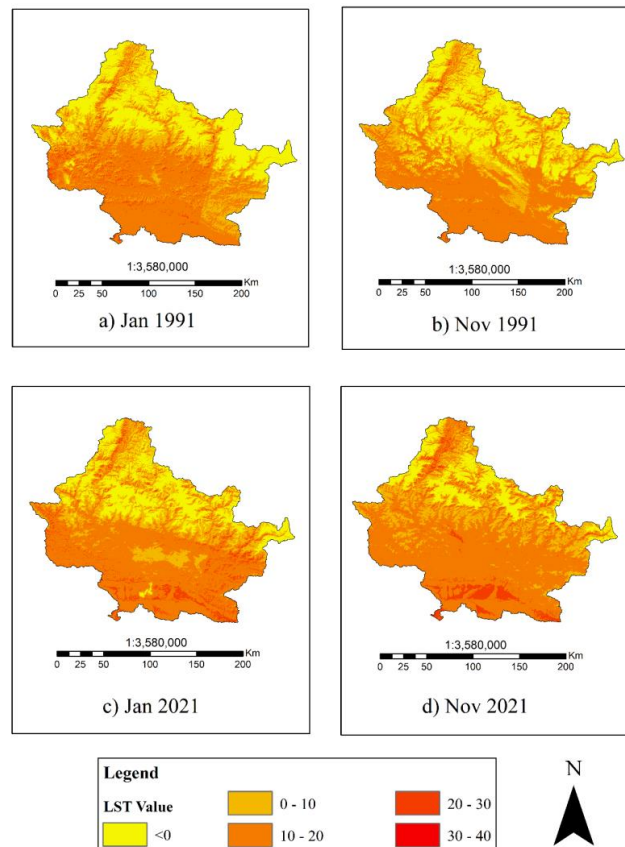


Fig 4. LST map of GRB

Table 3. Area in percentage of different land surface temperature

Temperature (Degree Celcius)	Area in Percentage			
	Jan 1991	Nov 1991	Jan 2021	Nov 2021
Less than 0	26.12	28.39	19.86	12.62
0 - 10	24.20	26.29	22.36	20.75
10-20	46.10	44.36	52.00	60.44
20-30	3.56	0.96	5.78	6.19
More than 30	0.01	0.00	0.01	0.01
Total	100	100	100	100

Temperature was found to be increasing in GRB between the years 1991 and 2021 (Figure 4 and Table 3). The increase in temperature in GRB is parallel to the results of Qin et al., (2009) and Ouyang et al., (2019), in the neighboring area of the Tibetan Plateau and Mao et al., (2017) in the South Asia region. The land area with temperature $<10^{\circ}\text{C}$ was decreased (Table 3), which might be due to the melting of Himalayan glaciers and low rainfall/snow in the region (global warming phenomenon) (Luintel et al., 2019). The land area with temperature $10\text{-}30^{\circ}\text{C}$ is increasing (Figure 4) due to urbanization, deforestation (Maillard et al., 2022), air pollution (Kahya et al., 2016) and land use change (Kafy et al., 2020) which results in increasing drought in the GRB. Negative relation between NDVI and temperature was discovered in our study, indicating

that the rising temperature in GRB had an adverse effect on vegetation (Figure 3 and Figure 4) which is parallel with the study of Das et al., (2023), in Bangladesh. The inverse correlation observed between vegetation NDVI and LST (Figure 3 and 4) may be attributed to decreased vegetation resistance and resilience, possibly resulting from the lasting impacts of drought (Das et al., 2023; Hossain et al., 2022; Hossain & Li, 2021; Isbell et al., 2015). The increasing LST has resulted in drought-induced stresses in GRB and led to climate-induced disturbances (Das et al., 2023).

4. Accuracy Assessment

Accuracy assessment of NDVI was carried out where overall accuracy was achieved more than 70% with kappa coefficient more than 65% (Table 4).

Table 4. Accuracy Assessment of NDVI for the months Jan and Feb of the year 1991 and 2021.

S. N.	Vegetation (Jan,1991)	Water	Built-up Area	Barren Land	Shrub and Grassland	Sparse Vegetation	Dense Vegetation	Total	User Accuracy	Kappa
1	Water	149	0	13	2	4	3	171	0.87	0
2	Builtup Area	0	54	25	4	4	6	93	0.58	0
3	Barren Land	0	0	25	2	7	4	38	0.66	0
4	Shrub and Grassland	0	0	8	57	5	5	75	0.76	0
5	Sparse Vegetation	0	0	0	2	46	8	56	0.82	0
6	Dense Vegetation	0	0	3	3	11	50	67	0.75	0
	Total	149	54	74	70	77	76	500	0	0
	P_Accuracy	1	1	0.33784	0.814286	0.597403	0.657895	0	0.762	0
	Kappa	0	0	0	0	0	0	0	0	0.705
S. N.	Vegetation (Nov,1991)	Water	Built up Area	Barren Land	Shrub and Grassland	Sparse Vegetation	Dense Vegetation	Total	User Accuracy	Kappa
1	Water	177	0	13	2	3	2	197	0.90	0
2	Builtup Area	0	75	25	8	6	6	120	0.63	0
3	Barren Land	0	5	28	1	1	2	37	0.76	0
4	Shrub and Grassland	0	0	3	54	9	12	78	0.69	0
5	Sparse Vegetation	0	0	1	3	33	9	46	0.72	0
6	Dense Vegetation	0	0	1	1	2	18	22	0.82	0
	Total	177	80	71	69	54	49	500	0	0
	P_Accuracy	1.00	0.94	0.39	0.78	0.61	0.37	0	0.77	0
	Kappa	0	0	0	0	0	0	0	0	0.77

Continue of Table 4. Accuracy Assessment of NDVI for the months Jan and Feb of the year 1991 and 2021.

S. N.	Vegetation (Jan,2021)	Water	Builtup Area	Barren Land	Shrub and Grassland	Sparse Vegetation	Dense Vegetation	Total	User Accuracy	Kappa
1	Water	73	0	2	0	0	0	75	0.97	0
2	Builtup Area	2	112	55	9	4	0	182	0.62	0
3	Barren Land	0	9	59	8	1	1	78	0.76	0
4	Shrub and Grassland	0	2	4	29	6	8	49	0.59	0
5	Sparse Vegetation	0	1	3	6	93	9	112	0.83	0
6	Dense Vegetation	0	0	3	1	1	5	10	0.50	0
	Total	75	124	126	53	105	23	506	0	0
	P_Accuracy	0.97	0.90	0.47	0.55	0.89	0.22	0	0.742	0
	Kappa	0	0	0	0	0	0	0	0	0.742

S. N.	Vegetation (Nov,2021)	Water	Builtup Area	Barren Land	Shrub and Grassland	Sparse Vegetation	Dense Vegetation	Total	User Accuracy	Kappa
1	Water	77	0	3	0	0	0	80	0.96	0
2	Builtup Area	5	44	38	5	4	6	102	0.43	0
3	Barren Land	0	0	19	8	4	4	35	0.54	0
4	Shrub and Grassland	1	2	4	60	6	16	89	0.67	0
5	Sparse Vegetation	0	0	1	6	105	10	122	0.86	0
6	Dense Vegetation	0	1	2	3	9	57	72	0.79	0
	Total	83	47	67	82	128	93	500	0	0
	P_Accuracy	0.93	0.94	0.28	0.73	0.82	0.61	0	0.724	0
	Kappa	0	0	0	0	0	0	0	0	0.724

5. Normalized Difference Drought Index (NDDI) as Drought Severity Map

The NDDI classes were classified into six NDDI categories (ANNEX 1.3). The abnormally drought area increased by 164.03% in January when compared between the year 1991 and 2021 (Figure 5 and Table 5). However, abnormally drought area declined by 40.5% in November when compared between the year 1991 and 2021. Moderately drought area increased by 34.58% and 44.36% in January and November respectively when compared between the year 1991 and 2021. Severe drought area decreased by 67.81% in January when compared between the year 1991 and 2021 (Table 5). Though

severe drought area increased by 39.49% in November when compared between the year 1991 and 2021. Extreme drought area decreased by 96.37% in January when compared between the year 1991 and 2021. However, the extreme drought area increased by 216.37% in November when compared between the year 1991 and 2021. Exceptional drought area decreased by 99.1% in January when compared between the year 1991 and 2021, though, increased by 984.66% in November when compared between the year 1991 and 2021 (Table 5). The water body/snow decreased by 45.91% and 47.91% in January and November respectively when compared between the year 1991 and 2021.

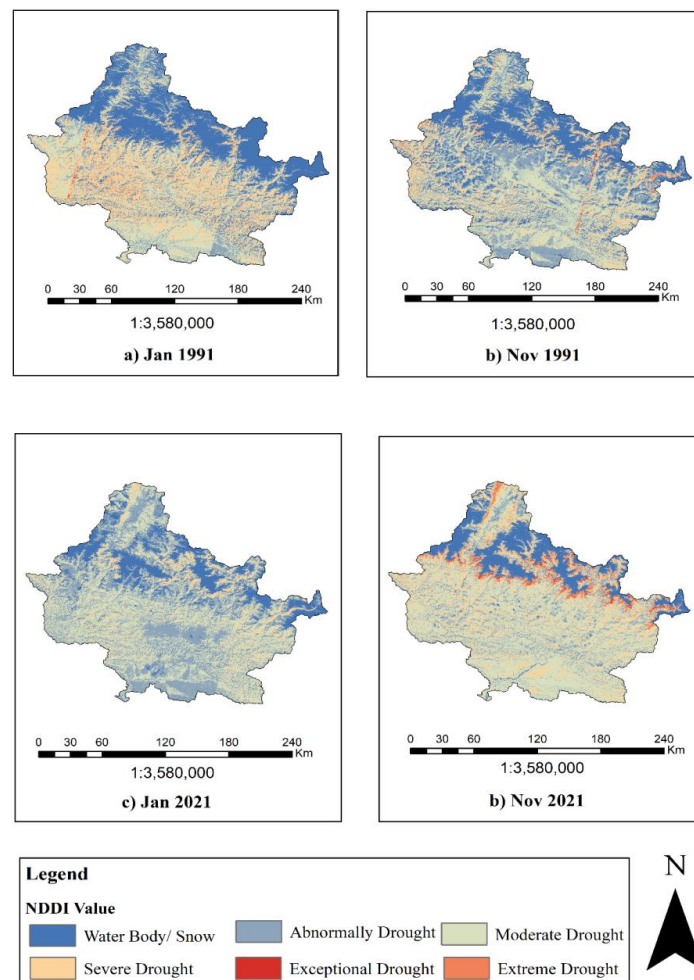


Fig 5. Drought map of GRB

Table 5. Area in percentage of different drought level

Drought Level	Area in Percentage			
	Jan 1991	Nov 1991	Jan 2021	Nov 2021
No Drought (Water/ Snow)	30.9	27.6	16.7	14.4
Abnormally Drought	13.8	25.1	36.3	14.9
Moderate Drought	29.0	32.5	39.1	47.0
Severe Drought	24.3	13.4	7.8	18.7
Extreme Drought	2.0	1.3	0.1	4.1
Exceptional Drought	0.0	0.1	0.0	0.9
Total	100	100	100	100

NDDI is recommended for measuring drought because it is a more recent and sensitive indicator and can provide a more accurate response in relation to the drought

rates (Tavazohi & Nadoushan, 2018). Our study found higher NDDI during the dry season of the year which is in full accord with the results of several studies

(Mongkolsawatu et al., 2009; Torres et al., 2010; Tavazohi & Nadoushan, 2018). Higher NDDI during the dry season is also similar to the study in Northeastern Thailand (Mongkolsawatu et al., 2009; Torres et al., 2010). In summer, NDDI was proven as an effective index in measuring drought (Gu et al., 2007). Considering the area of the GRB, study in Mongolia also concluded about the NDDI capacity to measure drought on a large scale (Erdenetuya et al., 2010). The abnormally drought, moderately drought and severe drought area were increased in January when compared between the year 1991 and 2021 whereas Moderate Drought area also increased in November (Table 5), which might be due to change in rainfall patterns (Tavazohi & Nadoushan, 2018), overpopulation (Young, 1995), climate change (Sayari et al., 2013), and anthropogenic activities (AghaKouchak et al., 2021). A study by Khatiwada & Pandey (2019) also recorded an increase in drought events in the Karnali river basin of Nepal. An escalation in drought conditions could have far-reaching consequences, impacting water availability, crop yields, and posing significant challenges across the environmental, economic, and social domains (Khatiwada & Pandey, 2019). Nepal witnessed consecutive and worsening drought conditions during 2005–2006 which was among the most difficult for Nepal's mountainous country's agriculture practices and water resource management (Bagale et al., 2021). Similar study shows the western and central region of Nepal as a highly affected drought area than eastern region. However, the abnormal drought area and severe drought area decreased in GRB due to the change in local weather patterns (Sayari et al., 2013). Drought has a direct impact on crops, resulting in financial losses and jeopardizing the

livelihoods of the people. Nations like Nepal, where a significant portion of the population depends heavily on rain-based agriculture for their sustenance, are especially susceptible to the adverse effects of drought (Gentle & Maraseni, 2012). Previous research indicated that Ethiopia experienced its worst extended droughts between 2002 and 2003, affecting the Awash River Basin. This finding aligns with our analysis of the drought tendency in the GRB between 1991 and 2021 (Getahun et al., 2023; Bayissa 2018; Mohammed et al., 2018; Suryabhagavan, 2017; Yadeta et al., 2020). Studies conducted around the world revealed that the current drought caused by climate change has increased in intensity, severity, and frequency over the past few decades (Band et al., 2022; Getahun et al., 2023; Sahana et al., 2021; Shamshirband et al., 2020). According to previous research (Fensholt et al., 2015; Nicholson et al., 1998), drought is an important factor in land degradation processes all over the world. GRB may be more susceptible to extreme dryness if drought persists, which could have a significant impact on local people and ecosystems (Leng et al., 2015). Similar findings were reported by the study of Orimoloye et al., (2019) in South Africa. Therefore, impact assessment studies of drought events are essential (Bagale et al., 2021).

It is evident that the basin is confronted with significant hurdles pertaining to the utilization of water resources, degradation in upstream areas, the vagaries of weather patterns, and a deficiency in public awareness, as highlighted in the work of Chhetri et al., (2020). Moreover, the absence of comprehensive data on actual water availability within the basin compounds the challenges faced in formulating effective drought mitigation strategies. Consequently, it is imperative to

conduct a comprehensive study in regions affected by drought to accurately assess water availability in the basin and address both present and future water demands and mitigate the impact of drought.

Conclusion

In conclusion, this study sheds light on the often underestimated and silent catastrophe of drought, with its far-reaching consequences including food and water shortages, displacement, and even the potential for conflict. Amidst the evident signs of ongoing climate change, there has been a notable lack of research focused on drought conditions within the GRB of Nepal. Through the rigorous analysis of four key indices NDVI, NDWI, LST, and NDDI in the period 1991 and 2021, and employing the power of GIS and remote sensing data, this study provides valuable insights into drought occurring in GRB. The findings are both compelling and concerning. They reveal a stark 93.26% decrease in dense vegetation and a striking 96.88% increase in built-up areas in the month of January, when comparing the years 1991 and 2021. Equally alarming is the 49.5% growth in high water-stressed areas observed in the same month. The NDDI further underscores the gravity of the situation, with an astounding 164.03% expansion in abnormally drought-affected areas in January over the three-decade span from 1991 to 2021.

What becomes unmistakably evident is that the increasing trend of drought in the GRB is not merely a product of natural climate variability but is significantly exacerbated by human activities. This necessitates urgent attention from policymakers and the wider community. In light of these findings, this study advocates for the exploration and utilization of modern tools such as GIS and Remote Sensing for the

prediction of drought and the continuous monitoring of its impact on both ecosystems and human populations. Such an approach offers a valuable resource for policymakers and stakeholders as they work to develop effective strategies for combatting the growing threats of drought and climate change. By harnessing the power of these technologies, we can better prepare, respond, and adapt to the evolving challenges posed by drought, ultimately fostering resilience and sustainability in the GRB and similar regions facing similar crises.

Acknowledgments

We also acknowledge the invaluable contributions of previous researchers in the field, the financial support from Department of Forest and Soil Conservation, Ministry of Forest and Environmental, Nepal, the guidance of our colleagues and advisors, and the unwavering support of our families and friends. This research underscores the significance of collaborative efforts, and we are grateful for the support of all those who contributed to its successful completion.

References

- Aadhar, S., & Mishra, V. (2020). On the projected decline in droughts over south Asia in CMIP6 multimodel Ensemble. *Journal of Geophysical Research: Atmospheres*, 125(20), e2020JD033587. <https://doi.org/10.1029/2020JD033587>
- Adhikari, S. (2018). Drought impact and adaptation strategies in the mid-hill farming system of western Nepal. *Environments*, 5, 101. <https://doi.org/10.3390/ENVIRONMENTS5090101>
- Ageta, Y., Naito, N., & IWATA, S. (2003). Glacier distribution in the Himalayas and glacier shrinkage from 1963 to 1993 in the Bhutan Himalayas. *Bulletin of Glaciological Research*, 20, 29-40.

- AghaKouchak, A., Mirchi, A., Madani, K., Di Baldassarre, G., Nazemi, A., Alborzi, A., ... & Wanders, N. (2021). Anthropogenic drought: definition, challenges, and opportunities. <https://doi.org/10.1029/2019RG000683>
- Ahmed, N., Mahbub, R. B., Hossain, M. M., & Sujauddin, M. (2020). Context of traditional and co-management paradigms. *Journal of Tropical Forest Science*, 32(1), 42–51. <https://www.jstor.org/stable/26872818>
- Bagale, D., Sigdel, M., & Aryal, D. (2021). Drought monitoring over Nepal for the last four decades and its connection with southern oscillation Index. *Water*, 13(23), 3411. <https://doi.org/10.3390/W13233411>
- Baidya, S. K., Shrestha, M. L., & Sheikh, M. M. (2008). Trends in daily climatic extremes of temperature and precipitation in Nepal. *Journal of Hydrology and Meteorology*, 5(1), 38–51.
- Bajracharya, T. R., Acharya, S., & Ale, B. B. (2011). Changing climatic parameters and its possible impacts in hydropower generation in Nepal (A case study on Gandaki river basin). *Journal of the Institute of Engineering*, 8(1–2), 160–173. <https://doi.org/10.3126/JIE.V8I1-2.5108>
- Band, S. S., Karami, H., Jeong, Y. W., Moslemzadeh, M., Farzin, S., Chau, K. W., Bateni, S. M., & Mosavi, A. (2022). Evaluation of time series models in simulating different monthly scales of drought index for improving their forecast accuracy. *Frontiers in Earth Science*, 10, 839527. <https://doi.org/10.3389/FEART.2022.839527>
- Baniya, B., Tang, Q., Huang, Z., Sun, S., & Techato, K.-a. (2018). Spatial and temporal variation of NDVI in response to climate change and the implication for carbon dynamics in Nepal. *Forests*, 9(6), 329. <https://doi.org/10.3390/F9060329>
- Bashit, N., Rišianti, N. S., & Ulfiana, D. (2022). Drought assessment using remote sensing and geographic information systems (GIS) techniques (Case study: Klaten district). *International Journal of Geoinformatics*, 18(5), 115–127. <https://doi.org/10.52939/ijg.v18i5.2393>
- Bayissa, Y.A. (2018). Developing an impact-based combined drought index for monitoring crop yield anomalies in the Upper Blue Nile Basin (Dissertation). Delft University of Technology.
- Bernstein, L., Bosch, P., Canziani, O., Chen, Z., & Christ, R. (2008). IPCC, 2007: AR4 climate change 2007: synthesis report. http://www.ipcc.ch/publications_and_data/ar4/syr/en/contents.html
- Bista, N., Mahat, D., Manandhar, S., Regmi, B., Panday, U. S., & Karki, S. (2021). Analyzing trend and pattern of agricultural drought: A case study of Karnali and Sudurpashchim provinces. *Journal on Geoinformatics, Nepal*, 20(1), 1–8. <https://doi.org/10.3126/NJG.V20I1.39470>
- Brown M.E., & Funk, C.C. (2005). A max-to-min technique for making projections of NDVI change in semi-arid Africa for food security early warning. In *AGU Fall Meeting Abstracts*.
- Central Bureau of Statistics (CBS). (2011). Nepal living standards survey 2010/2011. Kathmandu: Central Bureau of Statistics.
- Chaulagain, N. P., Nepal, M. S., & Hohmeyer, O. (2006). Impacts of climate change on water resources of Nepal, the physical and socioeconomic dimensions Gutachter (Dissertation). Flensburg University.
- Chen, B., Xu, G., Coops, N. C., Ciais, P., Innes, J. L., Wang, G., Myneni, R. B., Wang, T., Krzyzanowski, J., Li, Q., Cao, L., & Liu, Y. (2014). Changes in vegetation photosynthetic activity trends across the Asia–Pacific region over the last three decades. *Remote Sensing of Environment*, 144, 28–41. <https://doi.org/10.1016/J.RSE.2013.12.018>
- Chen, H., & Sun, J. (2015). Changes in drought characteristics over China using the standardized precipitation evapotranspiration index. *Journal of Climate*, 28(13), 5430–5447. <https://doi.org/10.1175/JCLI-D-14-00707.1>
- Chhetri, R., Kumar, P., Pandey, V. P., Singh, R.,

- & Pandey, S. (2020). Vulnerability assessment of water resources in Hilly Region of Nepal. *Sustainable Water Resources Management*, 2020.Springer, 6(3), 34. <https://doi.org/10.1007/s40899-020-00391-x>
- Ciais, P., Reichstein, M., Viovy, N., Granier, A., Ogee, J., Allard, V., Aubinet, M., Buchmann, N., Bernhofer, C., Carrara, A., Chevallier, F., De Noblet, N., Friend, A. D., Friedlingstein, P., Grünwald, T., Heinnesch, B., Keronen, P., Knohl, A., Krinner, G., ... Valentini, R. (2005). Europe-wide reduction in primary productivity caused by the heat and drought in 2003. *Nature*. 437(7058), 529–533. <https://doi.org/10.1038/nature03972>
- Cui, X., & Graf, H. F. (2009). Recent land cover changes on the Tibetan Plateau: A review. *Climatic Change*, 94(1–2), 47–61. <https://doi.org/10.1007/S10584-009-9556-8>
- Dahal, P., Shrestha, N. S., Shrestha, M. L., Krakauer, N. Y., Panthi, J., Pradhanang, S. M., Jha, A., & Lakhankar, T. (2016). Drought risk assessment in central Nepal: temporal and spatial analysis. *Natural Hazards*, 80(3), 1913–1932. <https://doi.org/10.1007/S11069-015-2055-5>
- Dandekhya, S., England, M., Ghate, R., Godrich, C., Nepal, S., Prakash, A., & Udas, P. (2017). The Gandaki basin: Maintaining livelihoods in the face of landslides, floods, and drought. In HI-AWARE Working Paper, 9.
- Das, A. C., Shahriar, S. A., Chowdhury, M. A., Hossain, M. L., Mahmud, S., Tusar, M. K., Ahmed, R., & Salam, M. A. (2023). Assessment of remote sensing-based indices for drought monitoring in the north-western region of Bangladesh. *Heliyon*, 9(2), e13016. <https://doi.org/10.1016/j.heliyon.2023.e13016>
- Dhakal, K., Silwal, S., & Khanal, G. (2010). Assessment of climate change impacts on water resources and vulnerability in hills of Nepal. A Case Study on Dhare Khola Watershed of Dhading District Submitted to National Adaptation Program of Action (NAPA) to Climate Change Ministry of Environment, Government of Nepal. https://www.climatenepal.org.np/sites/default/files/doc_resources/bshooe6hnfs_3.pdf
- Diego, R.T. , Martínez Izquierdo, M. E., Arquero Hidalgo, Á., & Sánchez Hernández, J. (2010). Drought estimation maps by means multirate landsat fused images. In: “30th EARSeL Symposium Remote Sensing for Science, Education, and Natural and Cultural Heritage”, 31 May-03 Jun 2010, Paris, Francia. <https://oa.upm.es/34984/>
- Eckstein, D., Künzel, V., y Schäfer, L. (2021). The global climate risk index 2021. Bonn: Germanwatch. *Recuperado de*. <https://bvearmb.do/handle/123456789/1306>
- Erdenetuya, M., Bulgan, D., & Erdenetseg, B. (2010). Drought monitoring and assessment using multi satellite data in Mongolia. 32nd Asian Conference on Remote Sensing, *TSI-Climate Change*.
- Food and Agricultural Organization (FAO) (2017). International Seminar on Drought & Agriculture-Predict, Plan, Prepare: Stop Drought Becoming Famine. <https://www.fao.org/3/bs902e/bs902e.pdf>.
- Fensholt, R., Horion, S., Tagesson, T., Ehammer, A., Grogan, K., Tian, F., Huber, S., Verbesselt, J., Prince, S. D., Tucker, C. J., & Rasmussen, K. (2015). Assessing drivers of vegetation changes in dry lands from time series of earth observation data. *Remote Sensing and Digital Image Processing*, 22, 183–202. https://doi.org/10.1007/978-3-319-15967-6_9
- Gao, B. (1996). NDWI—A normalized difference water index for remote sensing of vegetation liquid water from space. *Remote Sensing of Environment*, 58(3), 257–266. [https://doi.org/10.1016/S0034-4257\(96\)00067-3](https://doi.org/10.1016/S0034-4257(96)00067-3)
- GAR. (2021). <https://www.undrr.org/gar2021-drought>. Retrieved.
- Gautam, D. K., & Regmi, S. K. (2013). Recent trends in the onset and withdrawal of summer monsoon over Nepal. *ECOPERSIA*, 1(4), 353–367. <http://ecopersia.modares.ac.ir/article-24-11752-en.html>
- Gentle, P., & Maraseni, T. N. (2012). Cli-

- mate change, poverty and livelihoods: adaptation practices by rural mountain communities in Nepal. *Environmental Science & Policy*, 21, 24–34. <https://doi.org/10.1016/J.ENVSCI.2012.03.007>
- Getahun, Y., Li, M., Chen, Y., & Yate, T. (2023). Drought characterization and severity analysis using GRACE-TWS and MODIS datasets: a case study from the Awash River Basin (ARB), Ethiopia. *Journal of Water and Climate Change*, 14(2), 516–542. <https://iwaponline.com/jwcc/article-abstract/14/2/516/93369>
- Ghimire, P. (2019). A review of studies on climate change in Nepal. *The Geographic Base*, 6, 11–20. <https://doi.org/10.3126/TGB.V6I0.26163>
- Gu, Y., Brown, J. F., Verdin, J. P., Wardlow, B., Gu, Y., Brown, J. F., Verdin, J. P., & Wardlow, B. (2007). A five-year analysis of MODIS NDVI and NDWI for grassland drought assessment over the central Great Plains of the United States. *Geophysical Research Letters*, 34(6). <https://doi.org/10.1029/2006GL029127>
- Guha-Sapir, D., Hoyois, P., Wallemacq, P., & Below, R. (2017). Annual disaster statistical review 2016: the numbers and trends. <https://www.preventionweb.net/publication/annual-disaster-statistical-review-2016-numbers-and-trends>. Retired date.
- Gulácsi, A., & Kovács, F. (2018). Drought monitoring of forest vegetation using MODIS-based normalized difference drought index in Hungary. *Hungarian Geographical Bulletin*, 67(1), 29–42. <https://doi.org/10.15201/HUNGEOBULL.67.1.3>
- Gurung, G. B., & Bhandari, D. (2009). Integrated approach to climate change adaptation. *Journal of Forest and Livelihood*, 8(1), 90–98. <https://nepjol.info/index.php/JFL/article/view/1889>
- Hagman, G., Beer, H., Bendz, M., & Wijkman, A. (1984). Prevention better than cure. Report On Human And Environmental Disasters In The Third World. <https://kohahq.searo.who.int/cgi-bin/koha/opac-detail.pl?biblionumber=1479>
- Haile, T. (1988). Causes and characteristics of drought in Ethiopia. *Ethiopian Journal of Agricultural Sciences*, 10 (1–2), 85–97.
- Haitham, A., Supervisor, B., Károly, P., & János, R. (2021). Drought vulnerability and mitigation measures in Jordan based on spatio-temporal assessment of single and composite meteorological drought indices; [PHD dissertation]. Szeged, University of Szeged.
- Hamal, K., Sharma, S., Baniya, B., Khadka, N., & Zhou, X. (2020). Inter-annual variability of winter precipitation over Nepal coupled with ocean-atmospheric patterns during 1987–2015. *Frontiers in Earth Science*, 8, 511095. <https://doi.org/10.3389/FEART.2020.00161>
- Hisdal, H., Tallaksen, L., Peters, E., Stahl, K., & Zaidman, M. (2000). Assessment of regional impact of droughts in Europe (ARIDE). *Technical Rep*, 6, 15.
- Hofste, R., Reig, P., & Schleifer, L. (2019). 17 countries, home to one-quarter of the world's population, face extremely high water stress. <https://www.wri.org/insights/17-countries-home-one-quarter-worlds-population-face-extremely-high-water-stress>.
- Hossain, M. L., & Li, J. (2021). Biomass partitioning of C3- and C4-dominated grasslands in response to climatic variability and climate extremes. *Environmental Research Letters*, 16(7), 074016. <https://doi.org/10.1088/1748-9326/AC027A>
- Hossain, M. L., Li, J., Hoffmann, S., & Beierkuhnlein, C. (2022). Biodiversity showed positive effects on resistance but mixed effects on resilience to climatic extremes in a long-term grassland experiment. *Science of the Total Environment*, 827, 154322. <https://doi.org/10.1016/J.SCITOTENV.2022.154322>
- Ichii, K., Kawabata, A., & Yamaguchi, Y. (2002). Global correlation analysis for NDVI and climatic variables and NDVI trends: 1982–1990. *International Journal of Remote Sensing*, 23(18), 3873–3878. <https://doi.org/10.1080/01431160110119416>
- Intergovernmental Panel on Climate Change

- (IPCC). (2023). Climate change 2021—the physical science basis: working group I contribution to the Sixth assessment report of the intergovernmental panel on climate change. Cambridge: Cambridge University Press. Doi: 10.1017/9781009157896
- Isbell, F., Craven, D., Connolly, J., Loreau, M., Schmid, B., Beierkuhnlein, C., Bezemer, T. M., Bonin, C., Bruelheide, H., De Luca, E., Ebeling, A., Griffin, J. N., Guo, Q., Hautier, Y., Hector, A., Jentsch, A., Kreyling, J., Lanta, V., Manning, P., ... Eisenhauer, N. (2015). Biodiversity increases the resistance of ecosystem productivity to climate extremes. *Nature*, 526(7574), 574–577. <https://doi.org/10.1038/NATURE15374>
- Jonathan, K. H., & Suvarna Raju, P. (2017). Temperature variations in three regions of sultanate of Oman. *International Journal of Civil Engineering and Technology*, 8(2), 173–181.
- Jordaan, A., Bahta, Y. T., & Phatudi-Mphahlele, B. (2019). Ecological vulnerability indicators to drought: Case of communal farmers in Eastern Cape, South Africa. *Jamba: Journal of Disaster Risk Studies*, 11(1). <https://doi.org/10.4102/JAMBA.V11I1.591>
- Joshi, N., & Dongol, R. (2018). Severity of climate induced drought and its impact on migration: A study of Ramechhap district, Nepal. *Tropical Agricultural Research*, 29(2), 194–211.
- Kafy, A. Al, Rahman, M. S., Faisal, A. Al, Hasan, M. M., & Islam, M. (2020). Modelling future land use land cover changes and their impacts on land surface temperatures in Rajshahi, Bangladesh. *Remote Sensing Applications: Society and Environment*, 18, 100314. <https://doi.org/10.1016/J.RSASE.2020.100314>
- Kahya C, BektasBalcik F, BurakOztaner Y, Guney B. (2016). Determining land surface temperature relations with land use-land cover and air pollution. *Geophysical Research Abstracts*, 18, EGU2016-16489. <https://ui.adsabs.harvard.edu/abs/2016EGUGA..1816489K/abstract>
- Kawabata, A., Ichii, K., & Yamaguchi, Y. (2001). Global monitoring of internal changes in vegetation activities using NDVI and its relationships to temperature and precipitation. *International Journal of Remote Sensing*, 22(7), 1377–1382. <https://doi.org/10.1080/01431160119381>
- Khan, A.A, & Safdar, Q., & Khan, K. (2020). Occurrence pattern of meteorological droughts and associated problems in Cholistan region of Pakistan: A spatio-temporal view. *Basic Research Journal of Agricultural Science and Review*, 8(3). 38-51.
- Khatiwada, K. R., & Pandey, V. P. (2019). Characterization of hydro-meteorological drought in Nepal Himalaya: A case of Karnali River Basin. *Weather and Climate Extremes*, 26, 100239. <https://doi.org/10.1016/J.WACE.2019.100239>
- Leng, G., Tang, Q., & Rayburg, S. (2015). Climate change impacts on meteorological, agricultural and hydrological droughts in China. *Global and Planetary Change*, 126, 23–34. <https://doi.org/10.1016/J.GLOPLACHA.2015.01.003>
- Liu, W. C., Bravo De Guenni, L., Lee, H., Tsun, J., Yang, H., Ndayiragije, J. M., & Li, F. (2022). Effectiveness of drought indices in the assessment of different types of droughts, managing and mitigating their effects. *Climate*, 10(9), 125. <https://doi.org/10.3390/CLI10090125>
- Liu, X., Wang, S., Zhou, Y., Wang, F., Li, W., & Liu, W. (2015). Regionalization and spatiotemporal variation of drought in China based on standardized precipitation evapotranspiration index (1961-2013). *Advances in Meteorology*. <https://doi.org/10.1155/2015/950262>
- Lotfirad, M., Esmaeili-Gisavandani, H., & Adib, A. (2022). Drought monitoring and prediction using SPI, SPEI, and random forest model in various climates of Iran. *Journal of Water and Climate Change*, 13(2), 383–406. <https://doi.org/10.2166/WCC.2021.287>
- Luintel, N., Ma W., Ma Y, Wang B., & Subba, S. (2019). Spatial and temporal variation of daytime and nighttime MODIS land

- surface temperature across Nepal. *Atmospheric and Oceanic Science Letters*, 12(5), 305-312. <https://doi.org/10.1080/16742834.2019.1625701>
- Maharjan, A., Kochhar, I., Chitale, V. S., Hussain, A., & Gioli, G. (2020). Understanding rural outmigration and agricultural land use change in the Gandaki Basin, Nepal. *Applied Geography*, 124, 102278. <https://doi.org/10.1016/J.AP-GEOG.2020.102278>
- Maillard, O., Vides-Almonacid, R., Salazar, Á., & Larrea-Alcazar, D. M. (2022). Effect of deforestation on land surface temperature in the Chiquitania Region, Bolivia. *Land*, 12(1), 2. <https://doi.org/10.3390/LAND12010002>
- Mallick, D., Abbasi, S., Ali, M., Anwar, M., Batool, S., Bhadwal, S., & Varma, N. (2019). Participatory assessment of multiple socio-economic drivers and climate stresses leading to differentiated vulnerabilities in the Hindu Kush Himalaya; HI-AWARE Working Paper 24.
- Mao, K. B., Ma, Y., Tan, X. L., Shen, X. Y., Liu, G., Li, Z. L., Chen, J. M., & Xia, L. (2017). Global surface temperature change analysis based on MODIS data in recent twelve years. *Advances in Space Research*, 59(2), 503–512. <https://doi.org/10.1016/J.ASR.2016.11.007>
- Mašný, L. (2000). Melting of earth's ice cover reaches new high | HimalDoc. 2000. <https://lib.icimod.org/record/10441>
- McFeeters, S. K. (1996). The use of the Normalized Difference Water Index (NDWI) in the delineation of open water features. *International Journal of Remote Sensing*, 17(7), 1425–1432. <https://doi.org/10.1080/01431169608948714>
- McKee, T.B., Doesken, N.J., & Kleist, J. (1993). The relationship of drought frequency and duration to time scales. In Proceedings of the 8th Conference on Applied Climatology.
- Mehta, D. J., & Yadav, S. M. (2023). Meteorological drought analysis in Pali district of Rajasthan state using standard precipitation index. *International Journal of Hydrology Science and Technology*, 15(1), 1. <https://doi.org/10.1504/IJHST.2023.127880>
- Mehta, R. K., & Shah, S. C. (2012). Impact of climate change on water availability and food security of Nepal. *Hydro Nepal: Journal of Water, Energy and Environment*, 59–63. <https://doi.org/10.3126/HN.V11I1.7206>
- Mirza, M. M. Q. (2003). Climate change and extreme weather events: Can developing countries adapt? *Climate Policy*, 3(3), 233–248. <https://doi.org/10.3763/CPOL.2003.0330>
- Mishra, N. B., & Mainali, K. P. (2017). Greening and browning of the Himalaya: Spatial patterns and the role of climatic change and human drivers. *Science of the Total Environment*, 587–588, 326–339. <https://doi.org/10.1016/J.SCITOTENV.2017.02.156>
- Miyan, M. A. (2015). Droughts in Asian least developed countries: Vulnerability and sustainability. *Weather and Climate Extremes*, 7, 8–23. <https://doi.org/10.1016/J.WACE.2014.06.003>
- MOHA. (2009). National strategy for disaster risk management. <https://www.fao.org/faolex/results/details/en/c/LEX-FA-OC143046>.
- Mohammed, Y., Yimer, F., Tadesse, M., & Tesfaye, K. (2018). Meteorological drought assessment in north east highlands of Ethiopia. *International Journal of Climate Change Strategies and Management*, 10(1), 142–160. <https://doi.org/10.1108/IJCCSM-12-2016-0179>
- Mongkolsawat C, Wattanakij N, Kamchai T, Mongkolsawat K, Chuyakhai D. (2009). Exploration of spatio-temporal drought patterns using satellite-derived indices for crop management in Northeastern Thailand. In Proceedings of the 30th Asian Conference on Remote Sensing China.
- Mool, P., Tao, C., & Bajracharya, S.R. (2004). Monitoring of glaciers and glacial lakes from 1970s to 2000 in Poiqu basin, Tibet. Autonomous Region PR China by ICI-MOD, Kathmandu, Nepal

- Nagendra, H., Sudhira, H. S., Katti, M., & Schewenius, M. (2013). Sub-regional assessment of India: Effects of urbanization on land use, biodiversity and ecosystem services. *Urbanization, Biodiversity and Ecosystem Services: Challenges and Opportunities: A Global Assessment*, 65–74. https://doi.org/10.1007/978-94-007-7088-1_6
- Natarajan, N., & Vasudevan, M. (2020). Trend analysis of meteorological parameters of Adelaide, South Australia. *Environment Asia*, 13(3), 103–117. <https://doi.org/10.14456/EA.2020.46>
- Natarajan, N., Vasudevan, M., Raja, S. A., Mohanpradaap, K., Sneha, G., & Shanu, S. J. (2023). An assessment methodology for drought severity and vulnerability using precipitation-based indices for the arid, semi-arid and humid districts of Tamil Nadu, India. *Water Supply*, 23(1), 54–79. <https://doi.org/10.2166/WS.2022.415>
- Ndayiragije, J. M., & Li, F. (2022). Effectiveness of Drought Indices in the Assessment of Different Types of Droughts, Managing and Mitigating Their Effects. <https://doi.org/10.3390/cli10090125>
- Nepal, S., Tripathi, S., & Adhikari, H. (2021). Geospatial approach to the risk assessment of climate-induced disasters (drought and erosion) and impacts on out-migration in Nepal. *International Journal of Disaster Risk Reduction*, 59, 102241. <https://doi.org/10.1016/J.IJDRR.2021.102241>
- Nicholson, S. E., Tucker, C. J., & Ba, M. B. (1998). Desertification, drought, and surface vegetation: An example from the west African Sahel. *Bulletin of the American Meteorological Society*, 79(5), 815–830. [https://doi.org/10.1175/1520-0477\(1998\)079<0815:D-DASVA>2.0.CO;2](https://doi.org/10.1175/1520-0477(1998)079<0815:D-DASVA>2.0.CO;2)
- Orimoloye, I. R., Mazinyo, S. P., Nel, W., & Kalumba, A. M. (2018). Spatiotemporal monitoring of land surface temperature and estimated radiation using remote sensing: human health implications for East London, South Africa. *Environmental Earth Sciences*, 77(3), 1–10. <https://doi.org/10.1007/S12665-018-7252-6>
- Orimoloye, I. R., Ololade, O. O., Mazinyo, S. P., Kalumba, A. M., Ekundayo, O. Y., Busayo, E. T., Akinsanola, A. A., & Nel, W. (2019). Spatial assessment of drought severity in Cape Town area, South Africa. *Heliyon*, 5(7), e02148. <https://doi.org/10.1016/j.heliyon.2019.e02148>
- Ouyang, X., Chen, D., Feng, Y., & Lei, Y. (2019). Comparison of seasonal surface temperature trend, spatial variability, and elevation dependency from satellite-derived products and numerical simulations over the Tibetan Plateau from 2003 to 2011. *International Journal of Remote Sensing*, 40(5–6), 1844–1857. <https://doi.org/10.1080/01431161.2018.1482024>
- Palmer, W. C. (1968). Keeping Track of Crop Moisture Conditions, Nationwide: The new crop moisture Index. *Weatherwise*, 21(4), 156–161. <https://doi.org/10.1080/0431672.1968.9932814>
- Paniagua, M. T., Villalba, J., and Pasten, M. (2020). Spatial-temporal distribution of drought in the western region of Paraguay (2005–2017), *Int. Arch. Photogram. Remote Sens. Spatial Inf. Sci.*, XLII-3/W12-2020, 327–330, <https://doi.org/10.5194/isprs-archives-XLII-3-W12-2020-327-2020>
- Pant, R. R., Zhang, F., Rehman, F. U., Wang, G., Ye, M., Zeng, C., & Tang, H. (2018). Spatiotemporal variations of hydrogeochemistry and its controlling factors in the Gandaki River Basin, Central Himalaya Nepal. *Science of the Total Environment*, 622–623, 770–782. <https://doi.org/10.1016/J.SCITOTENV.2017.12.063>
- Panthi, J., Dahal, P., Shrestha, M. L., Aryal, S., Krakauer, N. Y., Pradhanang, S. M., Lakhankar, T., Jha, A. K., Sharma, M., & Karki, R. (2015). Spatial and temporal variability of rainfall in the Gandaki river basin of Nepal Himalaya. *Climate* 2015, Vol. 3, Pages 210–226, 3(1), 210–226. <https://doi.org/10.3390/CLI3010210>
- Park, S., Im, J., Jang, E., & Rhee, J. (2016). Drought assessment and monitoring through blending of multi-sensor indices using machine learning approaches for different climate regions. *Agric-*

- cultural and Forest Meteorology*, 216, 157–169. <https://doi.org/10.1016/J.AGR-FORMET.2015.10.011>
- Paudel, B., Wang, Z., Zhang, Y., Rai, M. K., & Paul, P. K. (2021). Climate change and its impacts on farmer's livelihood in different physiographic regions of the Trans-Boundary Koshi river basin, Central Himalayas. *International Journal of Environmental Research and Public Health*, 18(13), 7142. <https://doi.org/10.3390/IJERPH18137142>
- Qin, J., Yang, K., Liang, S., & Guo, X. (2009). The altitudinal dependence of recent rapid warming over the Tibetan Plateau. *Climatic Change*, 97(1), 321–327. <https://doi.org/10.1007/S10584-009-9733-9>
- Radmanesh, F., Esmaceli-Gisavandani, H., & Lotfirad, M. (2022). Climate change impacts on the shrinkage of Lake Urmia. *Journal of Water and Climate Change*, 13(6), 2255–2277. <https://doi.org/10.2166/WCC.2022.300>
- Rahaman, K. M., Ahmed, F. R. S., & Nazrul Islam, M. (2016). Modeling on climate induced drought of north-western region, Bangladesh. *Modeling Earth Systems and Environment*, 2(1), 1–21. <https://doi.org/10.1007/S40808-016-0089-7>
- Rai, R., Zhang, Y., Paudel, B., Acharya, B. K., & Basnet, L. (2018). Land use and land cover dynamics and assessing the ecosystem service values in the Trans-Boundary Gandaki river basin, Central Himalayas. *Sustainability*, 10(9), 3052. <https://doi.org/10.3390/SU10093052>
- Rai, R., Zhang, Y., Paudel, B., Li, S., & Khanal, N. R. (2017). A synthesis of studies on land use and land cover dynamics during 1930–2015 in Bangladesh. *Sustainability*, 9(10), 1866. <https://doi.org/10.3390/SU9101866>
- Ramachandraiah, C., & Prasad, S. (2004). Impact of urban growth on water bodies: The case of Hyderabad. Hyderabad: Centre for Economic and Social Studies. Working Paper no. 60. Center for Economic and Social Studies Begumpet, Hyderabad-500016. <https://core.ac.uk/download/pdf/6604874.pdf>
- Rebetez, M. (1996). Seasonal relationship between temperature, precipitation and snow cover in a mountainous region. *Theoretical and Applied Climatology*, 54(3–4), 99–106. <https://doi.org/10.1007/BF00865152>
- Regmi, B.R., Pandit, A. (2016). Classification of adaptation measures and criteria for evaluation: Case studies in the Gandaki river basin, Nepal. HI-AWARE Working Paper 6. Kathmandu: HI-AWARE. <file:///C:/Users/User/Downloads/Hi-AwareWP6.pdf>
- Rouse, J. W., Haas, R. H., Schell, J., & Deering, D. (1974). Monitoring vegetation systems in the Great Plains with ERTS. NASA Spec. Publ1974:351(1):309.
- Sahana, V., Mondal, A., & Sreekumar, P. (2021). Drought vulnerability and risk assessment in India: Sensitivity analysis and comparison of aggregation techniques. *Journal of Environmental Management*, 299, 113689. <https://doi.org/10.1016/J.JENVMAN.2021.113689>
- Sangita, D., & Dulal, G. (2021). Satellite mapping of land use land cover (LULC) changes and NDVI in the Subansiri river basin of eastern Himalayas and the Alaknanda river basin of western Himalayas: A comparative study based on spatial analysis. *Research Journal of Chemistry and Environment*, 25(7).
- Sayari, N., Bannayan, M., Alizadeh, A., & Farid, A. (2013). Using drought indices to assess climate change impacts on drought conditions in the northeast of Iran (case study: Kashafrud basin). *Meteorological Applications*, 20(1), 115–127. <https://doi.org/10.1002/MET.1347>
- Seto, K. C. (2011). Exploring the dynamics of migration to mega-delta cities in Asia and Africa: Contemporary drivers and future scenarios. *Global Environmental Change*, 21(SUPPL. 1), S94–S107. <https://doi.org/10.1016/J.GLOENV-CHA.2011.08.005>
- Shamshirband, S., Hashemi, S., Salimi, H., Samadianfard, S., Asadi, E., Shadkani, S.,

- Kargar, K., Mosavi, A., Nabipour, N., & Chau, K. W. (2020). Predicting standardized stream flow index for hydrological drought using machine learning models. *Engineering Applications of Computational Fluid Mechanics*, 14(1), 339–350. <https://doi.org/10.1080/19942060.2020.1715844>
- Sharma, S., Khadka, N., Hamal, K., Shrestha, D., Talchabhadel, R., & Chen, Y. (2020). How accurately can satellite products (TMPA and IMERG) detect precipitation patterns, extremities, and drought across the Nepalese Himalaya? *Earth and Space Science*, 7(8), e2020EA001315. <https://doi.org/10.1029/2020EA001315>
- Shrestha, A. B., Wake, C. P., Mayewski, P. A., & Dibb, J. E. (1999). Maximum temperature trends in the Himalaya and its vicinity: An analysis based on temperature records from Nepal for the period 1971–94. *Journal of Climate*, 12(9), 2775–2786. [https://doi.org/10.1175/1520-0442\(1999\)012](https://doi.org/10.1175/1520-0442(1999)012)
- Shrestha, M. S., Artan, G. A., Bajracharya, S. R., Gautam, D. K., & Tokar, S. A. (2011). Bias-adjusted satellite-based rainfall estimates for predicting floods: Narayani Basin. *Journal of Flood Risk Management*, 4(4), 360–373. <https://doi.org/10.1111/J.1753-318X.2011.01121.X>
- Shrestha, R. M., & Shrestha, R. M. (2020). Drought or wet assessment of daily rainfall pattern of the Budhi Gandaki river basin, Nepal: Standardized precipitation index approach using probabilistic model. *Nepalese Journal of Statistics*, 4, 57–72. <https://doi.org/10.3126/NJS.V4I0.33497>
- Shrestha, R. M., Sthapit, A. B., & Shrestha, S. L. (2018). A Probabilistic approach for assessment of future drought in Bagmati river basin, Nepal. *Nepalese Journal of Statistics*, 2, 75–88. <https://doi.org/10.3126/NJS.V2I0.21156>
- Sigdel, K. P., Ghimire, N. P., Pandeya, B., & Dawadi, B. (2022). Historical and projected variations of precipitation and temperature and their extremes in relation to climatic indices over the Gandaki river basin, Central Himalaya. *Atmosphere*, 13(11), 1866. <https://doi.org/10.3390/AT-MOS13111866>
- Sigdel, M., Ikeda, M., & Ikeda, M. (2010). Spatial and temporal analysis of drought in Nepal using Standardized Precipitation Index and its relationship with climate indices. *Journal of Hydrology and Meteorology*, 7(1), 59–74. <https://doi.org/10.3126/JHM.V7I1.5617>
- Sultana, M. S., Gazi, M. Y., & Mia, M. B. (2021). Multiple indices based agricultural drought assessment in the northwestern part of Bangladesh using geospatial techniques. *Environmental Challenges*, 4, 100120. <https://doi.org/10.1016/j.ENVC.2021.100120>
- Suryabhadgavan, K. V. (2017). GIS-based climate variability and drought characterization in Ethiopia over three decades. *Weather and Climate Extremes*, 15, 11–23. <https://doi.org/10.1016/j.WACE.2016.11.005>
- Tang, Q., Gao, H., Lu, H., & Lettenmaier, D. P. (2009). Remote sensing: hydrology. *Physical Geography* 33(4), 490–509. <https://doi.org/10.1177/0309133309346650>
- Tang, X. ling, Lv, X., & He, Y. (2013). Features of climate change and their effects on glacier snow melting in Xinjiang, China. *Comptes Rendus Geoscience*, 345(2), 93–100. <https://doi.org/10.1016/j.CRTE.2013.01.005>
- Tavazohi, E., & Nadoushan, M. A. (2018). Assessment of Drought in the Zayandehroud Basin during 2000-2015 Using NDDI and SPI Indices. *Fresenius Environmental Bulletin*, 27(4), 2332–2340.
- Tripathi, S., Subedi, R., & Adhikari, H. (2020). Forest cover change pattern after the intervention of community forestry management system in the Mid-Hill of Nepal: A case study. *Remote Sensing*, 12(17), 2756. <https://doi.org/10.3390/RS12172756>
- Turrall, H., Burke, J., & Faurès, J. (2011). Climate change, water and food security. <https://www.fao.org/3/i2096e/i2096e.pdf>
- UNCCD. (2022). Drought in numbers 2022 - Restoration for readiness and resilience. <https://reliefweb.int/report/world>

- drought-numbers-2022-restoration-readiness-and-resilience.
- UN-Water. (2021). Water scarcity. <https://www.unwater.org/water-facts/water-scarcity>.
- Vaglietti, G., Delacote, P., & Leblois, A. (2022). Droughts and deforestation: Does seasonality matter? *PLOS ONE*, 17(10), e0276667. <https://doi.org/10.1371/JOURNAL.PONE.0276667>
- Van Vliet, M. T. H., Sheffield, J., Wiberg, D., & Wood, E. F. (2016). Impacts of recent drought and warm years on water resources and electricity supply worldwide. *Environmental Research Letters*, 11(12), 124021. <https://doi.org/10.1088/1748-9326/11/12/124021>
- Vicente-Serrano, S. M., Beguería, S., & López-Moreno, J. I. (2010). A multi-scalar drought index sensitive to global warming: The standardized precipitation evapotranspiration index. *Journal of Climate*, 23(7), 1696–1718. <https://doi.org/10.1175/2009JCLI2909.1>
- Vohra, C. P. (1981). Note on recent glaciological expeditions in Himachal Pradesh. *Note on Recent Glaciological Expeditions in Himachal Pradesh*, 6, 26–29. <http://pas-cal-francis.inist.fr/vibad/index.php?action=getRecordDetail&idt=9555540>
- Wang, X., Wang, T., Liu, D., Guo, H., Huang, H., & Zhao, Y. (2017). Moisture-induced greening of the South Asia over the past three decades. *Global Change Biology*, 23(11), 4995–5005. <https://doi.org/10.1111/GCB.13762>
- Wassie, S. B. (2020). Natural resource degradation tendencies in Ethiopia: a review. *Environmental Systems Research*, 9(1), 1–29. <https://doi.org/10.1186/S40068-020-00194-1>
- World Meteorological Organization (WMO) and Global Water Partnership (GWP). (2016): Handbook of drought indicators and indices (M. Svoboda and B.A. Fuchs). Integrated drought management programmer (IDMP), Integrated Drought Management Tools and Guidelines Series 2. Geneva.
- World Wild Fund (WWF) (2019). Risiko dürre – Der weltweite Durst nach Wasser in Zeiten der Klimakrise. WWF Deutschland. Berlin, Germany. https://www.wwf.de/fileadmin/fm-wwf/Publikationen-PDF/WWF_Duerrebericht_DE_WEB.pdf
- Xu, G., Zhang, H., Chen, B., Zhang, H., Innes, J. L., Wang, G., Yan, J., Zheng, Y., Zhu, Z., & Myneni, R. B. (2014). Changes in vegetation growth dynamics and relations with climate over China's Landmass from 1982 to 2011. *Remote Sensing*, 6(4), 3263–3283. <https://doi.org/10.3390/RS6043263>
- Yadeta, D., Kebede, A., & Tessema, N. (2020). Climate change posed agricultural drought and potential of rainy season for effective agricultural water management, Kesem sub-basin, Awash Basin, Ethiopia. *Theoretical and Applied Climatology*, 140(1–2), 653–666. <https://doi.org/10.1007/S00704-020-03113-7>
- Yang, H., Munson, S. M., Huntingford, C., Carvalhais, N., Knapp, A. K., Li, X., Peñuelas, J., Zscheischler, J., & Chen, A. (2023). The detection and attribution of extreme reductions in vegetation growth across the global land surface. *Global Change Biology*, 29(8), 2351–2362. <https://doi.org/10.1111/GCB.16595>
- Young, R. A. (1995). Coping with a severe sustained drought on the Colorado Rwer: Introduction and overview. *Journal of the American Water Resources Association*, 31(5), 779–788. <https://doi.org/10.1111/J.1752-1688.1995.TB03400.X>
- Zhang, C., & Fang, Y. (2020). Application of capital-based approach in the measurement of livelihood sustainability: A case study from the Koshi River basin community in Nepal. *Ecological Indicators*, 116, 106474. <https://doi.org/10.1016/J.ECOLIND.2020.106474>
- Zhong, L., Ma, Y., Salama, M. S., & Su, Z. (2010). Assessment of vegetation dynamics and their response to variations in precipitation and temperature in the Tibetan Plateau. *Climatic Change*, 103(3), 519–535 <https://doi.org/10.1007/s10584->

009-9787-8 .

Zolotokrylin, A. N. (2010). Droughts: Causes, Distribution and consequences. *Natural Disasters*. <https://www.eolss.net/sample-chapters/c01/E4-06-02-01.pdf>

7. ANNEXES

ANNEX 1.1. NDVI Threshold

NDVI Threshold		
S.N.	Vegetation Level	Range
1	No Vegetation	-1 to -0.2
2	Low to Medium	-0.19 to 0.23
3	Medium	0.24 to 0.36
4	Medium to Dense	0.37 to 0.45
5	Very Dense	0.46 to 1

ANNEX 1.2. NDWI Threshold

NDWI Threshold		
S.N.	Water Stress Class	Range
1	Very High Water Stressed	-1 to -0.084
2	High Water Stressed	-0.084 to -0.05
3	Less Water Stressed	-0.05 to 0
4	No Effect	0 to 0.106
5	Normal Condition	0.106 to 0.24
6	Snow I Glacier	0.24 to 1

ANNEX 1.3. NDDI Threshold

NDDI Threshold		
S.N.	Drought Category	Range
1	Water Body I No Drought	-1 to -0
2	Abnormally Dry	0 to 0.1
3	Moderate Dry	0.1 to 0.2
4	Severe Drought	0.2 to 0.3
5	Extreme Drought	0.3 to 0.4
6	Exceptional Drought	0.4-1



A Biophysical Approach to Assess the Risks Associated with Climate Change for Spatial Analysis of Agricultural Drought Vulnerability

Mohammadreza Farzaneh^{1*}, Masoumeh Fakhri², Iman Fazeli-Farsani³, Maryam Najafi-Biragani⁴, Mohammad Abdolhosseini⁵

1. Research Group of Environmental Engineering and Pollution Monitoring, Research Center for Environment and Sustainable Development, RCESD, Department of Environment, Tehran, Iran.
2. Expert member of Agricultural Planning Economic and Rural Development Research Institute (APERDRI), Ministry of Agriculture, Tehran, Iran.
3. Soil Engineering Department, Shahrekord University, Shahrekord, Iran.
4. Water Engineering Department, Arak University, Arak, Iran.
5. Water Engineering Department, Gorgan University of Agricultural Sciences and Natural Resources, Gorgan, Iran.

*Corresponding author. Email: Mrf.farzaneh@rcesd.ac.ir mrf.farzaneh.env@gmail.com

Keywords:

Spatial analysis, Agricultural drought, Vulnerability, Isfahan, Iran.

Abstract

Global warming has led to changes in climate variability and different characteristics of extreme events. Recently, the study of compound extremes, defined as the co-occurrence of multiple events with extreme impacts, has attracted much attention because of their detrimental impacts on society and ecosystems. In countries like Iran with arid and semi-arid climate patterns, inter-annual climate variability causes severe influences on agriculture through compound dry and hot extremes. Such impacts are expected to increase due to climatic changes. Decreasing water availability as a consequence will have a direct impact on agriculture and could endanger socio-economic development and social sustainability in these regions. Assessment of the vulnerability to climate change and its resulting agricultural drought is fundamental for effective adaptation strategies in the future. This paper presents a spatial GIS-based assessment method for agricultural drought vulnerability in current and future climatic conditions in Isfahan Province, Iran, by constructing agricultural drought vulnerability maps. This assessment was conducted by evaluating changes in the severity, duration, and frequency of compound dry and hot extremes. The results expressed the spatio-temporal variability of the empirical probability of drought occurrence, and indicated the relation between the vulnerability of agricultural drought and the characteristics of drought occurrence. The results of the vulnerability assessment can be used to prioritise the counties for the implementation of long-term drought management plans and effective countermeasures, as well as to contribute to sustainable agricultural development.

Received:

13 June 2023

Revised:

24 July 2023

Accepted:

08 December 2023

How to cite this article:

Farzaneh, M., Fakhri, M., Fazeli-Farsani, I., Najafi-Biragani, M., & Abdolhosseini, M. (2024). A Biophysical Approach to Assess the Risks Associated with Climate Change for Spatial Analysis of Agricultural Drought Vulnerability. *Journal of Drought and Climate change Research (JDCR)*, 2(6), 27-56. [10.22077/jdcr.2023.6479.1027](https://doi.org/10.22077/jdcr.2023.6479.1027)



Introduction

The impacts of climate change on people, property, and nature become evident every year through more extreme weather events, including heat waves, droughts, and heavy rainfall (Clarke et al. 2022). The international disaster database, EM-DAT, has recorded 7,348 disaster events worldwide over the past twenty years, which represents a sharp increase in comparison with the previous twenty years. It records major increases in floods, storms, droughts, wildfires, and extreme temperature events (CRED & UNDRR, 2020)

Drought and hot extremes are among the most detrimental extremes, with impacts on agriculture, water availability, energy production, and human health (Mishra and Singh, 2010 ;Deryng et al., 2014 ; Zipper et al., 2016; Añel et al., 2017; Dosio et al., 2018; Hao et al., 2022).

Compound extremes may have lead to amplified impacts than individual extremes (or events) and have received increasing attention in the past decade (Hao et al., 2018).

A definition of the compound event (extreme) is given by the Intergovernmental Panel on Climate Change (IPCC) Special Report on Climate Extremes (SREX) in 2012 (Seneviratne et al., 2012): (1) two or more extreme events occurring simultaneously or successively, (2) combinations of extreme events with underlying conditions that amplify the impact of the events, or (3) combinations of events that are not themselves extremes but lead to an extreme event or impact when combined.

Right now, Iran is experiencing the most crucial negative impacts of climate change, due to its location at low latitude. Drought, as one of the most critical global hazards, is threatening the sustainable

agriculture and food security of nations. To provide food security and to minimize the negative impacts of climate change, following adaptation strategies would be essential. The assessment of the variability of drought and hot extreme characteristics provides useful information for the mitigation of extremes under global warming, but a more prior step could be the assessment of vulnerability to agricultural drought. The results of this task would make it possible to compare regions based on their vulnerability levels and identify the most vulnerable areas. Exploring drought characteristics from the vulnerability point of view leads to consideration of underlying conditions that can exacerbate impacts, and refers to the compound event definition. Likewise, it is necessary to explore the causes of vulnerability. Measuring agricultural drought vulnerability is essential for targeting interventions to improve and sustain agricultural performance for both rainfed and irrigated cultivation.

Most of the previous efforts in drought research in Iran have explored the nature of drought in terms of its characteristics (Zamani Nouri et al., 2015), duration of wet and dry periods (Fakhri et al., 2013), and different types of drought phenomena (Rostamian et al., 2013). Nevertheless, drought vulnerability is rarely assessed in Iran. Various authors from different countries have considered vulnerability as a key issue and explored the negative consequences of drought through the perspective of communities and sectors' vulnerability (Lures et al., 2003; Wilhelmi and Wilhite, 2002; Murthy et al., 2015; Jayanthi et al., 2013; Wu et al., 2011; Zhang et al., 2015; Wang et al., 2019; Tigkas et al., 2019). However, vulnerability is a dynamic process, changing on a variety of inter-linked temporal and spatial scales.

Detecting the impacts of climate change and evaluating vulnerability have a high level of priority in a growing population to provide food security countermeasures. As a step forward in this concern, some researchers have used the vulnerability to climate change through the projection of the future to emphasise the outcome of a system facing unfavourable disturbances or disasters (Cutter et al., 2003; Thirumalaivasan et al., 2003; Metzger et al., 2005; Calvo, 2008; Ravindranath et al., 2011; Zhang et al., 2019; Fazeli Farsani et al., 2019). But a crucial issue that has received less attention is the existence of uncertainty sources, especially, the uncertainty triggered by the differences between the 4th and the 5th assessment reports of the Intergovernmental Panel on Climate Change (IPCC).

Climate change researches and Projected climatic conditions (Fakkhar and Nazari, 2014, Farzaneh et al. 2024, Farzaneh and Banimostafaarab, 2023a, Farzaneh and Banimostafaarab, 2023b, Hamzeh et al. 2023a, Hamzeh et al. 2023b, HosseinSeddighi and Jalali, 2024, Rezaeei and Roshani, 2024) will have direct impacts on the agriculture sector and could endanger socio-economic development and social sustainability in different places, such as Isfahan province in central Iran, where agriculture is the primary occupation and means of subsistence for a large part of the population. In this study, a spatial analysis of agricultural drought vulnerability analysis for current and projected future climate conditions was conducted at representative sites of Isfahan province counties to depict the circumstances of drought events for current and future time horizons. Furthermore, the differences in projected conditions arising from IPCC recommendations in the 4th and 5th assessment reports were

analysed. From a theoretical point of view, the developed appropriate framework can be useful to recognise the spatial distribution of vulnerability and thus, can help in policy design, as understanding the vulnerability of a sector and its spatial distribution will orient policies towards a geographical area or population group with urgent requirements (UNDP, 2010; Ortega-Guacin et al., 2021; Ekrami et al., 2021).

Material and Methods

1. Study Area

This study is conducted in Isfahan province, located in central Iran, which covers a total area of 107045 km². The climatic pattern of the study area is arid and semi-arid. While the eastern part of the province is on the western margin of the arid and semi-arid zones of Iran, its western areas lie on the eastern hillslopes of the Zagros mountains. The mean annual temperature is 13.6 °C, and its annual amount of precipitation is about 160 mm. The amount of annual rainfall varies from 800 mm in the western region to 75 mm in the eastern part. The impact of drought in lower regions of the study area, where the amount of annual rainfall shows significant variability, can be widespread and affect various sectors like agriculture.

In this study, the precipitation records from 30 years (1975-2005) were selected to calculate the SPI index for the study area. The methodology of the study is based on extracted data and the investigation of characteristics considering uncertainty analysis, as illustrated in Fig 1.

2. Understanding the vulnerability concept

Vulnerability links with some ideas such as resilience, marginality, susceptibility, adaptability, fragility, and risk. Currently,

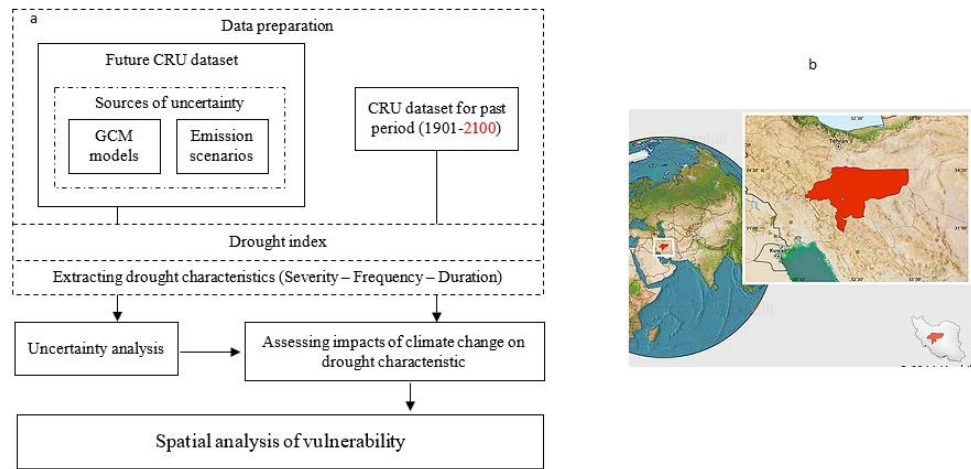


Fig 1. The methodology(a) and study area(b)

vulnerability is used in climate change research to emphasise the result of a system facing unfavourable disturbances or disasters. The literature on vulnerability has two major perspectives: the biophysical perspective and the social one. In the biophysical approach, the focus is predominantly on the event itself, in terms of magnitude, frequency, rapidity of onset, and spatial distribution. In contrast, the social perspective focuses primarily on the human determinants or drivers of

vulnerability, namely, the social, political, and economic conditions that make exposure unsafe or challenging.

3. Quantifying vulnerability

In this research, the vulnerability of the agricultural system in Isfahan province is explored from a biophysical perspective. The conceptual model for the vulnerability of the community to climate change is outlined here as follows:

$$\text{Agricultural drought vulnerability} = \frac{\text{Drought characteristic} \times \text{Agricultural area of each county}}{\text{The total area of each county}} \quad (1)$$

4. Preparing data

In this study, the downscaled CRU dataset at a 0.5° grid resolution was used. Rainfall data of the past 100 years and the data of the future period were extracted from CRU under uncertainties induced from HadCM3, PCM, ECHAM, CGCM, and CCSIRO general circulation models (GCMs) as well as A1, A2, B1, and B2 emission scenarios.

5. Calibration and validation

As it can be seen in Fig. 2, drought characteristics in Isfahan station were extracted primarily based on observed

rainfall data and then based on CRU rainfall data for both calibration and validation. The results were evaluated using the Nash-Sutcliffe efficiency index.

$$E = 1 - \frac{\sum_{i=1}^n (P_i - O_i)^2}{\sum_{i=1}^n (O_i - \bar{O})^2} \quad (2)$$

where P_i is the amount of rainfall calculated by GCMs; O_i is the observed rainfall value; \bar{O} is the number of samples; and \bar{O} is the average of observed values.

The Nash-Sutcliffe efficiency index varies in the range of $(-\infty, 1)$ and the models with values higher than 0.5 are acceptable.

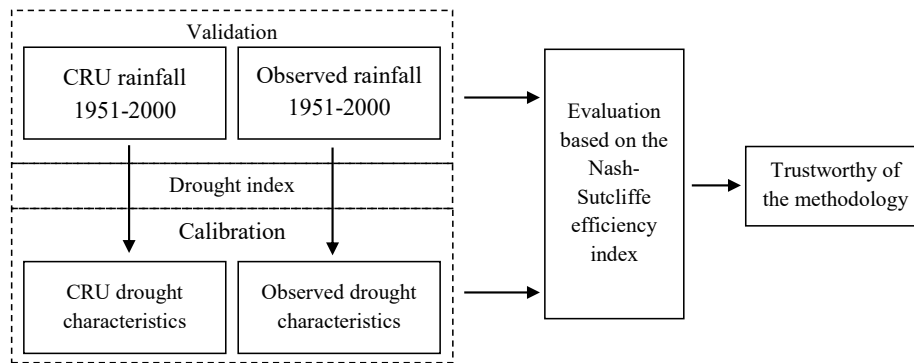


Fig 2. Procedural framework for calibration and validation

6. Drought monitoring

In this research, drought analysis was carried out using the standardised precipitation index (SPI). McKee et al. (1993) developed SPI for the identification and monitoring of droughts through recorded precipitation data. Different time scales (1, 3, 6, 12, 24 and 48-months) can be used to compute the SPI index; the longer time scales relate to hydrological drought while, the shorter ones may represent agricultural drought. Although SPI is more suited to monitoring meteorological and hydrological droughts than agricultural droughts, it is flexible enough to inform on some aspects of agricultural droughts. Due to its simplicity of calculations, decent reliability, and ability to address a variety of drought-

related issues, and because it just needs rainfall data as input, it is a popular index for monitoring different kinds of drought. Essentially, SPI is the standard deviation index of a given precipitation deficiency. Positive SPI values indicate higher than median precipitations, and negative values indicate less than median ones. Its values are generally between ± 2.0 . Table 1 shows the SPI thresholds defined by McKee et al. (1993). A drought event starts when the SPI values are continuously negative and reach an intensity of -1.0. The drought event ends when the SPI values return to positive. Based on normalised SPI values, an event is considered normal, moderate, severe, or extreme.

Table 1. SPI drought severity classes for wet and dry periods

SPI Classes	SPI Value
Extremely wet	> 2
Severely wet	1.5 - 1.99
Moderately wet	1 - 1.49
Normal	-0.99 - 0.99
Moderately dry	-1.49 - -1
Severely dry	-1.99 - -1.5
Extremely dry	< -2

The computation of SPI is conducted using a software programme developed at the University of Nebraska and downloadable from the website of the

National Drought Mitigation Center which provides comprehensive information and a complete formulation for SPI calculation. The SPI in each time scale is the difference

between precipitation on the time series (X_i) and the mean value \bar{X} , divided by the standard deviation (S):

$$SPI = \frac{x_i - \bar{x}}{s} \quad (3)$$

It quantifies observed precipitation as a standardised departure from a selected probability distribution function that models the precipitation data. The precipitation data are typically fitted to a gamma or Pearson Type III distribution or applied to a rank-based non-parametric method to find their empirical cumulative probabilities and then transformed to a normal distribution.

The severity and duration of SPI were evaluated using 30 years of monthly rainfall data from 22 stations in arid and semi-arid regions of Isfahan province, Iran. Drought characteristics, including severity, duration, and frequency, identified based on SPI at a 3-month time scale, were used as indicators of exposure to drought for different counties in the study area. The selection of the 3-month time scale was due to the importance of agricultural drought in the study area.

7. The uncertainty analysis

Emission scenarios and GCMs are among the most important sources of uncertainty in climate change studies. Creating the probable decision space for the future requires using an efficient method of uncertainty analysis. On the other hand, samples should be excellent examples of the target community. For this purpose, the bootstrap technique was applied to estimate the confidence interval (Fakhri et al., 2014). Using this method, drought characteristics for the future period were estimated at a 95% confidence level. The drought characteristics, including frequency, severity, and duration, were

investigated using linear correlation for the past-time horizon and also for the future period, through analysing the uncertainty band arising from agreement and disagreement between models.

Result and Discussion

Some constraints limit the investigation of the drought index. The first one is the lack of observed data, as well as the non-regular data distribution in some stations. The second problem is the short-term recorded dataset, which can lead to a lack of consideration of extreme events compared to the long-term return period. In this regard, we attempt to provide a methodology for regions without recorded hydrological data and also for regions with a short period that is capable of investigating climatic change scenarios for the future. In the first step, the drought severity, frequency, and duration characteristics were calculated for the past period from the SPI index for each county. The calibration and validation processes were conducted next. As agriculture is among the first sectors to experience economic damage from exposure to drought, the agricultural drought vulnerability for each county was calculated at the next step based on the model presented in Section 2.4. Finally, the expected effects of climate change on counties' agricultural drought vulnerability were assessed based on the projected climatic variability for the future period.

1. The results of SPI index

Fig. 3 shows the efficiency of the SPI index in the estimation of the drought events that occurred in 2000, 2008, and 2010. As the only input variable for the SPI index is rainfall, the annual and monthly changes in rainfall were investigated more precisely to provide a better understanding

of the study area (Fig. 4). The minimum and maximum amounts of annual rainfall are 40 mm and 349 mm, respectively. The fluctuation of rainfall is considerable in the yearly time series and shows a significant reducing trend with respect to time in such a way that the amount of long-term average rainfall for this station is 123 mm. Monthly precipitation also shows severe fluctuations during different seasons. The highest amount was in March with 22 mm, and the lowest was in September with near zero value. The presented monthly and annual fluctuations are two important indicators, indicating the extreme vulnerability of the region to drought.

2. Spatial analysis of drought characteristics

In this study, the occurrence of drought was

investigated based on severity, duration, and frequency characteristics over a 3-month timescale. The resulting SPI values at corresponding drought categories were mapped for each county, for drought severity, duration, and frequency per year in Isfahan province using the inverse distance weighting (IDW) interpolation method in Arc GIS. The IDW method was chosen for all data interpolation processes as it provides a reasonable level of accuracy in data prediction and is much less time-consuming in comparison to other interpolation methods, such as Kriging. Fig. 5 shows the severity, duration, and frequency characteristics of drought for each county.

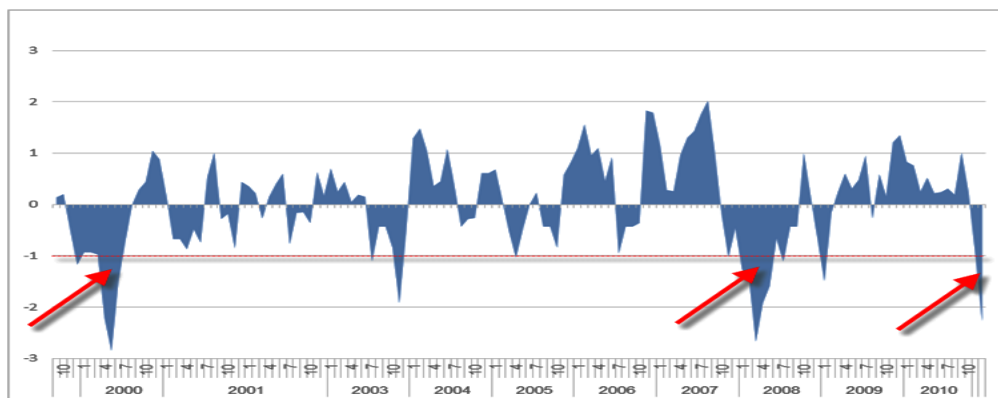


Fig 3. Description of past drought events in Isfahan province based on SPI index

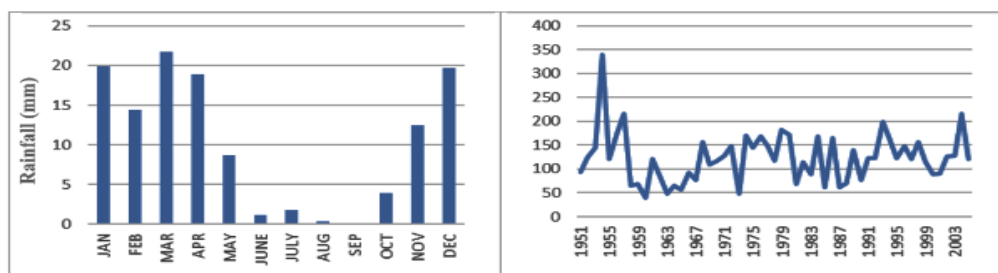


Fig 4. The annual and monthly time series of rainfall in Isfahan synoptic station

As presented in Fig (5), the distributions of characteristics show variability. The counties that are most affected by drought severity are located in the western zone (such as Fereydown Shahr, Chadegan, and

Najafabad), while the least affected ones are in the east. The spatial analysis of drought duration indicates that eastern counties, a part of north and south (especially in Naeen, Semirrom, Kashan, and Aran-va-

Bidgol) have experienced the longest drought duration, while the central region has faced the shortest (Fig. 5). By jointly looking at both characteristics, the severity and duration of the drought are affecting the majority of counties, such as Kashan, Aran-va-Bidgol, and Semirrom. Northern and western regions (Kashan, Barkhar-va-Meimeh and Fereydan) have

more frequent droughts than other areas, and Natanz and the west of Ardestan counties have less. Generally speaking, the drought frequency is lower in the east of the study area.

Since the drought damage differs between counties, the comparison of vulnerability should be undertaken at the level of counties.

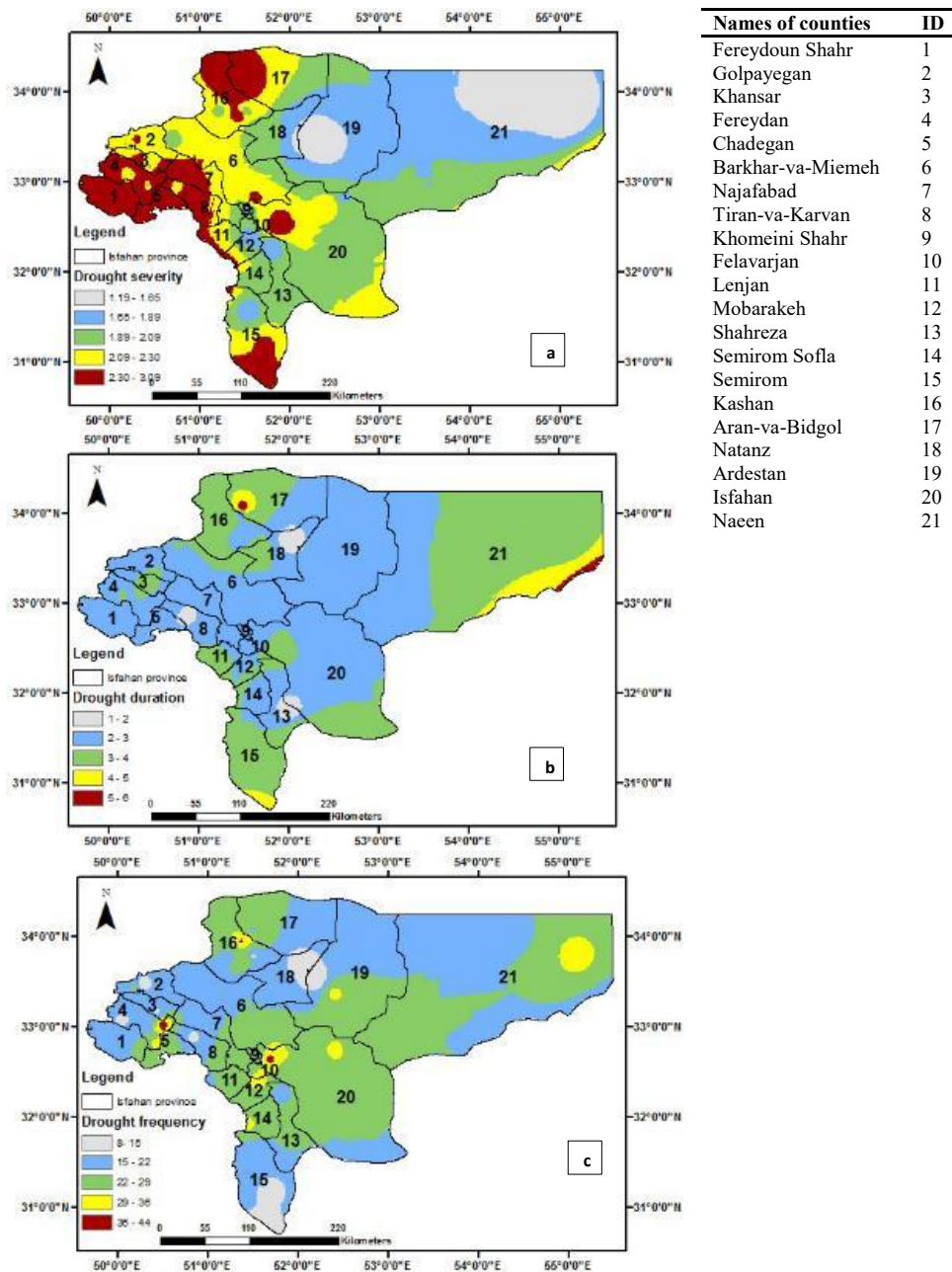


Fig 5. Drought (a) severity, (b) duration, and (c) frequency per year in Isfahan province, Iran

3. Calculating agricultural vulnerability

Exposure maps for intensity, frequency, and severity characteristics of drought were extracted based on observed data. Then, by considering the ratio between total land and agricultural area, the agricultural drought vulnerability for each county was evaluated based on the vulnerability model presented in

Eq. 1.

Fig (6) shows the vulnerability to drought in different counties. Though considering total area, drought vulnerability differs for each characteristic, showing more homogeneity for only agricultural areas. The vulnerability of agriculture to drought in the counties of Isfahan and Barkhar-va-Meimeh was as its maximum (Black line),

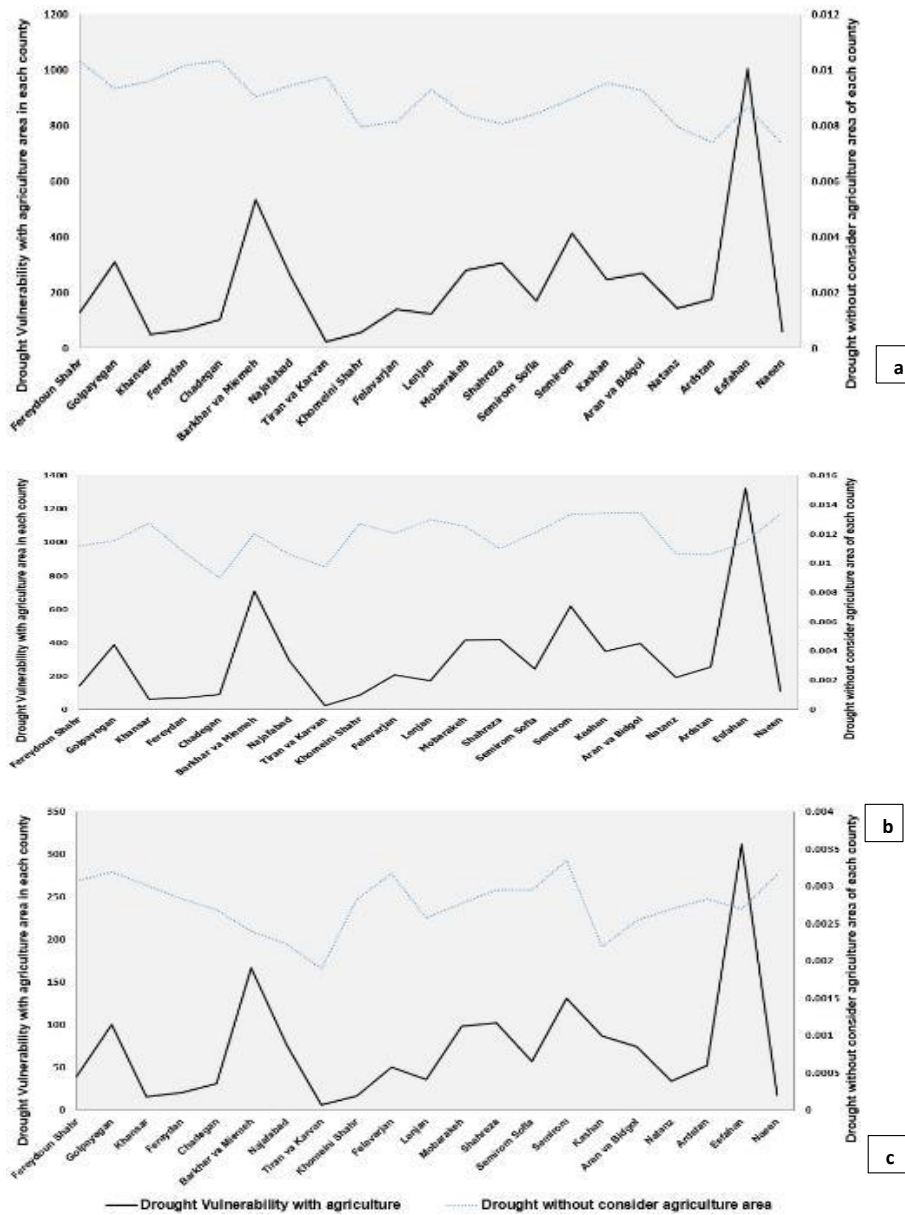


Fig 6. Drought vulnerability of (a) severity, (b) duration, and (c) frequency with and without considering agriculture in each county

while these counties in the total area have a low vulnerability (Fig 6). It is evident that when the agriculture area of each county is applied, the trend of drought will change. Moreover, while some counties have less total area, they have more agricultural areas, in contrast to some other counties with more total area and fewer agricultural areas. In these counties (such as Tiran-va-Karvan, Khomeini-Shahr, and Naeen), the agricultural area can have a significant impact on drought vulnerability.

In counties of Isfahan province, by the heppening of drought in a county with more agricultural areas and gardens, people in the center, west and south are more faced with damages (Fig. 1) and this circumstance is more critical for counties that have lessened areas, such as Khomeini Shahr and Felavarjan. Exposure with damages means that people who live in agricultural areas will gradually abandon agriculture and turn to other careers. In occupations in the west and south, agriculture is a popular job for people and thus, during drought, it has more vulnerability. In Felavarjan county, people are employed in agriculture and gardening, and after Khomeini Shahr, this county is the smallest town in this matter. Likewise,

farmers in Isfahan and Felavarjan counties are cultivating rice, which requires plenty of water to grow, and the drought events in the past years have caused a considerable reduction in its production. Therefore, these counties are much more sensitive to drought than other areas.

4. Calibration, validation, and uncertainty analysis of the CRU data based on observation data

In this study, 50 grids of CRU data with a 0.5-degree resolution for Isfahan province were used. For calibration, the CRU data were analysed based on observation data at the Isfahan station. The accuracy of the proposed methodology was evaluated using an observational and simulated rainfall performance evaluation over a 50-year-long period at Isfahan station. The results, presented in Table 2, indicate acceptable accuracy in May to excellent accuracy in June. Regarding CRU acceptable calibration results at Isfahan station, at the stage of validation, the vulnerability of agricultural drought characteristics was considered for each county using observation and CRU data for a common period of 1951 to 2005, and then the results were normalised.

Table 2. The result of Nash-Sutcliffe efficiency index for the validation period

Jan	Feb	Mar	Apr	May	Jun	Jul	Aug	Sep	Oct	Nov	Dec
0.97	0.82	0.87	0.91	0.50	0.99	0.85	0.63	0.98	0.73	0.93	0.89

Fig (7) shows the results of validation as well as the uncertainty band for each county. Regarding Fig. (7), the uncertainty of agricultural drought vulnerability is different between counties. The highest uncertainty is related to Felavarjan, Mobarakeh, Esfahan, and Ardestan, due to the high level of farming area in these

counties. The lowest uncertainty was related to Khansar, Fereydan and Tiran-va-Karvan. Furthermore, the most significant difference between observed data and the 95 PPU band, was found in Isfahan and Barkhar-va-Meimeh, and the lowest difference was related to Fereydan and Tiran-va-Karvan, respectively.

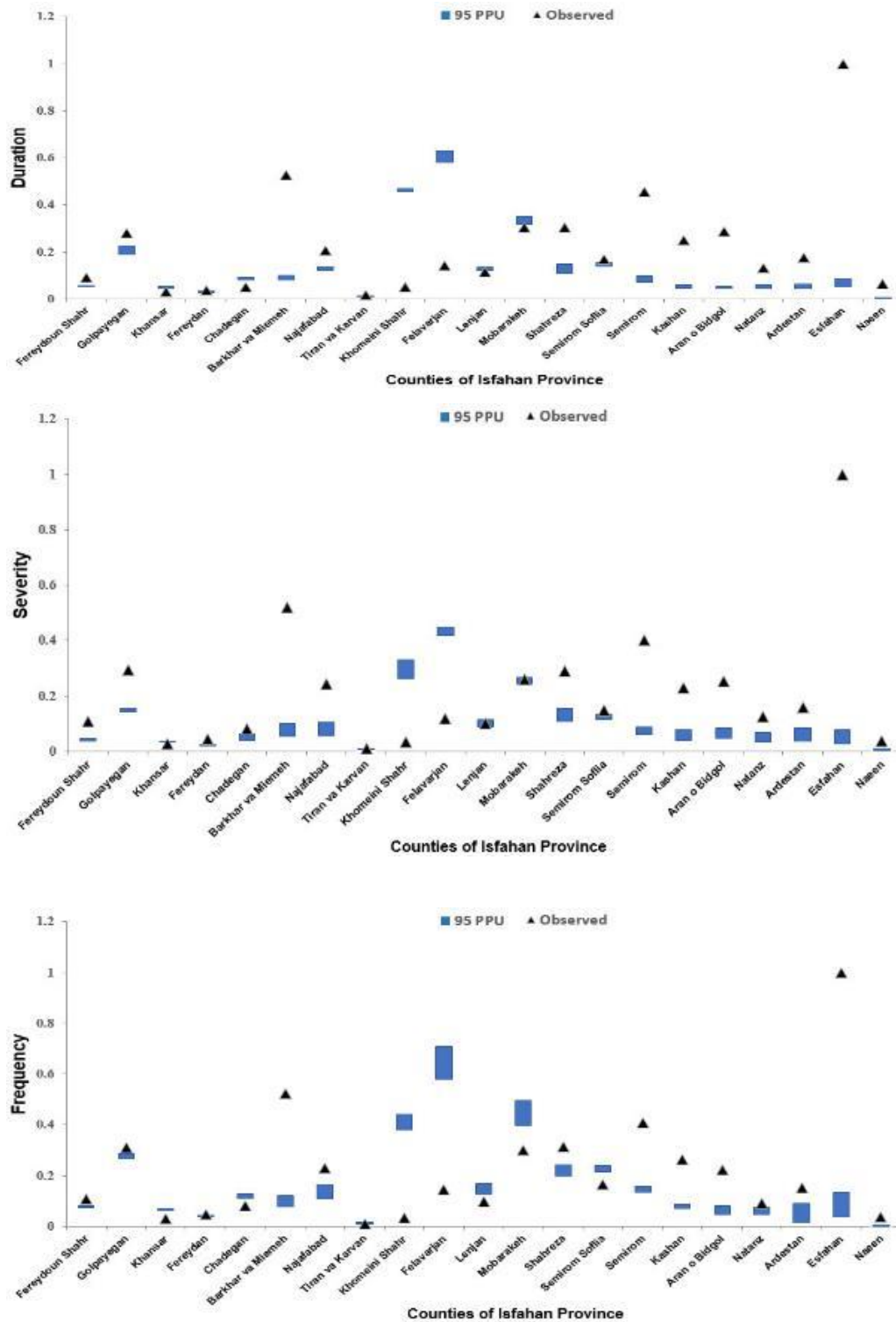


Fig 7. Comparison of 95PPU ranges of drought vulnerability of severity (a), duration (b) and frequently (c) characteristics in counties, with CRU data for the period of 1951–2005 (In these figures, blue band is the range of CRU)

5. Effects of climate change on drought characteristics in the future period

Results with a value higher than 0.5 for the Nash-Sutcliffe efficiency index (in the calibration and validation) approve the effectiveness of the proposed methodology. To be able to take into account events with long return periods, the duration of the statistical period was extended to a long period of 100 years. Drought characteristics based on CRU data for the twentieth century were calculated. These characteristics were assessed for the twenty-first century under different sources of uncertainty due to emission scenarios

and AOGCM models.

Fig. 8a shows the impact of climate change on drought severity. The A1 emission scenario, representative of the most critical condition for all GCM models, shows an increase in drought intensity. Some models represent a considerable difference, and some of them are more close to the result of the past period. Other scenarios have shown a decreasing trend in the incidence of drought intensity, and meanwhile, the most optimistic intensity is projected to occur under the B1 scenario.

Fig. 8b shows the impact of climate change on drought duration. The results presented

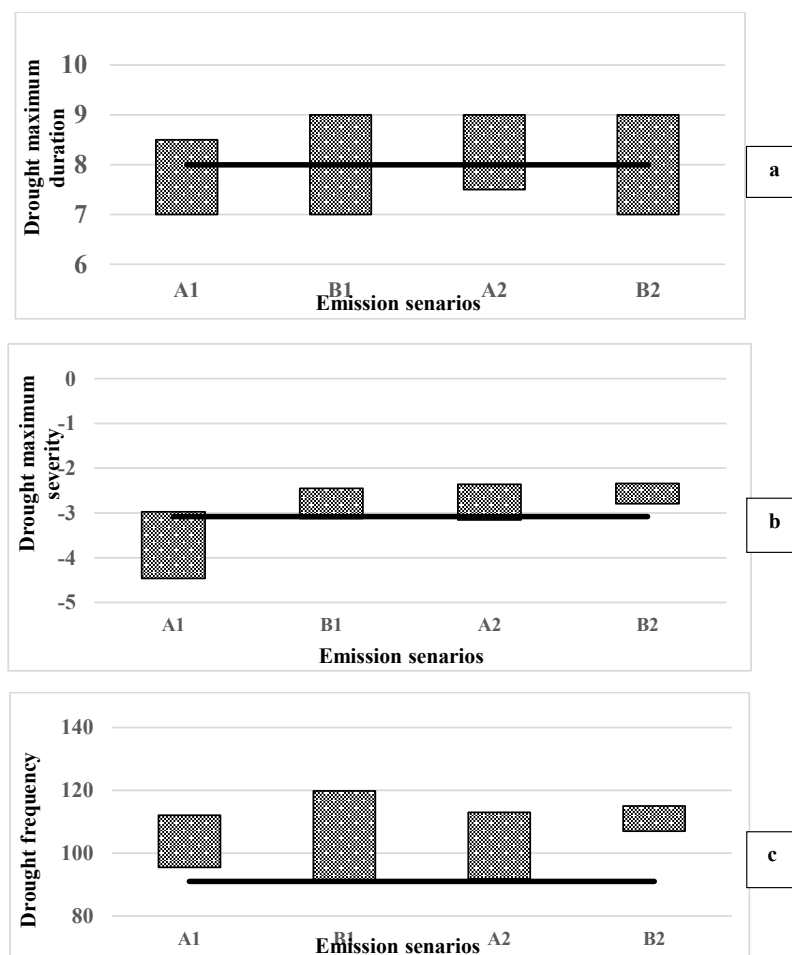


Fig 8. Assessment of drought duration, severity, and frequency characteristics under climate change

in this figure show disagreement between the results of different models in terms of projected drought duration. The most disagreement was related to B1, and B2 scenarios, and the lowest was observed in the group with an emission scenario.

Fig. 8c indicates that all four scenarios are projecting an increasing trend for drought frequency characteristics in the future period. B1 and B2 scenarios show the widest and thinnest ranges of uncertainty bands, respectively. Although the uncertainty of the B2 scenario is less than that of other scenarios, its considerable difference from the observed values of the past period implies the criticality of the condition from the perspective of this scenario. All models have consensus in this respect.

6. Agricultural drought vulnerability under the effects of climate change in the future period

In this section, the vulnerability of the agriculture sector was investigated under the effect of climate change under different emission scenarios, related to the fourth and fifth assessment reports of the IPCC. The first step is to investigate the spatial distribution of drought characteristics, including intensity, duration, and frequency under A1, A2, B1, and B2 emission scenarios of the IPCC 4th assessment report. Investigation of these characteristics under 2.6, 4.5, 6.0, and 8.5 scenarios of the 5th assessment report is the next step. Then, the Bootstrap method was applied for both a 2.5% and 97.5% confidence interval to investigate the drought intensity, duration, and frequency characteristics for the future period and their spatial distribution in the province. The uncertainty band, along with historic base values, was calculated to investigate each characteristic at the county level. Figures 15 to 18 show the results.

6.1. Spatial analysis of agricultural drought vulnerability under the effects of climate change, according to AR4

Figures 9 to 11 represent the spatial distribution of duration, frequency, and intensity characteristics of drought for the base period and also under the effect of climate change considering A1, A2, B1, and B2 emission scenarios, at a confidence band of both 2.5% and 97.5%.

Fig. 9 shows that in the eastern part of the province, the duration of drought will increase under the effect of climate change at 97.5% confidence interval level; the most pessimistic scenarios are related to B1, and the most optimistic are related to A2 at 2.5% confidence interval level; all scenarios show an increase in drought duration for eastern counties, and also a decrease for western counties. According to Fig. 10, the probable effect of climate change in all emission scenarios, will cause an increasing trend in drought frequency, in the northeastern and southern parts. The maximum frequency is projected for the central part; the most pessimistic scenarios are related to the A2 emission scenario at the level of 97.5%, and the most optimistic scenario is related to the B1 scenario at the 2.5% confidence interval level. For both 2.5% and 97.5% confidence interval levels, the frequency of drought is projected to undergo a decreasing trend under the effect of climate change.

Fig. 11 shows the severity of droughts under the effect of climate change, based on emission scenarios for AR4. It can be seen that in all scenarios, the severity of drought events will increase. In general, for all scenarios, the drought severity will increase in the eastern part of the province, while the western part of the province will experience a decreasing trend.

6.2. Spatial analysis of agricultural drought vulnerability under the effect of climate change, according to the fifth assessment report

Based on this assumption that the uncertainties in the fifth assessment report have been reduced, the drought characteristics of frequency, severity, and intensity were also analysed based on the fifth assessment report of the IPCC.

Fig. 12 shows the spatial distribution of agricultural drought vulnerability based on drought duration for the AR5 scenario at a level of 2.5 % and a 97.5 % confidence interval. The most pessimistic projection is related to the 2.6 emission scenario at the level of 97.5 %, and the most optimistic one is related to the 2.6 emission scenario at the level of a 2.5% confidence interval. In contrast to the results of the fourth report, the results extracted based on the fifth report, suggest that the northern and west-northern parts of the province will be affected by the duration characteristic, more than the eastern part.

Fig. 13 shows the spatial distribution of agricultural drought vulnerability under climate change, based on the frequency of drought for AR5 scenarios at 2.5% and 97.5% confidence intervals. The most pessimistic scenario is related to the 2.6 emission scenario at the level of 97.5%, and the most optimistic one is related to the 4.5 emission scenario at the 2.5% confidence interval level. In contrast to the results suggested by AR4, results based on AR5 suggest that western parts of the province will be affected by the frequency characteristic more than the eastern part.

Fig. 14 shows the spatial distribution of agricultural drought vulnerability based on drought severity for the AR5 scenario at 2.5% and 97.5% confidence intervals. The most pessimistic scenario is related to the 2.6 emission scenario at the level of

97.5%, and the most optimistic scenario is related to the 4.5 and 2.6 scenarios at the 2.5% confidence interval level. Based on this characteristic, the western parts of the province will be exposed to more frequent drought events, and these parts of the province will be more vulnerable in comparison to the base period. These results have a significant difference from the results derived from AR4.

6.3. Uncertainty bound of agricultural drought vulnerability for each county under the effects of climate change based on the fourth report

Figs. 15 and 16 show uncertainty bounds for agricultural drought vulnerability related to drought characteristics of intensity, duration, and frequency under the effect of climate change for A1, A2, B1, and B2 emission scenarios based on AR4 for each county of Isfahan province. The most uncertainty in all three characteristics and all emission scenarios in terms of agricultural drought vulnerability is related to Isfahan and then Barkhar-va-Meimeh. The maximum numerical value in terms of drought severity and duration was also observed in these counties. Tiran-va-Karvan counties show the lowest agricultural drought vulnerability based on all three drought characteristics.

In some counties, the future uncertainty bound for drought severity, frequency, and duration is greater than the historical average. In contrast, some counties show a lower value. But, for most counties, the duration is within the uncertainty bound range. As can be seen in Figs. 15 and 16, the most significant difference in uncertainty bound associated with the base and future periods, is related to the severity characteristic. Regarding emission scenarios, the B2 scenario shows the lowest uncertainty bound for all drought characteristics.

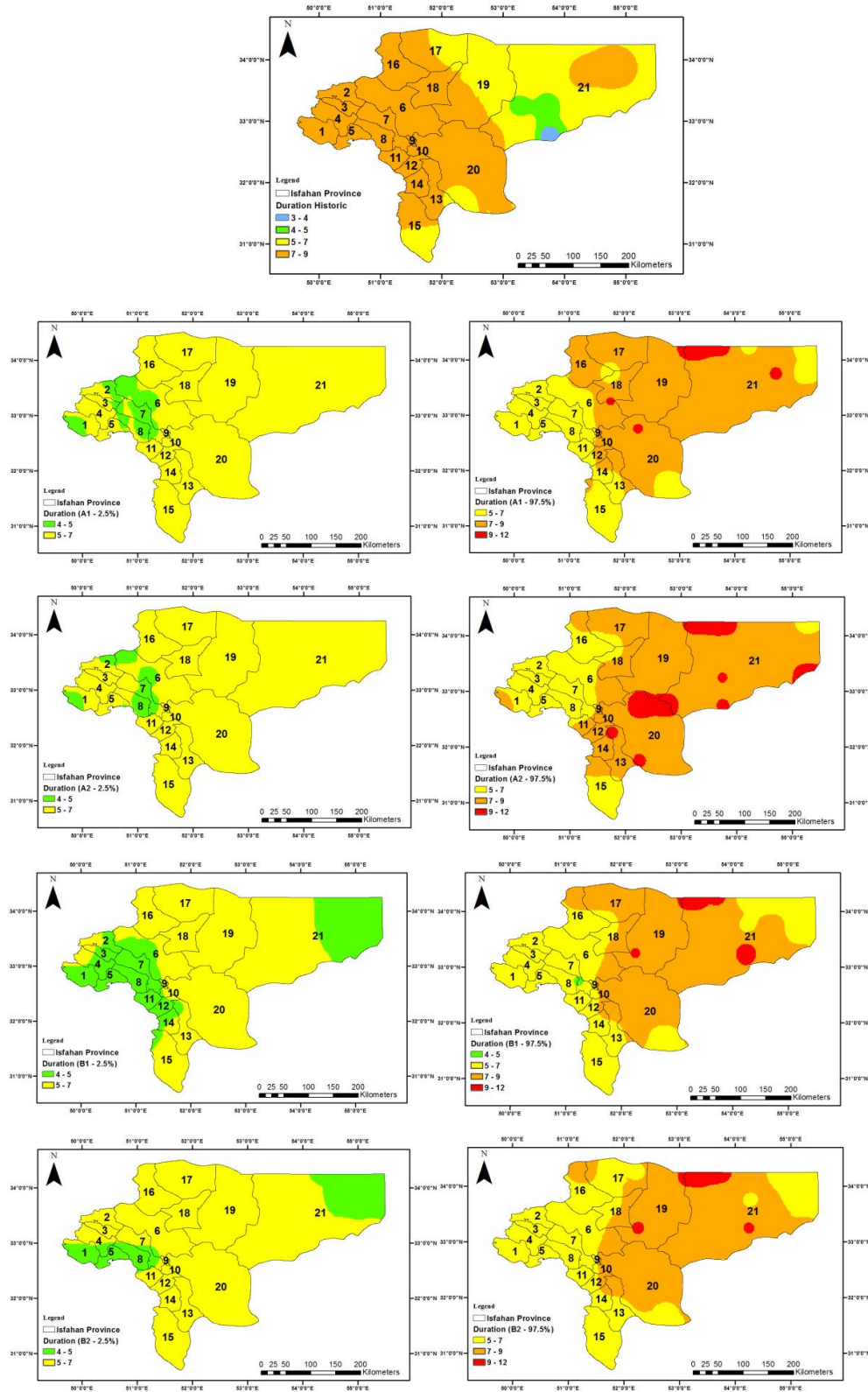


Fig 9. Assessment of drought duration under the effect of climate change based on AR4 report (A1 – 2.5% means A1 scenario in 2.5% uncertainty level)

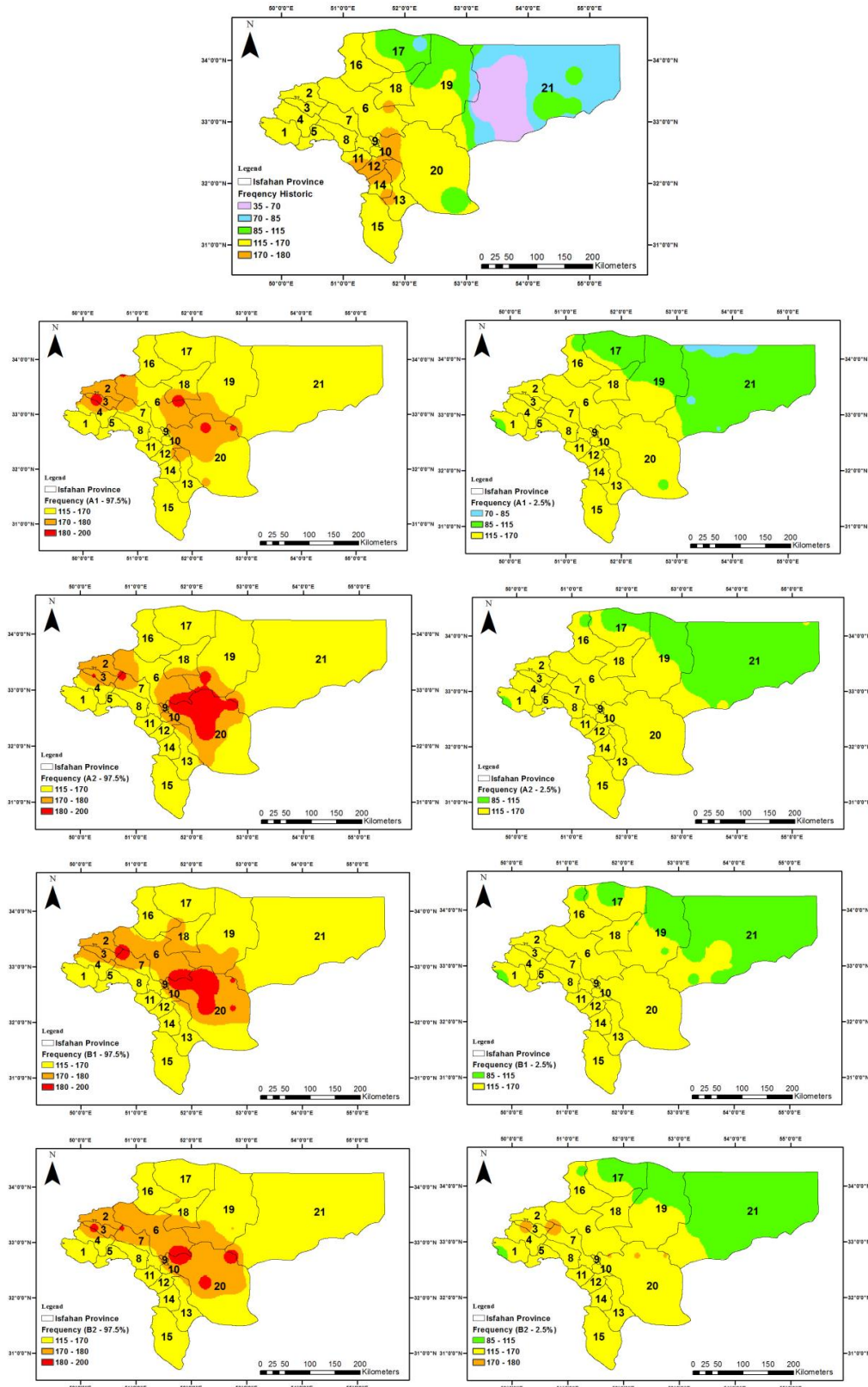


Fig 10. Assessment of drought frequency under the effect of climate change based on AR4 report

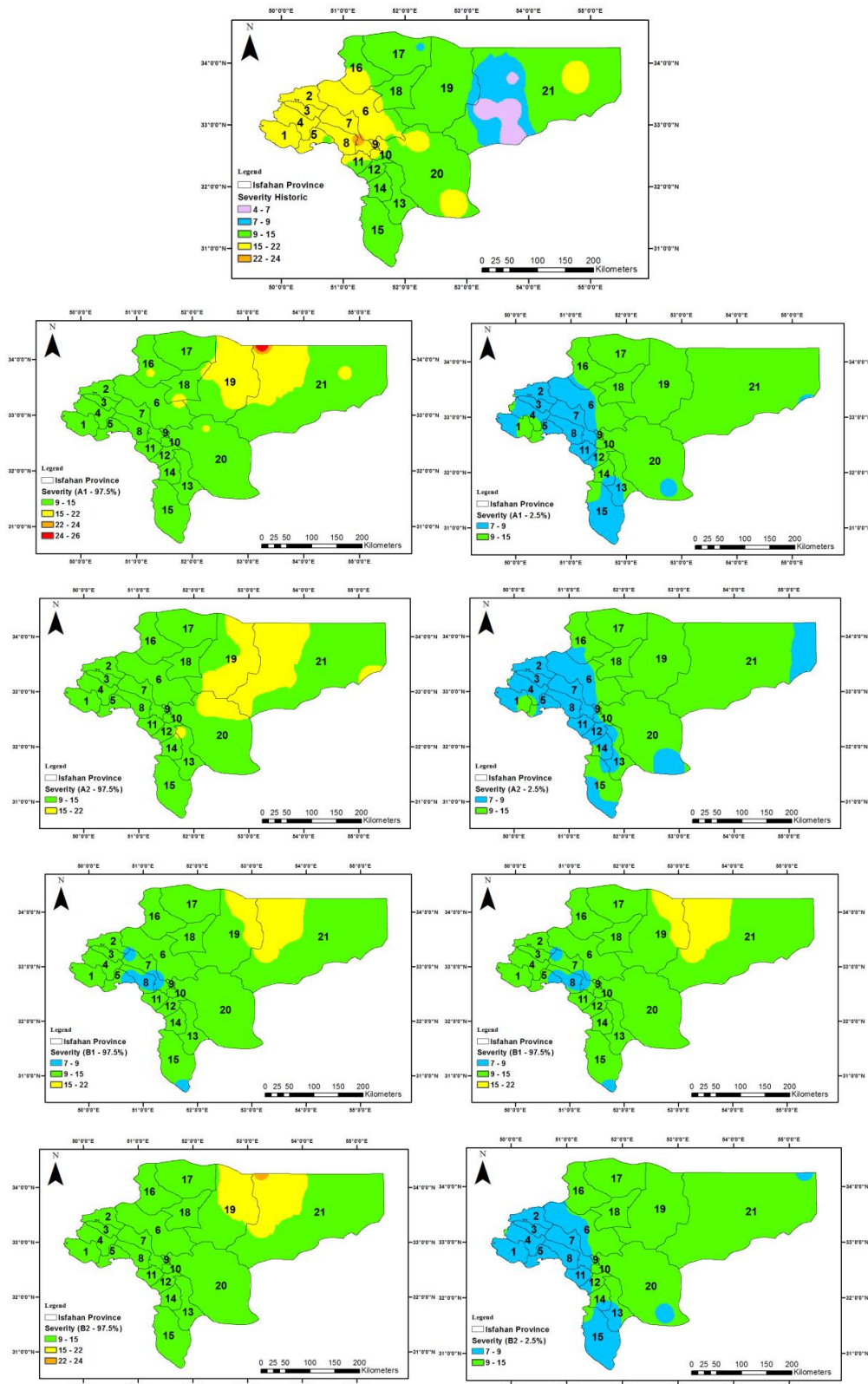


Fig 11. Assessment of drought severity under the effect of climate change based on AR4 report

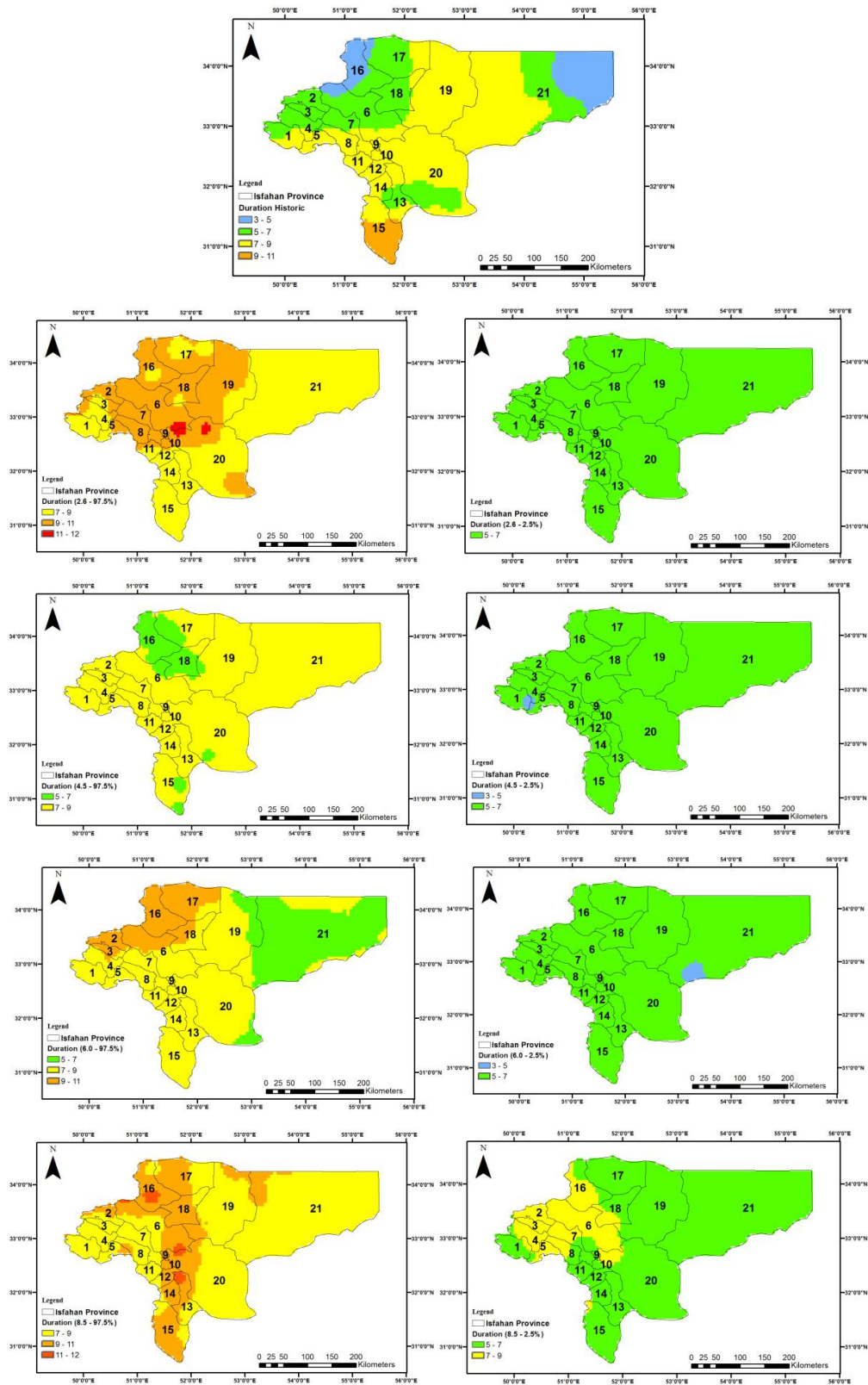


Fig 12. Assessment of drought duration under the effect of climate change based on AR5 report

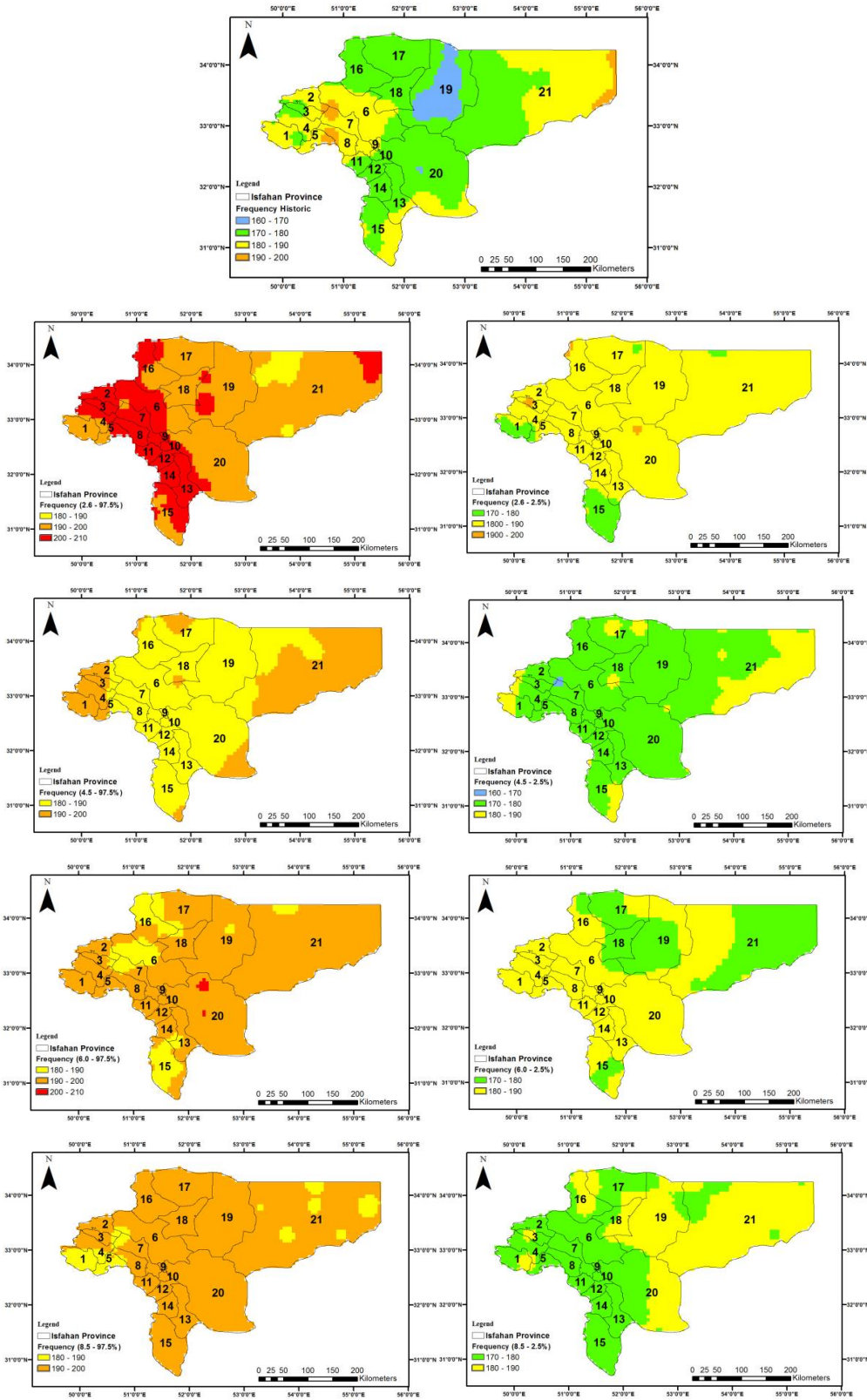


Fig 13. Assessment of drought frequency under the effect of climate change based on AR5 report

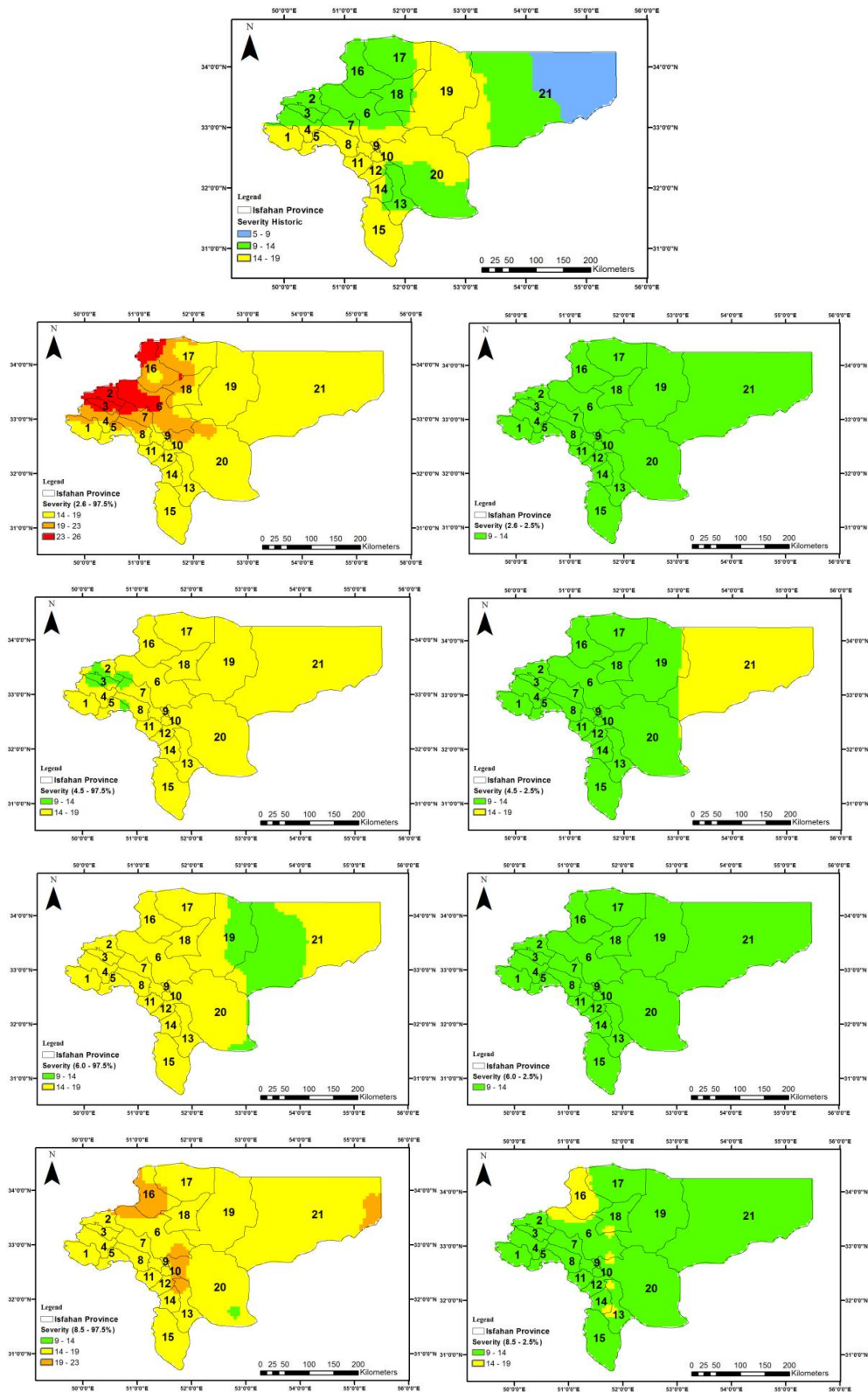


Fig 14. Assessment of drought severity under the effect of climatic change condition, based on AR5 report

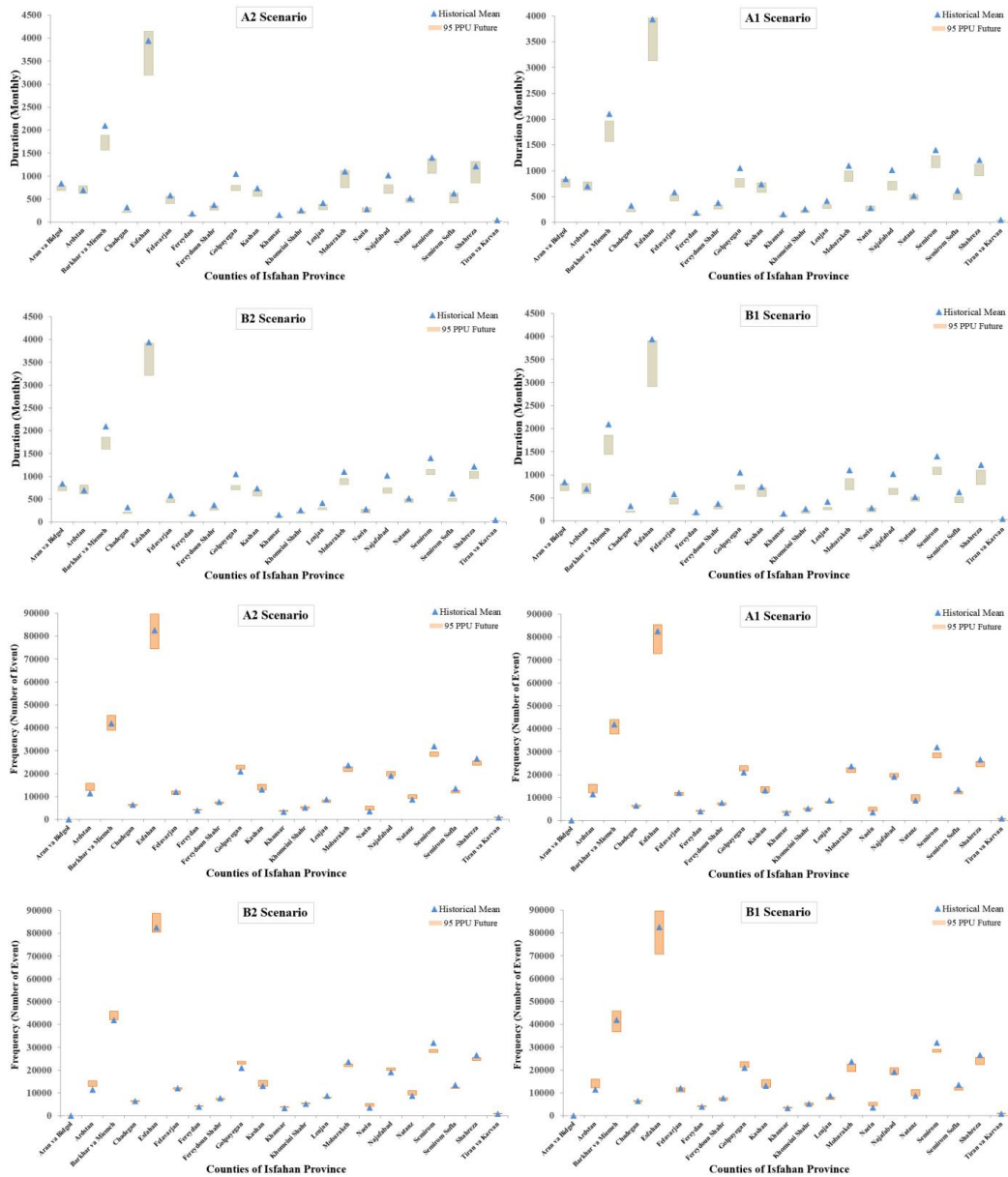


Fig 15. Comparison of 95PPU ranges of drought vulnerability for duration and frequently characteristics under the effect of climate change with AR4 emission scenarios in Isfahan counties

6.4. Uncertainty bound of agricultural drought vulnerability for each county, under the effects of climate change based on AR5 Figs. 17 and 18 show uncertainty bounds for drought characteristics of intensity, duration, and frequency, under the effect of climate change for emission scenarios of 2.6, 4.5, 6, and 8.5 based on AR5 for each county of Isfahan province. As the results

from AR4, the most uncertainty in all three characteristics and all emission scenarios is related to Isfahan and then Barkhar-va-Meimeh. Maximum numerical values in terms of drought severity and duration were also observed in these two counties. Tiran-va-Karvan county shows the lowest agricultural drought vulnerability based on all three drought characteristics.

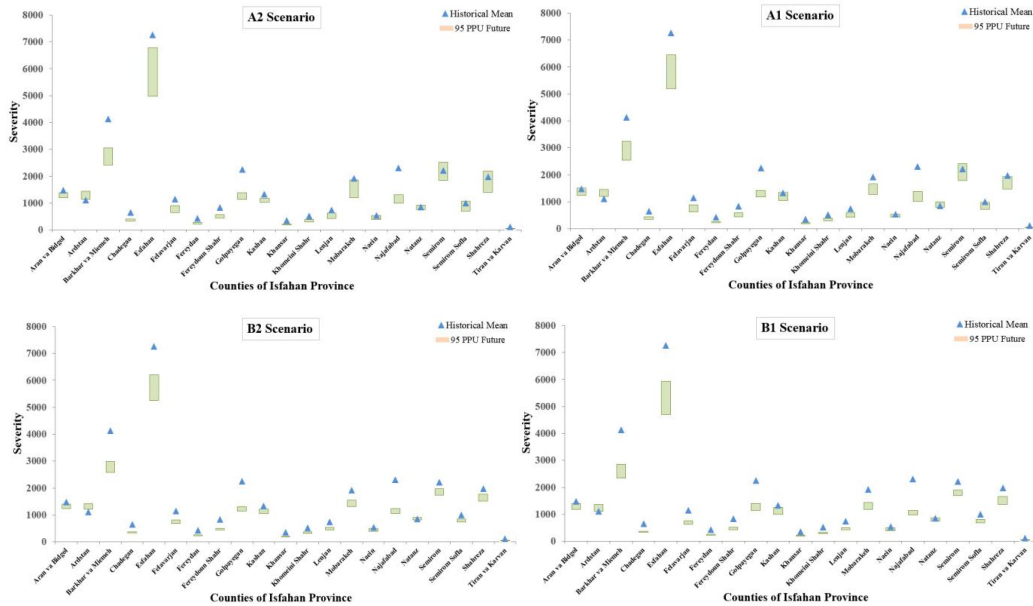


Fig 16. Comparison of 95PPU ranges of drought vulnerability for severity characteristic under the effect of climate change with AR4 emission scenarios in Isfahan counties

The most numerical value of the future uncertainty bound for drought duration is shown under the emission scenario of 2.6 while in contrast, the 4.5 scenario shows the lowest value.

In terms of drought frequency, the widest uncertainty bound belongs to the 8.5 and the lowest to the 4.5 emission scenarios. Also, the lowest difference between the historical average and the uncertainty bound is observed in the 4.5 emission scenario. For drought severity, the lowest uncertainty bound belongs to the 8.5 emission scenario, and the widest one is for the 2.6 scenario.

7. IPCC-AR6

The Intergovernmental Panel on Climate Change (IPCC) sixth Assessment Report (AR6) serves as a crucial scientific resource for investigating the impact of climate change on drought. Utilizing the precipitation projections outlined in AR6 enables researchers to comprehensively examine the implications of climate change on water resources and the occurrence of

drought events. AR6 not only provides a robust foundation for understanding future precipitation patterns but also incorporates diverse uncertainty sources, such as greenhouse gas emission scenarios, climate model variability, and socio-economic factors. By considering these uncertainties, scientists can refine their analyses and offer a more nuanced understanding of the potential impacts of climate change on drought severity, frequency, and spatial distribution. The comprehensive and up-to-date information from IPCC AR6, therefore, serves as a valuable tool for researchers aiming to unravel the intricate connections between climate change and drought, ultimately contributing to informed decision-making and adaptive strategies for mitigating the consequences of a changing climate. The results presented in Table 3 show the amount of precipitation for 2020-2039 for Isfahan province under different uncertainty sources (39 models and 5 scenarios: median, low 10-90th percentile range and high 10-90th percentile range). Using the methodology presented in this

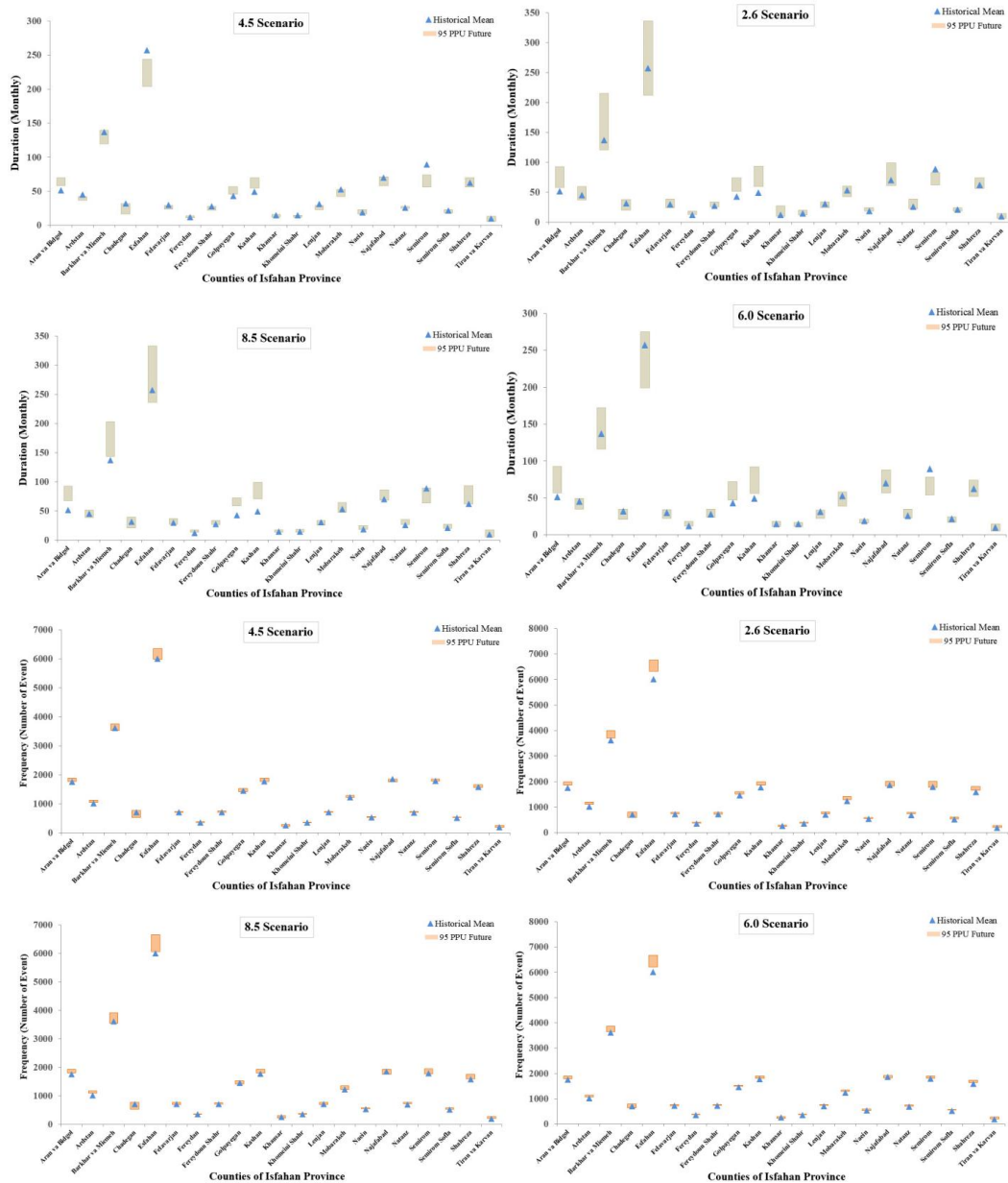


Fig 17. Comparison of 95PPU ranges of drought vulnerability of duration and frequently characteristics under the effect of climate change with AR5 emission scenarios in Isfahan counties

article, results similar to those presented in Table 3 can be extracted for each of the pixels in the study area, and the agricultural drought vulnerability can be analysed for each point. Similar to the near future (2020-2039), these results can be calculated and analysed for the middle (2040-2059 and 2060-2079) and distant future (2080-2099) as well.

Conclusions

The aim of this study was to perform analysis of the vulnerability for current and future climatic conditions, to depict drought conditions for current and future time horizons, while considering uncertainties arising from general circulation models and emission scenarios.

Assessing the vulnerability of different

Table 3. projected climatology of precipitation for 2020-2039 for Esfahan province scale under different uncertainty sources (models and scenarios)

Index	monthe	Historical Ref. Period, 1995- 2014	2020-2039				
			SSP1- 2.6	SSP2- 4.5	SSP2- 4.5	SSP3- 7.0	SSP5- 8.5
Median	Jan	26.92	29.41	29.51	29.51	28.46	29.16
	Feb	23.89	25.15	23.96	23.96	24.36	23.52
	Mar	27.66	29.02	29.59	29.59	29.15	26.82
	Apr	22.51	23.73	23.22	23.22	20.99	22.96
	May	8.52	9.41	9.18	9.18	8.95	9.05
	Jun	0.18	0.21	0.17	0.17	0.20	0.21
	Jul	0.00	0.00	0.00	0.00	0.00	0.00
	Aug	0.00	0.00	0.00	0.00	0.00	0.00
	Sep	0.00	0.00	0.00	0.00	0.00	0.00
	Oct	2.72	2.94	2.49	2.49	2.70	2.92
	Nov	15.17	14.98	15.93	15.93	14.54	15.35
	Dec	22.19	23.27	23.41	23.41	24.41	24.73
10-90th Percentile Range (low)	Jan	26.92	24.16	22.40	22.40	21.82	23.36
	Feb	23.89	19.35	18.77	18.77	19.73	17.93
	Mar	27.66	22.87	23.27	23.27	22.88	22.08
	Apr	22.51	18.41	17.27	17.27	17.03	17.27
	May	8.52	6.76	7.38	7.38	6.40	6.94
	Jun	0.18	0.08	0.07	0.07	0.06	0.07
	Jul	0.00	0.00	0.00	0.00	0.00	0.00
	Aug	0.00	0.00	0.00	0.00	0.00	0.00
	Sep	0.00	0.00	0.00	0.00	0.00	0.00
	Oct	2.72	1.60	1.46	1.46	1.39	1.43
	Nov	15.17	10.61	11.18	11.18	9.99	10.23
	Dec	22.19	18.05	17.90	17.90	20.49	17.88
10-90th Percentile Range (high)	Jan	26.92	33.05	33.46	33.46	34.37	37.24
	Feb	23.89	29.96	28.67	28.67	29.28	27.67
	Mar	27.66	34.78	34.47	34.47	34.40	32.80
	Apr	22.51	29.14	29.20	29.20	27.71	28.22
	May	8.52	11.61	11.46	11.46	11.27	11.77
	Jun	0.18	0.46	0.40	0.40	0.40	0.44
	Jul	0.00	0.00	0.00	0.00	0.00	0.00
	Aug	0.00	0.00	0.00	0.00	0.00	0.00
	Sep	0.00	0.00	0.01	0.01	0.01	0.00
	Oct	2.72	4.36	4.28	4.28	3.89	4.33
	Nov	15.17	20.08	19.72	19.72	20.89	21.90
	Dec	22.19	29.85	30.39	30.39	28.94	30.97

counties in Isfahan province in Iran, led to a ranking of the vulnerability of the counties. This ranking can support decision-makers in the identification of counties characterized by a high level of vulnerability.

Results showed that the agricultural vulnerability of drought in Isfahan and Barkhar-va-Meimeh was highest, while these counties had a low level of vulnerability in the total area. It was evident that, when the agricultural area of each county is applied, the trend of drought will change.

Moreover, some counties have more agricultural areas with less total area, in contrast to counties with a higher amount of total area. In these counties (such as Tiran-va-Karvan, Khomeini Shahr, and Naein), the agricultural area has a significant impact on drought vulnerability.

Based on these results in the studied area, each county with more agricultural area and gardens will experience the most crucial damage from exposure to drought because agriculture is among the first sectors to suffer from climate change and the resulting drought episodes.

Future improvements to the applied methodology can be obtained by incorporating applied indicators to create a spatial vulnerability map.

Finally, the proposed methodology represents a useful tool for decision-makers to rank priority areas and take appropriate management strategies.

References

- Añel, J. A., Fernández-González, M., Labandeira, X., López-Otero, X., & De la Torre, L. (2017). Impact of cold waves and heat waves on the energy production sector. *Atmosphere*, 8(11), 209. <https://doi.org/10.3390/atmos8110209>
- Calvo, C. (2008). Vulnerability to multidimensional poverty: Peru, 1998–2002. *World Development*, 36(6), 1011-1020. <https://doi.org/10.1016/j.worlddev.2007.10.001>
- Clarke, B., Otto, F., Stuart-Smith, R., & Harrington, L. (2022). Extreme weather impacts of climate change: an attribution perspective. *Environmental Research: Climate*, 1(1), 012001. <https://doi.org/10.1088/2752-5295/ac6e7d>
- Cred and UNDRR (2020). Human Cost of Disasters. An Overview of the last 20 years: 2000–2019. CRED, UNDRR, Geneva.
- Cutter, S. L., Boruff, B. J., & Shirley, W. L. (2012). Social vulnerability to environmental hazards. In *Hazards vulnerability and environmental justice* (pp. 143-160). Routledge. <https://doi.org/10.1111/1540-6237.8402002>
- Deryng, D., Conway, D., Ramankutty, N., Price, J., & Warren, R. (2014). Global crop yield response to extreme heat stress under multiple climate change futures. *Environmental Research Letters*, 9(3), 034011. <https://doi.org/10.1088/1748-9326/9/3/034011>
- Dosio, A., Mentaschi, L., Fischer, E. M., & Wyser, K. (2018). Extreme heat waves under 1.5 C and 2 C global warming. *Environmental research letters*, 13(5), 054006. <https://doi.org/10.1088/1748-9326/aab827>
- Ekrami, M., Mahdavi Najaf Abadi, R., Rezai, M., Vagharfard, H., & Barkhordari, J. (2021). Spatial Analysis and Assessment of Agricultural Drought Vulnerability in Arid Regions (Case Study: Pishkouh Watershed, Yazd Province). *Watershed Engineering and Management*, 13(1), 197-212. <https://doi.org/10.22092/ijwmse.2020.341878.1772>
- Fakhri, M., Dokohaki, H., Eslamian, S., Fazeli Farsani, I., & Farzaneh, M. R. (2014). Flow and sediment transport modeling

- in rivers. *Handbook of Engineering Hydrology*, 2, 233-275. <https://doi.org/10.1201/b16683-14>
- Fakhri, M., Farzaneh, M. R., Eslamian, S., & Khordadi, M. J. (2013). Confidence interval assessment to estimate dry and wet spells under climate change in Shahrekord Station, Iran. *Journal of Hydrologic Engineering*, 18(7), 911-918. [https://doi.org/10.1061/\(ASCE\)HE.1943-5584.0000688](https://doi.org/10.1061/(ASCE)HE.1943-5584.0000688)
- Fakhar, M. S., & Nazari, B. (2024). Multitemporal Analysis of Drought in Iran: Monitoring and Evaluation of Spatial and Temporal Characteristics Using MODIS Indices. *Journal of Drought and Climate Change Research*, 2(1), 39-58. doi: 10.22077/jdcr.2024.7011.1050
- Farzaneh, M., Bani mostafa arab, F., & Hussein Hamarashid, S. (2024). Preservation and Restoration of the Hamon Wetland is a Common Solution for Iran and Afghanistan in the Field of Facing the Phenomenon of Climate Change. *Journal of Drought and Climate Change Research*, 2(1), 15-38. doi: 10.22077/jdcr.2023.6658.1037
- Farzaneh, M., & Bani mostafa arab, F. (2023a). Analysis of Climate Change Adaptation Laws in Developed Countries. *Journal of Drought and Climate Change Research*, 1(1), 49-70. doi: 10.22077/jdcr.2023.6024.1009
- Farz Farzaneh, M., & Banimostafaarab, F. (2023b). Analysis of climate change adaptation laws in developing countries. *Climate Change Research*, 4(13), 35-54. doi: 10.30488/ccr.2023.394431.1128
- Fazeli Farsani, I., Farzaneh, M. R., Besalatpour, A. A., Salehi, M. H., & Faramarzi, M. (2019). Assessment of the impact of climate change on spatiotemporal variability of blue and green water resources under CMIP3 and CMIP5 models in a highly mountainous watershed. *Theoretical and Applied Climatology*, 136, 169-184. <https://doi.org/10.1007/s00704-018-2474-9>
- Hamzeh, A., Farzaneh, M., Khordadi, M. J., & Banimostafaarab, F. (2024). The non-structural strategy of insurance in developed countries to adapt to climate change. *Journal of Climate Research*, 1402(54), 179-199.
- Hamzeh, A., Farzaneh, M., Khordadi, M. J., & Banimostafa Arab, F. (2023). Challenges of Developing Countries to Exploitation Non-structured Insurance Strategy to Climate Change Adaptation. *Journal of Climate Research*, 1401(52), 169-182.
- Hao, Z., Hao, F., Singh, V. P., & Zhang, X. (2018). Changes in the severity of compound drought and hot extremes over global land areas. *Environmental Research Letters*, 13(12), 124022. <https://doi.org/10.1088/1748-9326/aace96>
- Hao, Z., Hao, F., Xia, Y., Feng, S., Sun, C., Zhang, X., ... & Meng, Y. (2022). Compound droughts and hot extremes: Characteristics, drivers, changes, and impacts. *Earth-Science Reviews*, 104241. <https://doi.org/10.1016/j.earscirev.2022.104241>
- Hosseini Seddigh, S. M., & Jalali, M. (2024). Analysis of Iran's Drought Changes with Palmer's Self-Adjustment Index. *Journal of Drought and Climate Change Research*, 2(1), 93-106. doi: 10.22077/jdcr.2024.6149.1016
- Jayanthi, H., Husak, G. J., Funk, C., Magadzire, T., Chavula, A., & Verdin, J. P. (2013). Modeling rain-fed maize vulnerability to droughts using the standardized precipitation index from satellite estimated rainfall—Southern Malawi case study. *International Journal of Disaster Risk Reduction*, 4, 71-81. <https://doi.org/10.1016/j.ijdrr.2013.02.001>
- McKee, T. B., Doesken, N. J., & Kleist, J. (1993). Analysis of Standardized

- Precipitation Index (SPI) data for drought assessment. *Water*, 26(2), 1-72.
- Luers, A. L., Lobell, D. B., Sklar, L. S., Addams, C. L., & Matson, P. A. (2003). A method for quantifying vulnerability, applied to the agricultural system of the Yaqui Valley, Mexico. *Global Environmental Change*, 13(4), 255-267. [https://doi.org/10.1016/S0959-3780\(03\)00054-2](https://doi.org/10.1016/S0959-3780(03)00054-2)
- Murthy, C. S., Laxman, B., & Sai, M. S. (2015). Geospatial analysis of agricultural drought vulnerability using a composite index based on exposure, sensitivity and adaptive capacity. *International journal of disaster risk reduction*, 12, 163-171. <https://doi.org/10.1016/j.ijdr.2015.01.004>
- Metzger, M. J., Leemans, R., & Schröter, D. (2005). A multidisciplinary multi-scale framework for assessing vulnerabilities to global change. *International Journal of Applied Earth Observation and Geoinformation*, 7(4), 253-267. <https://doi.org/10.1016/j.jag.2005.06.011>
- Mishra, A. K., & Singh, V. P. (2010). A review of drought concepts. *Journal of hydrology*, 391(1-2), 202-216. <https://doi.org/10.1016/j.jhydrol.2010.07.012>
- Ortega-Gaucin, D., Ceballos-Tavares, J. A., Ordoñez Sánchez, A., & Castellano-Bahena, H. V. (2021). Agricultural drought risk assessment: A spatial analysis of hazard, exposure, and vulnerability in Zacatecas, Mexico. *Water*, 13(10), 1431. <https://doi.org/10.3390/w13101431>
- Ravindranath, N. H., Rao, S., Sharma, N., Nair, M., Gopalakrishnan, R., Rao, A. S., ... & Bala, G. (2011). Climate change vulnerability profiles for North East India. *Current Science*, 384-394.
- Rezaei, A. R., & Roshani, A. (2024). Prioritization of Factors Affecting Drought using the Fuzzy Analytic Hierarchy Process Method (Study Case: Torbat Heydarieh City). *Journal of Drought and Climate Change Research*, 2(1), 77-92. doi: 10.22077/jdcr.2024.7255.1057
- Rostamian, R., Eslamian, S., & Farzaneh, M. R. (2013). Application of standardised precipitation index for predicting meteorological drought intensity in Beheshtabad watershed, central Iran. *International Journal of Hydrology Science and Technology*, 3(1), 63-76. <https://doi.org/10.1504/IJHSt.2013.055233>
- Seneviratne, S., Nicholls, N., Easterling, D., Goodess, C., Kanae, S., Kossin, J., ... & Zwiers, F. W. (2012). Changes in climate extremes and their impacts on the natural physical environment.
- Thirumalaivasan, D., Karmegam, M., & Venugopal, K. (2003). AHP-DRAStIC: software for specific aquifer vulnerability assessment using DRAStIC model and GIS. *Environmental Modelling & Software*, 18(7), 645-656. [https://doi.org/10.1016/S1364-8152\(03\)00051-3](https://doi.org/10.1016/S1364-8152(03)00051-3)
- Tigkas, D., Vangelis, H., & Tsakiris, G. (2019). Drought characterisation based on an agriculture-oriented standardised precipitation index. *Theoretical and applied climatology*, 135, 1435-1447. <https://doi.org/10.30638/eemj.2015.156>
- UNDP (2010). Mapping Climate Change Vulnerability and Impact Scenarios – A Guidebook for Sub-National Planners. United Nations Development Programme.
- Wang, R., Zhang, J., Guo, E., Alu, S., Li, D., Ha, S., & Dong, Z. (2019). Integrated drought risk assessment of multi-hazard-affected bodies based on copulas in the Taoerhe Basin, China. *Theoretical and Applied Climatology*, 135, 577-592. <https://doi.org/10.1007/s00704-018-2374-z>
- Wilhelmi, O. V., & Wilhite, D. A. (2002). Assessing vulnerability to agricultural drought: a Nebraska case study. *Natural Hazards*, 25, 37-58. <https://doi.org/10.1023/A:1013388814894>

- Wu, J., He, B., Lü, A., Zhou, L., Liu, M., & Zhao, L. (2011). Quantitative assessment and spatial characteristics analysis of agricultural drought vulnerability in China. *Natural Hazards*, *56*, 785-801. <https://doi.org/10.1007/s11069-010-9591-9>
- Zamani Nouri, A., Farsani, I.F., & Farzaneh, M.R. (2015). Assessment of multi-index agricultural drought vulnerability and spatial characteristics analysis. *IJBPAS*, *4*(12), 440-452.
- Zhang, Q., Sun, P., Li, J., Xiao, M., & Singh, V. P. (2015). Assessment of drought vulnerability of the Tarim River basin, Xinjiang, China. *Theoretical and applied climatology*, *121*, 337-347. <https://doi.org/10.1007/s00704-014-1234-8>
- Zhang, Q., Yao, Y., Wang, Y., Wang, S., Wang, J., Yang, J., ... & Li, W. (2019). Characteristics of drought in Southern China under climatic warming, the risk, and countermeasures for prevention and control. *Theoretical and Applied Climatology*, *136*, 1157-1173. <https://doi.org/10.1007/s00704-018-2541-2>
- Zipper, S. C., Qiu, J., & Kucharik, C. J. (2016). Drought effects on US maize and soybean production: spatiotemporal patterns and historical changes. *Environmental Research Letters*, *11*(9), 094021. <https://doi.org/10.1088/1748-9326/11/9/094021>



Assessment of Water, Food, and Energy Efficiency Indicators with a Nexus Approach and Sustainable Agricultural Management

Seyyed Ali Moasheri¹, Saman Javadi^{2*}, Mahmoud Mashal², Behzad Azadegan², Hamid Kardan Moghadam³

1. Ph.D, Irrigation and drainage, Aburihan Campus, University of Tehran, Tehran and Expert of Yazd Regional Water Company, Yazd, Iran.
2. Associate Professor, Department of Water Engineering, Aburihan Campus, University of Tehran, Tehran, Iran.
3. Assistant Professor at Water Research Institute, Ministry of Energy, Tehran, Iran.

*Corresponding Author: javadis@ut.ac.ir

Keywords:

Climate Change, Sustainable Management, Resources and Utilization, Nexus Approach, Efficiency, Irrigation Planning.

Abstract

Sustainable management of water, food, and energy resources and increasing efficiency is one of the key challenges in sustainable management and development. Given climate change, global population growth, and growing demands, sustainable utilization of these resources is essential to ensure the possibility of human survival and sustainable growth. Achieving sustainable development goals requires a comprehensive and interactive approach, and resource management with an integrative perspective is a necessary component of sustainable development, where all stakeholders participate in the decision-making process and implementation of actions. This study aims to enhance the efficiency of water, food, and energy in the Plusgan watershed and develop a validated tool for evaluating agricultural management strategies in relation to the nexus of water, food, and energy security. The study was conducted in two stages. In the first stage, management scenarios were identified to increase efficiency, and in the second stage, nexus-oriented management scenarios were evaluated and prioritized. In the second part of this research, among the 30 sub-scenarios introduced for improving efficiency, the sub-scenarios that involved a 20%, 10%, and 30% increase in forage maize cultivation showed positive effects on water, food, and energy efficiency indicators. After prioritizing the influential sub-scenarios using the TOPSIS multi-criteria decision-making model, the sub-scenario with a 30% increase in forage maize cultivation had the greatest positive impact on water, food, and energy efficiency. It was identified as the key scenario for evaluating efficiency in sustainable agricultural management.

Received:

16 July 2023

Revised:

07 August 2023

Accepted:

12 August 2023

How to cite this article:

Moasheri, S.A., Javadi, S., Mashal, M., Azadegan, B., & Kardan Moghadam, H. (2024). Assessment of Water, Food, and Energy Efficiency Indicators with a Nexus Approach and Sustainable Agricultural Management. *Journal of Drought and Climate change Research (JDCR)*, 2(6), 57-76. [10.22077/jdcr.2023.6585.1031](https://doi.org/10.22077/jdcr.2023.6585.1031)



Introduction

One of the most significant challenges facing humanity today is water supply in the face of associated stresses, which highlights the need for effective water resource management (FAO, 2012). Population growth has increased the demand for appropriate allocation of water resources, and this issue has always been accompanied by stress due to the reduction of freshwater resources. It is crucial to have a proper understanding of the water resource system in a region for planning and making informed decisions, considering both climate and human-induced stresses (Tork et al., 2021). However, it seems that there is a lack of useful information for decision-making related to water management (Hirwa et al., 2022). Given the significant role of water availability in the social, economic, and environmental well-being of a region, a holistic approach to water resource management should consider the sustainable dimensions of resources and consumption. To achieve sustainability, a better understanding of the variables affecting the water supply and demand sustainability and their interrelationships is necessary. Therefore, there is a need for an index that connects the elements of the water balance to quantify the water sustainability status and the level of water protection required for proper water resource management (Karamouz et al., 2017). On the other hand, with the finite nature of water resources and the depletion of renewable water sources, optimal utilization of water resources, particularly in the agricultural sector, is of the utmost importance. On Iran's central plateau, surface water resources are limited. Therefore, the main volume of water supply, especially in terms of sustainability, relies on groundwater resources, which play a crucial role in

meeting the region's water needs.

One of today's concerns is ensuring water supply in the face of associated stresses. This issue emphasizes the attention and importance of effective water resource management (FAO, 2012). Population growth has increased the demand for appropriate allocation of water resources, and this issue has always been accompanied by stress due to the reduction of freshwater resources. Understanding the water resource system of a region is of great importance for proper planning and decision-making regarding water management, considering climate and human-induced stresses (Tork et al., 2021). However, it appears that we face a lack of useful information for decision-making concerning water management (Hirwa et al., 2022). Given the crucial role of water availability in the social, economic, and environmental well-being of a region, a holistic approach to water resource management should focus on water resources considering the dimensions of resource sustainability and consumption patterns. To achieve sustainability, a better understanding of the variables influencing water supply and demand sustainability and their interrelationships is essential. Therefore, the use of an index that connects various elements of the water balance to determine the water sustainability status and the level of water protection required for proper water resource management is necessary (Karamouz et al., 2017). On the other hand, with the fixed amount of available water and the reduction of renewable water resources, optimal utilization of water resources and soil, especially in the agricultural sector, is crucial. On Iran's central plateau, surface water resources are limited. Therefore, the main source of water supply, especially in terms of sustainability, is related to

groundwater resources. These resources play a significant role in meeting the region's water needs. Additionally, groundwater tables have been affected by unregulated extraction and imbalanced use, resulting in many Iranian plains being classified as prohibited areas. The failure of past water management policies and climate stresses has led to a significant reduction in water levels, resulting in a decline in groundwater levels and reservoir volume in aquifers.

The sharp decline in water levels in most of the country's aquifers and the importance of the issue have led to increased attention to the quantitative and qualitative development of groundwater resource balancing projects. The groundwater balancing and restoration project has started in recent years in collaboration with the Ministry of Energy and the Agricultural Jihad Organization in the country. The main objective of this project is to reduce aquifer depletion with minimal economic and social stress. Furthermore, in line with the implementation of the resolutions of the Supreme Water Council and the organizational goals of the Ministry of Energy, estimating and communicating the amount of water available for planning purposes is essential.

Considering the research objectives, the implementation of the groundwater balancing project in line with water scarcity adaptation programs should be approached with a nexus perspective. This should encompass the three dimensions of water, food, and energy efficiency. This approach represents a novel approach to integrated water resource management. To select an effective solution and prioritize the proposed solutions, the TOPSIS multi-criteria decision-making model will be utilized. This decision-making model aims to identify the best solution among the

proposed alternatives and prioritize it. Water productivity, in simple terms, refers to producing more food or obtaining greater benefits with less water. In this regard, physical water productivity is defined as the ratio of the amount of product to the amount of water consumed. Economic water productivity represents the value obtained from each unit of water consumed. Water productivity is often calculated for specific crops or livestock (Molden., 2007). Nevertheless, the water saved from improving water productivity can be used in other sectors. There are various ways to improve water productivity, and international trade in agricultural products provides a pathway for enhancing global water use efficiency through virtual water transfers to water-stressed regions (Dalin et al., 2014). Since water use efficiency varies significantly in different regions, international or domestic trade in food can contribute to significant water savings at the global or national level (Chapagain et al., 2011). While virtual water transfers may not solve the inequities of water consumption globally (Seekell et al., 2011), they can reduce social vulnerability to drought under certain scenarios (D'Odorico et al., 2012). This model is based on maximizing food production, minimizing energy consumption, minimizing water use, and increasing groundwater reserves. Without water-energy-food trade-offs, risks in this sector increase. Therefore, it is necessary to analyze and address the risks affecting the water, food, and energy sector in the agricultural water supply and distribution system before any incidents occur. Examining the water-food-energy nexus based on risk can provide opportunities for improving the sustainability of these resources in agricultural water supply and distribution systems.

Economic and social development, population growth, and climate change pose significant challenges to sustainability and food security, which are among the most pressing concerns of societies (Vörösmarty et al., 2000; Gleick, 2008). Consequently, water resources, essential for human survival, sustainable livelihoods, food security, and ecosystem preservation, are under pressure. Many believe that the world is facing an unprecedented water crisis, and without progress and improved management of water resources, as well as integrated decision-making in developed and developing countries, water-related issues are expected to become increasingly critical in the coming decades (Scheierling et al., 2014). Iran, located in a dry and semi-dry climate, also faces severe water scarcity. In 2014, Iran's water per capita was 1644 cubic meters, indicating an unfavorable water availability compared to the global average of 6225 cubic meters per person per year (World Bank, 2014). The trend and patterns of water per capita are worrisome, with the country's water per capita decreasing from 5570 cubic meters in 1962 to 1876 cubic meters in 2008 and further to 1644 cubic meters in 2014 (Aquastat, 2010). The current status of water resources in Iran, the trends shaping them, and the inadequate spatial and temporal distribution of limited water availability highlight the need for demand management, consumption moderation, and achieving a balance between water supply and demand.

In this regard, understanding two facts is crucial to comprehending the role of agriculture in the water crisis. First, agriculture is the largest water user, accounting for a significant proportion (80%) of water consumption (Rost, 2008). Second, agricultural water use is relatively less efficient and productive compared to

other water users (Yong, 2005). Therefore, when water becomes scarce in many parts of the world, other sectors and users tend to view agriculture as a potential water source (Scheierling et al., 2014). Many experts believe that in addition to the global water crisis, agriculture and related activities are facing an unprecedented crisis worldwide. Continuous population growth, changes in dietary patterns (increased consumption of dairy and meat), and the expansion of biofuel use have increased the pressure on the agricultural sector (Scheierling et al., 2014). Recent yield growth in major crops has raised concerns that without substantial investment in low-yield areas and the implementation of appropriate strategies to sustain yield increases in high-yield areas, agricultural productivity will not be sufficient to meet future demands quickly (Ray et al., 2013). To shed light on the subject, reviewing recent projections for agricultural production and its water requirements would be useful. It is projected that the world population will reach 9.6 billion by 2050 (United Nations, 2013). According to the FAO model for the period from 2005 to 2050, the growth rate of agricultural product consumption is estimated at 1.1% annually. To meet this global demand, agricultural production in 2050 needs to be 60% higher than the production in 2005. Consequently, the water required for irrigation needs to increase from 2761 to 2926 cubic kilometers (Bruinsma & Alexandratos, 2012). Considering the limited potential for increasing water supply in many parts of the world, it is strongly recommended to focus efforts and actions on improving water productivity in agriculture. Given the large amount of water consumed in agriculture and the relatively low efficiency, even slight improvements in agricultural water productivity can have a

considerable impact on global and regional water budgets. This process of enhancing water productivity enables increased agricultural production with the same amount of water or the production of the same agricultural output with less water. Indicators of agricultural water efficiency are suitable tools for evaluating agricultural management, particularly in dry and semi-arid regions. Low water efficiency in the agricultural sector is one of the pressing issues that have caused significant changes and transformations in human life due to various reasons, including climate change, improper water management on farms, and the depletion of renewable resources as the primary supplier of water needs in the country.

It has been mentioned that to feed a growing population accompanied by improvements in per capita income and diverse dietary patterns, we will need more water based on per capita average needs. The increased demand for water in agriculture will put pressure on water and soil systems and intensify competition for water resources (Molden, 2007). In this regard, improving the physical water productivity in agriculture reduces the need for additional water and soil in irrigation and rainfed systems, thus providing a suitable response to increasing water scarcity.

There are promising pathways to increasing water efficiency in both rainfed and irrigated agricultural systems. Supplementary irrigation for rainfed lands, soil fertility preservation, deficit irrigation, small-scale operations for water storage, delivery, and utilization, modern irrigation technologies, soil moisture conservation through minimum or zero tillage, reduced biomass through increased pest and disease resistance, and rapid initial growth for quick ground cover are among these pathways. However, the benefits derived

from improving water efficiency depend on specific conditions and can only be assessed through a holistic watershed-level perspective (Molden., 2007). Increasing water efficiency, especially the value created per unit of water, can be an important path to poverty reduction, provided that the benefits of water efficiency reach the poor, particularly rural women.

In general, the path to improving water efficiency can be achieved through evapotranspiration, soil fertility, international trade, and reducing evaporation or water delivery (Molden, 2007). Adopting methods to enhance water efficiency requires a capable institutional and political environment to balance the incentives of producers, resource managers, and the community and to develop a process for coordinating stakeholders. Despite sufficient managerial operations and technologies, realizing net benefits from water efficiency is challenging due to various reasons. The low price of agricultural products and the high production risks for farmers are factors that hinder significant progress (Molden, 2007). Increasing water efficiency through increased agricultural production puts pressure on the market prices of these products, and the benefits obtained by one group often come at the expense of other groups, indicating that incentive systems and the adoption of modern technologies do not support each other adequately. Proposed strategies need to identify these challenges and provide incentive policies and compensation schemes to promote greater fairness between those who benefit from the water efficiency process and those who are adversely affected (Molden., 2007).

Human economic efforts have always aimed to maximize results with minimal

effort and resources. Water efficiency is defined as the ratio of output to the amount of water applied for plant growth (Choudhury and Bhattacharya, 2018). In essence, water efficiency determines how much produce is generated for a given amount of water used, and its unit is kilograms per cubic meter.

Determining and analyzing agricultural water efficiency indicators is not always a straightforward task because water is not solely used for agricultural production. In assessing and evaluating the effectiveness of water in plant production, besides the amount of produce, the value of the produced material should also be considered. For example, the income derived from the consumption of each cubic meter of water or the amount of protein and calories produced per a specific amount of water can also be important considerations in evaluations. Agricultural water efficiency is related to water resources and the benefits derived from them, and many parameters in this regard are qualitative and not easily measurable. Additionally, a significant challenge in studying water efficiency is the insufficient availability of basic information to calculate monetary and non-monetary indicators of agricultural water efficiency. Integrated water resources management is a set of strategies and practices that aim to address the complex challenges related to the sustainable and equitable management of water resources and water-related services. It recognizes the interconnectedness, interdependencies, and interactions between water resources and various sectors, including agriculture, industry, energy, and the environment (Rogers and Hall, 2003).

Managing groundwater resources and their uses is a crucial component of integrated water resources management. It involves

the sustainable utilization and management of groundwater and surface water resources to achieve a balanced and equitable distribution of water and the efficient utilization of water resources. Proper governance and management of water resources require effective administrative and legal frameworks, which can facilitate stakeholder participation and ensure effective decision-making processes (Saunier and Meganck, 2009). Such frameworks should consider the technical, economic, and social dimensions of water management to promote sustainable and integrated practices (GEF, 2015). Water governance and management in transboundary river basins, where different countries share water resources, require international cooperation, collaborative approaches, and sound governance mechanisms (Varady et al., 2012; Chilton and Smidt, 2014).

The implementation of integrated water resources management involves various challenges and constraints, including the fragmented nature of water-related institutions, limited financial resources, and the lack of coordination among different stakeholders (Halbe et al., 2015). Overcoming these challenges requires a holistic and interdisciplinary approach that integrates elements of water management, governance, and policy. Effective implementation of integrated water resources management can lead to improved water security, increased resilience to climate change impacts, and sustainable development (Megdal and Perlman, 2018).

In recent years, the concept of the linkage and nexus between water, food, and energy security has gained significant attention in the context of sustainable water management. Each of these elements, water, energy, and food,

is influenced by increasing population growth, urbanization, changing lifestyles, and climate change, leading to complex interlink ages and challenges that require integrated solutions (Beisheim, 2013). The total cost includes the sum of energy, water supply, electricity generation, food production, and CO₂ reduction costs.

WEFEN enables us to comprehensively and dynamically understand the interconnections and dynamics of water, food, and energy elements, allowing for safe and sustainable management and utilization. By effectively integrating equations and considering the interactions of these elements, we can achieve a coordinated and optimized approach to resource management (FAO, 2014).

In practical terms, WEFEN can be defined as an approach to assessing, developing, and implementing policies that simultaneously emphasize water, energy, and food security (Bizikova et al., 2014). Specifically, WEFEN provides a conceptual and analytical framework for socio-ecological systems and proposes a framework for the coordinated management and utilization of natural resources across all sectors and scales (FAO, 2014). Gupta (2017) emphasizes the interactions and collaboration of all involved elements, aiming to maximize the benefits derived from their utilization and preserve environmental integrity. Holtz et al. (2013) integrated the land, energy, and water resources systems using the CLEWs framework. Instead of developing a completely new unified analysis tool, they integrated their perspectives based on existing evaluation methods for each of the three resources, which yielded good results. The land-use model, energy model, and water resource management model were connected using recent data and predicted scenarios.

Outputs from one module served as inputs for the other two modules, which were then solved continuously, transferring data between the models. This process was iterated until a convergent solution was reached. The Republic of Mauritius was selected as the first CLEWs case study due to its water scarcity and contribution to climate change mitigation. The country's priority is to reduce energy imports while committing to greenhouse gas emissions reductions. The majority of the island's surface is dedicated to sugarcane cultivation, playing a significant role in the economy as the primary export and foreign exchange income. Reducing oil imports would increase energy independence, reduce oil import costs, and mitigate greenhouse gas emissions. Whether this strategy is desirable or not depends on the cost of domestic ethanol production, overall public and socioeconomic benefits, the price ratio between oil and sugar development, the value assigned to energy security and greenhouse gas emissions reduction, as well as the unintended and secondary effects.

The WEFO model was developed by Zhang and Vesselingh (2017) to answer the question of how to plan energy, water, electricity generation, and food production to minimize the overall system cost while controlling greenhouse gas emissions. A hypothetical system including two thermal power plants (coal and natural gas) for electricity generation was used to demonstrate the application of the WEF approach. The WEFO planning was conducted over three consecutive five-year periods. Electricity production requires water from three different sources: groundwater, surface water, and reclaimed water. The generated electricity is not only used within the WEF system (e.g., water supply for power plants and

food production) but also for meeting social and economic needs. Water (excluding reclaimed water due to human health concerns) and energy (in the form of electricity in this study) are required for food production and processing. Additionally, greenhouse gas emissions are associated with electricity and food production. The interactions within the WEFO model, as well as the existing social-economic and environmental constraints, were examined. The decision variables in the WEFO model include 1) energy values available from coal and natural gas, 2) power plant capacity for electricity generation, 3) groundwater and surface water values required for food production, 4) groundwater, surface water, and reclaimed water values required for electricity generation, and 5) social and economic demands for WEF production over a planning horizon.

A comprehensive three-stage plan has been proposed in Taiwan to investigate the synergies of Nexus Water-Food-Energy through the optimization of a multi-purpose reservoir combined with short-term/long-term joint operation of irrigation ponds to address increasing urbanization. The three-stage plan has been implemented step by step. (1) Short-term optimization (daily scale) of reservoir operation to maximize hydropower generation and reservoir storage during typhoon seasons (July-October). (2) Long-term water scarcity simulation (ten-day scale) considering the inventory of irrigation ponds for the agricultural and public sectors during non-typhoon seasons (November-June of the following year). And (3) promotion of one-year horizon benefits of WFE Nexus through the integration of short-term optimization and long-term simulation of reservoir operation. The results of short-term/long-term joint operation throughout

the year showed a potential reduction of water scarcity by more than 10%, food production increase up to 47%, and water-electricity benefits up to 9.33 million USD per year, in a wet year (Zhu et al., 2022). Karlberg et al. (2015) conducted a comprehensive study on the feasibility of integrating agriculture, energy, and water management in the Tana River basin in Kenya, with the aim of optimizing the water use efficiency. Their study revealed the potential benefits of optimizing water, energy, and agriculture sectors in terms of water savings, improved food production, and increased economic benefits. However, the implementation of such integrated approaches requires proper planning, management, and coordination to ensure sustainable water resources management and to overcome various technical, institutional, and socio-economic challenges (Garg and Dadhich, 2014).

Moreover, the integration of water, energy, and food sectors in water-scarce regions has been recognized as a key strategy to address the challenges of water scarcity, food security, and sustainable development. This integrated approach can help minimize water use conflicts, increase water use efficiency, and promote sustainable agricultural practices (El-Gafy, 2017). By considering the interdependencies and trade-offs among water, energy, and food, this approach can provide a more holistic and integrated framework for water resources management and planning (El-Gafy et al., 2017a). The optimization of water, energy, and food systems in water-scarce regions can lead to significant water savings, increased energy efficiency, and improved agricultural productivity (Sadeghi et al., 2020). The implementation of such integrated approaches requires a comprehensive understanding of the water-

energy-food nexus and the development of innovative strategies to enhance resource efficiency and sustainability (El-Gafy et al., 2017b).

The report “Critical Challenges and Priorities for Integrated Water Resources Management in Iran” (2017CSS) addresses 100 important and challenging issues in Iran. Among these topics, 12 titles, including water scarcity, drought and desertification, water pollution and contamination, groundwater depletion, institutional coordination, climate change impacts, water basin management, agricultural practices, irrigation efficiency, low energy productivity, inefficient water markets, groundwater management, and social conflicts, are identified as crucial in achieving water, energy, and food security and sustainability.

Water plays a vital role in agricultural production, industrial processes, domestic consumption, and hydropower generation. Its efficient use, proper allocation, sustainable management, and the nexus between water, energy, and food are significant factors in Iran’s development. Moreover, understanding the complexity of interrelationships in multi-sectoral systems is essential for achieving a safe and prosperous future (Rasul and Sharma, 2016; Cai, X et al., 2018).

By adopting an integrated approach, cohesive structures, and continuous linkages, the report aims to develop strategies and approaches for water, food, and energy security and sustainable development. Learning from trial and error experiences, it seeks to rectify the deficiencies and shortcomings in the decision-making processes of managers and stakeholders. It also emphasizes the importance of adopting comprehensive, cross-sectoral approaches to address water, food, and energy challenges and to promote

resilience in the face of uncertainties (Hettiarachchi and Ardakanian, 2016). In this study, a suitable model has been developed to prioritize solutions for enhancing water and land productivity, reducing resource uncertainties, and optimizing water, food, and energy interlinkages at the regional level. The model considers the interconnectedness between the water, food, and energy sectors in order to guide decision-making processes and formulate effective strategies for sustainable water, food, and energy management.

Material and Methods

Study Area

Study area considering the objectives and needs of this research, the Plasjan watershed, located upstream of the Zayandehrud Dam in Iran, was selected as the study area. The Plasjan watershed is situated in the northwestern part of the upstream region of Zayandehrud Dam, covering an area of 1854 square kilometers, ranging from eastern longitude °50 to °45 and northern latitude °32 to °33. The location of the study area is depicted in Figure (1). The maximum elevation of this watershed is 3877 meters, while the minimum elevation in the outlet section is 2056 meters above mean sea level. The watershed is divided into three sub-basins: Damandan (code 4214), Chehelkhaneh (code 4213), and Boein-Miandasht (code 4212). An examination of the water resources in this watershed reveals that 218 million cubic meters of water are utilized, with 177 million cubic meters sourced from groundwater and 41 million cubic meters from surface water. The selection of this area was based on the declining groundwater levels and reservoir deficits in the aquifers within the study area, emphasizing the need for aquifer balancing. Additionally, the availability of remote

sensing data in the study area played a role in choosing the Plasjan watershed. In these three aquifers, water level measurements are conducted monthly using 53 observation wells. Analysis of groundwater levels in these aquifers indicates a decline of 1.1 meters and 0.5 meters in the Boein-

Miandasht and Chehelkhaneh regions, respectively, and a decrease of 1.5 meters in the Damandan aquifer. Therefore, the Plasjan watershed was selected as the study area for further investigations.

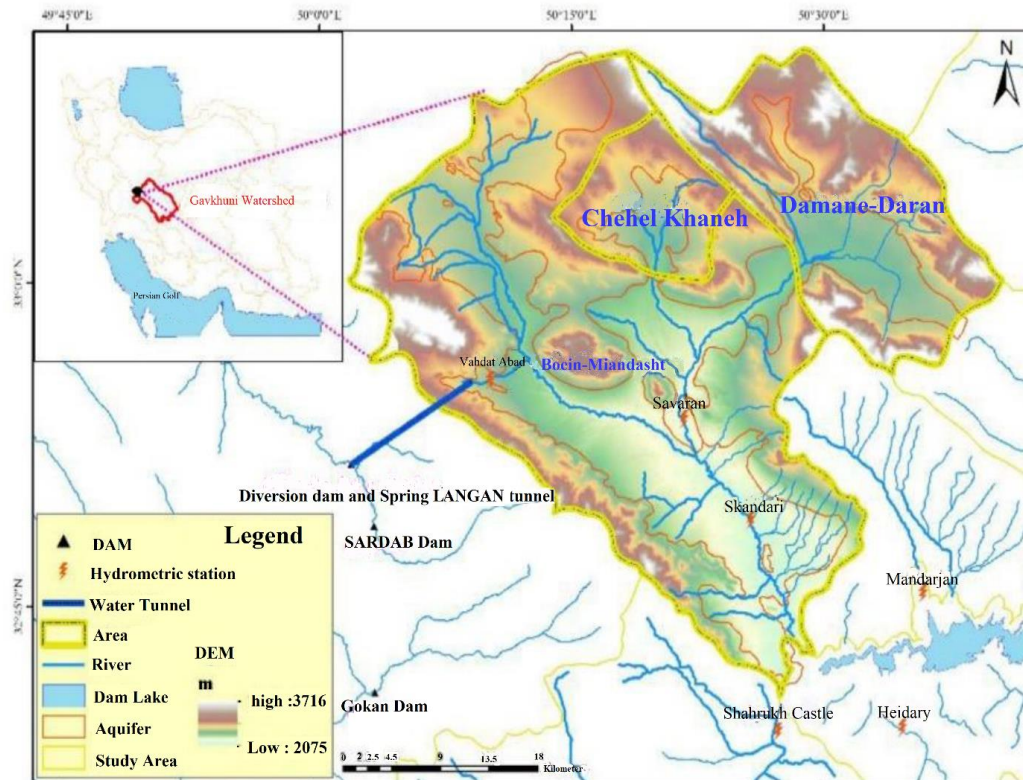


Fig 1. Study Area (Rahimzadeh et al., 2021)

The majority of water consumption in this area is allocated to agricultural users, while less than 10 million cubic meters of water are allocated to the industrial and drinking water supply sectors. The central part of this region is influenced by agricultural activities, which have resulted in the highest water consumption from available resources. However, less emphasis has been placed on the industrial and drinking water supply sectors, indicating that agriculture holds greater importance in this area. The cropping pattern and agricultural productivity of this watershed, based on

land use classification as presented in Table 1 according to the Agricultural Statistical Yearbook of Isfahan Province in the water year 2017-2018, are provided.

The agricultural cropping pattern in the Plasjan watershed in the water year 2017-2018 in Isfahan province primarily consisted of wheat and barley cereals, oilseeds such as rapeseed, and forage crops including alfalfa and maize. The agricultural productivity in the region shows that wheat and barley, despite having lower yields compared to forage

Table 1. Cropping pattern and representative crop yields in the Plasjan watershed (Agricultural Statistical Yearbook 2017-2018, Jihad-e Agriculture of Isfahan Province)

Class	Product Representative	Yield (Kg/ha)	Cultivation type	Cultivated area (ha)
Cereal	Wheat	4000	Irrigated	3000
	Wheat	700	Rainfed	2000
	Atmosphere	4000	Irrigated	700
Oil Seeds	Canola	2214	Irrigated	14
Fodder plants	Alfalfa	10000	Irrigated	5000
	Fodder corn	60000	Irrigated	1200

crops (alfalfa) and forage maize, were cultivated on a larger area. Additionally, rapeseed, as an oilseed crop, holds a special position in the cropping pattern of this watershed with a smaller cultivated area but higher yields compared to wheat and barley. This agricultural cropping pattern and crop performance can serve as a basis for appropriate planning by farmers and relevant authorities in Isfahan province to optimize water and soil resources, increase agricultural productivity and efficiency. Furthermore, the wheat cropping pattern in the Plasjan watershed in the water year 2017-2018 was divided into two types: irrigated and rainfed. This division, based on the water availability for cultivation, indicates lower wheat yields in rainfed cultivation compared to irrigated cultivation. Based on this agricultural cropping pattern and crop performance in the Plasjan watershed in Isfahan province, efforts can be made in agricultural planning to increase productivity and efficiency by optimizing irrigated and rainfed cultivation of different crops, utilizing improved technologies in production and water and soil resource management, and selecting high-performance and climate- and water-compatible crops.

Considering the research objectives, the work is structured into five sections: The first section introduces scenarios for improving water efficiency based on the opinions of experts and specialists.

The second section determines the effectiveness of scenarios for improving efficiency by employing a linked approach in three indices of water, food, and energy efficiency.

The third section identifies the changes in the impact of implementing scenarios for improving efficiency, employing a linked approach to three indices of water, food, and energy efficiency compared to the current situation.

The fourth section determines scenarios with positive impacts on improving water, food, and energy efficiency.

The fifth section prioritizes scenarios for improving efficiency using a linked approach in three indices of water, food, and energy efficiency through the multi-criteria evaluation method of Technique for Order of Preference by Similarity to the Ideal Solution (TOPSIS).

Management Scenarios

Considering the current status of water resources and the water balance in the study area, and based on the opinions of agricultural experts and specialists, 30 sub-scenarios were defined to enhance and achieve positive effectiveness in efficiency from a linked perspective. These sub-scenarios focused on changes in the cultivated area of crops.

Based on the defined approach for increasing efficiency, which is essentially a comprehensive approach, 30 sub-scenarios

were identified for each dominant crop in the region. These sub-scenarios were based on six conditions: a 20%, 10%, or 30% increase in the cultivated area, or a 10%, 20%, or 30% decrease in the cultivated area. In this case, simulations were conducted based on a set of scenarios using the three indices of water efficiency, food efficiency, and energy efficiency.

Nexus Assessment of Water, Food, and Energy Efficiency Scenarios

One of the tools used to study these relationships is the Water-Food-Energy Nexus concept. The water-food-energy nexus has gained international attention since the Bonn Nexus Conference in 2011 (Salam et al., 2017). The linkage of water, energy, and food resources is highly complex, as the impacts of each sector have direct and indirect consequences for the others. The demand for each of these resources has been increasing over time, and it is expected to continue in the future, raising important questions about sustainable resource management (Shinde, 2017).

Link-related indicators will be used to assess the nexus based on the introduced scenarios in the previous step. The methodology involves calculating the linkage indicators before and after implementing the scenarios and evaluating the changes for each scenario. Three efficiency indicators, namely water efficiency, energy efficiency, and food efficiency, will be calculated based on available regional statistics and information.

Water Efficiency Indicator: In the study by El-Gafy (2017), the water efficiency indicator (ton/m^3) is presented as Equation 1:

$$W_{pro.t} = Y_{c.t}/W_{c.t} \quad (1)$$

Where $Y_{c,t}$ represents the performance

of product c in time period t , and $W_{c,t}$ represents the amount of water consumed for producing product c at time t .

The energy efficiency indicator is defined by El-Gafy (2017) in Equation 2:

$$E_{pro.t} = Y_{c.t}/E_{c.t} \quad (2)$$

Where $Y_{c,t}$ represents the performance of product c , and $E_{c,t}$ represents the energy consumed for product c at time t .

The food efficiency indicator is introduced in this study to analyze the water-energy-food nexus more effectively, and it is defined by Equation 3:

$$F_{pro.t} = Y_{c.t}/Y_{TOTAL} \quad (3)$$

Where $Y_{c,t}$ is the absolute difference between the food supplied and the food demand, and Y_{TOTAL} represents the total food supplied in the specified region.

The parameters of this model include the level of water resources exploitation (surface and groundwater), the energy extraction from water resources, the production and consumption of non-conventional water in the region, water consumption in the drinking, agricultural, and industrial sectors, and the energy flow in the agricultural production system of the region.

To calculate the energy indicators for the studied products, the energy of input factors, including seeds, fertilizers, pesticides, machinery, water, labor, etc., used in agricultural operations, along with the product yield, were calculated based on their energy equivalents.

The inputs in agricultural systems can be divided into two forms: direct (renewable) and indirect (non-renewable) energy. Based on this categorization, direct energy includes human labor, diesel fuel, irrigation water, and electricity, while indirect

energy includes seeds, chemical fertilizers, animal manure, pesticides, and machinery (Yilmaz et al., 2005). Furthermore, human labor, seeds, irrigation water, and animal manure are considered renewable energy sources, while chemical fertilizers, diesel fuel, pesticides, and machinery are classified as non-renewable energy sources (Yilmaz et al., 2005). In the present study, the input energy for the studied products was calculated according to these categorizations.

Results and Discussion

Water, Food, and Energy Efficiency Indices under Different Scenarios

Based on the introduced efficiency indices in the previous step, the values of each of these indices were calculated (Table 2) to evaluate their interrelationships. The methodology involved calculating the levels of all three efficiency indices in the current state and after implementing each of the scenarios, thereby assessing the changes in the indices for each scenario. Considering the constraints considered for this optimization, a set of solutions (30 solutions) was obtained, and the results, according to the definition of the three water, food, and energy efficiency indices, are presented in Table 2. The aim was to select an optimal level of cultivation to achieve aquifer balance using a nexus approach with the three indices of water, food, and energy. Accordingly, the water, energy, and food efficiency indices was calculated based on the available statistics and information in the region.

Nexus Evaluation

After introducing corrective management sub-scenarios and determining the efficiency indices, these sub-scenarios were subjected to a nexus evaluation. Ultimately, out of the 30 defined sub-scenarios, 3 sub-scenarios were selected

for increasing efficiency in the three indices of water, food, and energy, taking into account their positive impact on these three indices simultaneously. These sub-scenarios were ranked using the TOPSIS method. In this method, the sub-scenario with the highest score is ranked first. Table 3 presents the final scores and rankings using this method.

Among the 30 proposed sub-scenarios, the sub-scenario of a 30% increase in the cultivation area of forage maize ranked first as the selected sub-scenario in terms of its positive impact on all three efficiency indices of water, food, and energy. As observed, according to this method, the sub-scenarios involving changes in the cultivation area of other dominant crops in the region such as wheat, barley, alfalfa, and canola had a negative impact on the efficiency indices.

Considering the environmental conditions of the region, recommending a 30% increase in the cultivation area of forage maize not only leads to an increase in food efficiency but also improves water and energy efficiency. This is because with the same amount of water and energy consumption, the crop yield increases within the same cultivation area. It should be noted that this prioritization is based on equal weighting of the three efficiency indices of water, food, and energy.

Figure 2 illustrates the performance comparison of implementing efficiency enhancement sub-scenarios with a nexus approach. As mentioned earlier, sub-scenarios involving changes in wheat varieties with full irrigation had the greatest positive impact on the nexus indices.

Prioritization of Selected Sub-scenarios with Equal Importance of Indices

Using the TOPSIS method and considering the specified weighting, the selected sub-scenarios are evaluated for prioritization.

Table 2. Water, Food, and Energy Efficiency under Different Scenarios

Scenario	sSb-scenarios	Energy efficiency (joules/kg)	Food efficiency	Water efficiency
	Scp1	26.716	0.808	8.537
	Scp2	25.292	0.745	8.537
	Scp3	23.825	0.682	8.537
	Scp4	28.100	0.871	8.537
	Scp5	28.102	0.871	8.537
	Scp6	28.105	0.871	8.537
	Scp7	28.979	0.845	8.537
	Scp8	29.971	0.819	8.537
	Scp9	31.096	0.793	8.537
	Scp10	28.195	0.869	8.537
	Scp11	28.293	0.867	8.537
	Scp12	28.393	0.864	8.537
	Scp13	28.538	0.863	8.537
	Scp14	29.001	0.855	8.537
	Scp15	29.487	0.847	8.537
	Scp16	29.440	0.934	8.537
	Scp17	30.744	0.997	8.537
	Scp18	32.012	1.061	8.537
	Scp19	28.095	0.871	8.537
	Scp20	28.090	0.872	8.537
	Scp21	28.095	0.871	8.537
	Scp22	27.309	0.898	8.537
	Scp23	26.601	0.924	8.537
	Scp24	25.960	0.950	8.537
	Scp25	28.001	0.874	8.537
	Scp26	27.906	0.876	8.537
	Scp27	27.812	0.879	8.537
	Scp28	27.677	0.880	8.537
	Scp29	27.275	0.888	8.537
	Scp30	26.891	0.896	8.537

The scenario of optimizing the cultivated area

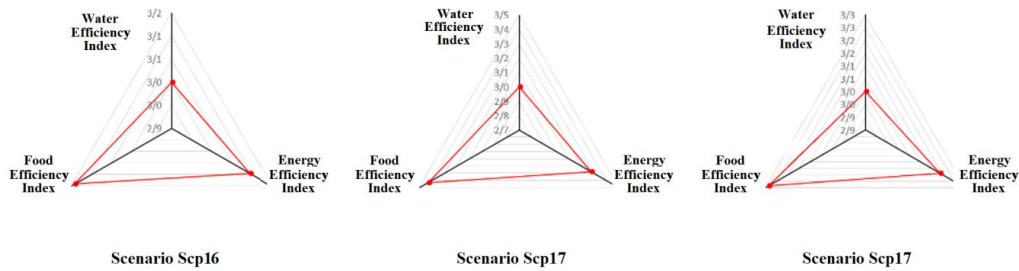


Fig 2. Radar graph of productivity increase scenarios with a Nexus approach

The TOPSIS method is a multi-criteria decision-making method used to prioritize different options based on various criteria. In this method, the importance of the indices is determined through weighting. Here, equal weights are assigned to the three efficiency indices of water, food, and energy, meaning that each of these indices is considered equally important in the prioritization process.

Table 3 illustrates the results of this prioritization. Based on this table, the sub-

scenarios can be ranked in order of priority based on the importance of different indices. By considering the importance level of each index, the prioritization of the proposed scenarios can be determined. In this study, for prioritizing the selected sub-scenarios conducted through the TOPSIS method (Table 3), equal weights are assigned to the three efficiency indices of water, food, and energy. However, it is possible to modify these weights based on specific decisions and policies.

Table 3. Prioritization of Selected Sub-scenarios using the TOPSIS method.

Prioritizing sub-scenarios	Description of sub scenarios	Sub-scenarios	Energy efficiency (joules/kg)	Food efficiency	Water efficiency
1	30% increase in the area under fodder corn cultivation scenarios	Scp18	3/279	3/431	3
2	20% increase in the area under fodder corn cultivation scenarios	Scp17	3/188	3/286	3
3	10% increase in the area under fodder corn cultivation scenarios	Scp16	3/096	3/142	3

Conclusion

The integration of water and energy consumption indices and food production in the analysis of management planning scenarios using a multi-criteria decision-making method can provide a more accurate analysis in selecting a powerful decision-making scenario for increasing efficiency with a nexus approach. By using a nexus approach, the effects of different

scenarios on water, food, and energy can be evaluated simultaneously. Ranking and analyzing the impact of implementing management scenarios in each of the water, food, and energy sectors enables managers to have a broader insight into the interests of the involved sectors. By considering the comprehensive impacts of these three interconnected sectors and weighing the effects of each criterion based on variable

policies, the management system of water resources and consumption can be directed towards increasing efficiency in water, food, and energy simultaneously. To improve the decision-making structure in agricultural production, the focus should shift from providing purely technical and structural scenarios to the modification of policies and infrastructures in the three sectors of water, food, and energy that significantly affect water and energy consumption and food production. This includes considering water, food, and energy efficiency and conducting detailed assessments of water resources and consumption.

The nexus approach to water resources and consumption management indicates that providing solutions to address crises in one sector without considering the other sectors will lead to greater problems. According to the nexus evaluation, sub-scenarios for changing the cultivation area of dominant crops in the region such as wheat, barley, alfalfa, and rapeseed not only carry high risks in terms of water supply, but also exhibit low efficiency in water, food, and energy criteria, resulting in negative scores compared to other sub-scenarios. Finally, among the 30 introduced sub-scenarios for improving efficiency, sub-scenarios for a 20%, 10%, and 30% increase in the cultivation area of forage maize showed positive impacts on the water, food, and energy efficiency indices. After prioritizing the influential sub-scenarios using the TOPSIS multi-criteria decision-making model, the sub-scenario for a 30% increase in the cultivation area of forage maize had the highest positive impact on water, food, and energy efficiency and was identified as the key scenario for evaluating efficiency in sustainable agricultural management.

Reference

- Alexandratos, N., & Bruinsma, J. (2012). World agriculture towards 2050/2030: the 2012 revision. *Rome, FAO: ESA working paper*. <https://doi.org/10.22004/ag.econ.288998>.
- Beisheim, M. (2013). The water, energy and food security nexus: how to govern complex risks to sustainable supply. *Stiftung Wissenschaft und Politik (SWP) Comments*. German Institute for International and Security Affairs. 32, 1-8. <https://www.swp-berlin.org/en/publication/water-energy-food-security-nexus>.
- Bizikova, L., Roy, D., Venema, H. D., McCandless, M., Swanson, D., Khachtryan, A., ... Zubrycki, K. (2014). Water-Energy-Food Nexus and Agricultural Investment: A Sustainable Development Guidebook. International Institute for Sustainable Development. <https://www.iisd.org/publications/report/water-energy-food-security-nexus-towards-practical-planning-and-decision>.
- Cai, X., Wallington, K., Shafiee-Jood, M., & Marston, L. (2018). Understanding and managing the food-energy-water nexus – opportunities for water resources research. *Advances in Water Resources*, 111, 259-273. <https://doi.org/10.1016/j.advwatres.2017.11.014>.
- Chapagain, A. K., & Hoekstra, A.Y. (2011). The blue, green and grey water footprint of rice from production and consumption perspectives. *Ecological Economics*, 70(4), 749-758. <https://doi.org/10.1016/j.ecolecon.2010.11.012>.
- Chilton, J., & Smidt, E. (2014). Diagnostic report UNECE region (2nd Draft). Groundwater governance—A global framework for action, GEF, UNESCO-IHP, FAO, World Bank and IAH. <http://www.groundwater-governance.org>
- Choudhury, I., & Bhattacharya, B. (2018). An assessment of satellite-based agricultural water productivity over the Indian region,

- International Journal of Remote Sensing*, 39(8), 2294-2311. <https://doi.org/10.1080/01431161.2017.1421792>.
- Dalin, C., Hanasaki, N., Qiu, H., Mauzerall, D. L. & Rodriguez-Iturbe, I. (2014). Water resources transfer through Chinese interprovincial and foreign food trade. *Proceedings of the National Academy of Sciences of the United States of America*, 111(27), 9774-9779. <https://doi.org/10.1073/pnas.1404749111>.
- D'Odorico, P., Carr, J., Laio, F., & Ridol, L. (2012). Spatial organization and drivers of the virtual water trade: a community-structure analysis. *Environ. Res. Lett.* <https://doi.org/10.1088/1748-9326/7/3/034007>.
- El-Gafy, I. (2017). Water–food–energy nexus index: analysis of water-energy-food nexus of crop's production system applying the indicators approach. *Applied Water Science*, 7, 2857-2868. <https://doi.org/10.1007/s13201-017-0551-3>.
- El-Gafy, I., Grigg, N. & Reagan, W. (2017a). Water-food-energy: nexus and non-nexus approaches for optimal cropping pattern. *Water Resource Management*, 31, 4971-4980. <https://doi.org/10.1007/s11269-0-1789-017>.
- FAO. (2012). Coping with water scarcity; an action framework for agriculture and food security, FAO water reports 38, FAO, Rom. <https://www.fao.org/>
- Garg, N.K. & Dadhich, S.M. (2014). Integrated non-linear model for optimal cropping pattern and irrigation scheduling under deficit irrigation. *Agric. Water Management*. 140, 1-13. <https://doi.org/10.1016/j.agwat.2014.03.008>.
- GEF. (2015). Global diagnostic on groundwater governance. Special Edition for WWF7. UNESCO.IHP. World Bank, FAO.
- Giordano, M., Scheierling, S. M., Tréguer, D. O., Turrall, H., & McCornick, P.G. (2019). Moving beyond 'more crop per drop': insights from two decades of research on agricultural water productivity. *International Journal of Water Resources Development*, 37(1), 137–161. <https://doi.org/10.1080/07900627.2019.1576508>.
- Gupta, A.D. (2017). Water-Energy-Food (WEF) Nexus and Sustainable Development. *Water-Energy-Food Nexus: Principles and Practices*, 229, 223. <https://doi.org/10.1002/9781119243175.ch19>.
- Halbe, J., Pahl-Wostl, C., Lange, M.A., & Velonis, C. (2015). Governance of transitions towards sustainable development – the water–energy–food nexus in Cyprus, *Water International*, 40(5-6), 877-894. <https://doi.org/10.1080/02508060.2015.1070328>.
- Hettiarachchi, H., & Ardkanian, R. (2016). Managing water, soil, and waste in the context of global change. Environmental resource management and the nexus approach. *Springer Cham Press*. <https://doi.org/10.1007/978-3-319-28593-1>.
- Hirwa, H., Zhang, Q., Li, F., Qiao, Y., Measho, S., Muhirwa, F., Xu, N., Tian, C., Cheng, H., Chen, G. & Ngwijabagabo, H. (2022). Water Accounting and Productivity Analysis to Improve Water Savings of Nile River Basin, East Africa: From Accountability to Sustainability. *Agronomy*, 12(4), 818. <https://doi.org/10.3390/agronomy12040818>.
- Holtz, G. (2013). Coherence of social practices: the case of meat consumption. Unpublished working paper, *Institute of Environmental Systems Research*, <http://www.usf.uos.de>.
- Kabote, S. J., & John, P. (2017). Water governance in Tanzania: performance of governance structures and institutions. *World Journal of Social Sciences and*

- Humanities*, 3(1), 15-25. <https://doi.org/10.12691/wjssh-3-1-3>
- Karamouz, M., Mohammadpour, P. & Mahmoodzadeh, D. (2017). Assessment of sustainability in water supply-demand considering uncertainties. *Water Resources Management*, 31(12), 3761-3778. <https://doi.org/10.1007/s11269-017-1703-9>.
- Karlberg, L., Hoff, H., Amsalu, T., Andersson, K., Binnington, T., Flores-López, F., de Bruin, A., Gebrehiwot, S. G., Gedif, B., zur Heide, F., Johnson, O., Osbeck, M., & Young, C. (2015). Tackling complexity: Understanding the food-energy-environment nexus in Ethiopia's lake TANA sub-basin. *Water Alternatives*, 8(1), 710-734. <http://www.water-alternatives.org/index.php/alldoc/articles/vol8/v8issue1/273-a8-1-6/file?auid=21>.
- Megdal, S. B., & Petersen-Perlman, J. D. (2018). Decentralized Groundwater Governance and Water Nexus Implications in the United State. *Jurimetrics*, 59(1), 99–119. <https://www.jstor.org/stable/27189255>.
- Molden, D. (Ed.). (2007). *Water for Food Water for Life: A Comprehensive Assessment of Water Management in Agriculture* (1st ed.). *Routledge*. <https://doi.org/10.4324/9781849773799>
- Rahimzadeh, Z., Javadi, S., Karimi, N., Hashemi Shahdani, S. M., & Kardan Moghadam, H. (2021). The WA+ Water Accounting Approach in Analyzing Water Resources and Water Use Balance (Case Study: Plasjan Watershed). *Journal of Water and Irrigation Management*, 12(1), 188-199. [In Persian] <https://doi.org/10.22059/jwim.2022.323091.868>.
- Rasul, G. & Sharma, B. (2016). The nexus approach to water-energy-food security: an option for adaptation to climate change. *Climate Policy*. 16, 682-702.
- Ray, D.K., N. Ramankutty, N.D. Mueller, P.C. West, & Foley, J.A. (2013). Yield trends are insufficient to double global crop production by 2050. *PLOS ONE*, 8(6), 1-8. <https://doi.org/10.1080/14693062.2015.1029865>.
- Rogers P, & Hall AW. (2003). Effective water governance. TEC Background Papers No. 7. Global Water Partnership. Stockholm, Sweden. <https://doi.org/10.12691/wjssh-3-1-3>.
- Sadeghi, S. H., Sharifi Moghadam, E., Delavar, M., & Zarghami, M. (2020). Application of water-energy-food nexus approach for designating optimal agricultural management pattern at a watershed scale. *Agricultural Water Management*, 233, 106071. <https://doi.org/10.1016/j.agwat.2020.106071>
- Salam, P. A., Pandey, V. P., Shrestha, S., & Anal, A. K. (2017). The need for the nexus approach. *Water-Energy-Food Nexus: Principles and Practices*, 1-10. <https://doi.org/10.1002/9781119243175.ch1>
- Saunier RE, Meganck RA. Meganck, R.A., & Saunier, R.E. (2009). *Dictionary and Introduction to Global Environmental Governance* (2nd ed.). *Routledge*. <https://doi.org/10.4324/9781849771009>.
- Shinde, VR. (2017). Water-Energy-Food Nexus: Selected Tools and Models in Practice. In: *Water-Energy-Food Nexus: Principles and Practices*. <https://doi.org/10.1002/9781119243175.ch7>
- Seekell, D., D'Odorico, P., & Pace, M. (2011). Virtual water transfers unlikely to redress inequality in global water use. *Environ Res Lett*, 6, 455-468. <https://doi.org/10.1088/1748-9326/6/2/024017>.
- Tork, H., Javadi, S., & Hashemy Shahdany, S.M. (2021). A new framework of a multi-criteria decision making for agri-

- culture water distribution system. *Journal of Cleaner Production*. <https://doi.org/10.1016/J.JCLEPRO.2021.127178>.
- UN. (2007). System of Environmental Economic Accounting for Water, United Nation Statistics Division, Geneva.
- UNDP. (2014). *Human Development Report*. <http://www.undp.org>.
- United Nations. (2013). World Population Prospects: The 2012 Revision, Key Findings and Advance Tables. Department of Economic and Social Affairs, ESA/P/WP.227. New York: United Nations.
- Varady RG, Weert F, Megdal SB, Gerlak A, Iskandar CA, House-Peters L, & McGovern ED. (2012). Groundwater policy and governance. Thematic Paper No 5. Groundwater Governance, a Global Framework for Action. GEF, WorldBank. UNESCO-IHP. FAO and IAH.
- Vörösmarty, C. J., Green, P., Salisbury, J., & Lammers, R. B. (2000). Global water resources: vulnerability from climate change and population growth. *Science* (New York, N.Y.), 289(5477), 284–288. <https://doi.org/10.1126/science.289.5477.284>.
- Yilmaz, I., Akcaoz, H., & Ozkan, B. (2005). An analysis of energy use and input costs for cotton production in Turkey. *Renewable Energy* 30, 145-155. <https://doi.org/10.1016/j.renene.2004.06.001>.
- Zhang, X., & Vesselinov, V.V. (2017). Integrated modeling approach for optimal management of water, energy and food security nexus. *Advances in Water Resources*, 101, 1–10. <https://doi.org/10.1016/j.advwatres.2016.12.017>.
- Zhu, Y., Zhang, C., Fang, J., & Miao, Y. (2022). Paths and strategies for a resilient megacity based on the water-energy-food nexus. *Sustainable Cities and Society*, 82, 103892. <https://doi.org/10.1016/j.scs.2022.103892>.



Monitoring Changes in Rice Cultivation Area Using Multi-Temporal Satellite Images (Case Study: Beiranshahr Region, Iran)

Samad Abdi¹, Mohsen Ahmadede², Rabee Rustum³, Anahid Salmanpour¹

1. Soil and water research institute, Lorestan Agricultural and Natural Resources Research and Education Center, Agricultural Research, Education and Extension Organization (AREEO), Khoramabad, Iran.
2. Lorestan Agricultural and Natural Resources Research Center, AREEO, Khorramabad, Iran.
3. Heriot-Watt University, Dubai Campus, Dubai Knowledge Park, Dubai, UAE.

*Corresponding author: S.abdi@areeo.ac.ir

Keywords:

Landsat 8; Mann-Kendall test; NDVI; Rice Cultivation; Sentinel 1.

Abstract

In arid and semi-arid regions, cultivating crops with high water demand can seriously threaten water resources. This research was conducted to investigate the expansion of rice cultivation areas from 2013 to 2021 in this region. For this purpose, using Landsat 8 and Sentinel 1 satellite images, the changes in rice cultivation in this area were determined. After radiometric and atmospheric corrections, the Normalized Difference Vegetation Index (NDVI) was calculated. The vegetation area in hectares was obtained using the pixel size of the images. Finally, the change in vegetation area with time was plotted graphically. For more certainty, the cultivated area in August 2021 was also determined with radar images. After performing the preprocess corrections (thermal noise removal, calibration, terrain flattening, multilink, speckle filter and terrain correction), a suitable RGB image was created. Then sampling was done on different classes of land. The final land cover map was prepared using a random forest algorithm. In order to estimate the trend in the time series of area change, the MannKendall test was used and the nonparametric Sen's method was used to determine the slope of a linear trend. The results showed that the area under rice cultivation has increased from 2,564 hectares in 2013 to 4,771 hectares in 2021. The results of the Mann-Kendall test showed that a positive increasing trend exists in the data series. Investigating the underground water level showed that the depth of the water in some parts of the region has reached 10 meters, while in the past, the depth of the underground water in this region was less than 2 meters. These findings show that increasing rice planting in this region can endanger the region's water resources, and in the long term, the region will face serious challenges. Therefore, it is recommended to limit rice cultivation in the region and cultivate crops with less water demand instead.

Received:

03 September 2023

Revised:

11 October 2023

Accepted:

13 October 2023

How to cite this article:

Abd, S., Ahmadede, M., Rustum, R., & Salmanpour, A. (2024). Monitoring Changes in Rice Cultivation Area Using Multi-Temporal Satellite Images (Case Study: Beiranshahr Region, Iran). *Journal of Drought and Climate change Research (JDCR)*, 2(6), 77-92. [10.22077/jdcr.2023.6743.1040](https://doi.org/10.22077/jdcr.2023.6743.1040)



Introduction

Determining the agricultural area is one of the most important stages for monitoring the crop produced in each region. Knowing the type of crops cultivated in each region helps policymakers to make correct decisions regarding the food needs of the population covered by each region (IPBES, 2019; Sadoghi *et al.*, 2021). This issue is so important, especially for developing countries, including Iran, since accurate agricultural statistics are important for food security and economic planning (Nicholson *et al.*, 2021). On the other hand, rural life and food security depend on agricultural lands, especially in Iran. Optimal land use requires correct and accurate management by national and provincial officials. Policymakers, knowing the level of crops under cultivation, can provide services and equipment according to the existing assets. In addition, this information will determine the real potential of agricultural areas and prevent them from changing their use. The first step in managing and controlling agricultural land is to observe the current situation and examine the trend of land use changes in the last few decades.

Remote sensing technology provides this information with low time and cost to achieve sustainable goals (Weiss *et al.*, 2020). In fact, remote sensing is one of the fast and most suitable tools for monitoring the cultivated area. Using this tool, it is possible to determine the expansion or reduction of the cultivated area even for years when data are unavailable without going to the fields and spending time and money (Mousavi *et al.*, 2022). Multi-temporal satellite images have the ability to distinguish different types of agricultural crops from each other (Pourgholam and Rahimzadegan, 2017). This method has been applied by researchers in recent years. In Iran, Pourgholam and Rahimzadegan

(2017) investigated the area of saffron cultivation in Torbat Heydarieh using this method. These researchers reported that if the normalized difference vegetation index (NDVI) index is used as one of the vegetation survey methods (Renza *et al.*, 2017), the cultivated area will only be 5.7% different from the observational data collection. Research conducted by Riahi *et al.* (2019) also showed the appropriate accuracy of using remote sensing in Iran. Tamela and Hailu (2020) integrated Sentinel-1A Synthetic Aperture Radar (SAR) with Sentinel-2 multispectral sensor (MSI) images to map rice field extent in a tropical area, Fogera Wereda, Ethiopia. These researchers concluded that the VH polarization of Sentinel-1A is suitable for rice field mapping. Mansaray *et al.* (2017) used optical and Radio Detection and Ranging (RADAR) remote sensing data to map and monitor rice growth.

Rice (*Oryza sativa* L) is one of the most important food sources in the world. It is the food of half of the world's people, and its consumption is increasing every year (FAO, 2017). The average area under rice production in Iran in the last five years has been about 517 thousand hectares, and the average production has been 1980 thousand tons, which has increased by about 7.5% compared to 2012 (Anonymous, 2018). In Iran, with an average rainfall of 250 mm per year, only two provinces, Mazandaran and Gilan, have a high average rainfall of about 1000 mm per year. Other provinces are facing water shortage problems (Anonymous, 2021). Therefore, about 71% of rice cultivation is in these two abovementioned provinces, and other provinces cover the remaining 29% (Anonymous, 2018). Based on various factors, including high profit and short growing seasons, the desire of farmers in other provinces to

cultivate rice has increased in recent years. This subject is noticeable considering Iran's arid and semi-arid climate and the problems caused by water scarcity (Yaghoobzadeh *et al.*, 2017a, b). On the other hand, the rainy season in Iran is from mid-Autumn (October) to late winter (April), which does not coincide with the rice-growing season in summer. For this reason, rice cultivation in Iran has always faced various challenges and problems. Lorestan province, in Iran, where rice cultivation has expanded in recent years, faces water scarcity. The average cultivated area in this province is estimated to be around 10 thousand hectares (Anonymous, 2018). However, according to some local data, due to a lack of water, this amount has decreased to less than 7 thousand hectares in 2021. This subject has caused pressure on the water resources of this province. Because there were no accurate statistics on the change in rice cultivation in some areas of this province, including the Beiranshahr region, this research evaluated the change in rice cultivation area using multi-temporal satellite data.

Material and Methods

Study Area

Beiranshahr region is located in the north of Khorramabad city in Lorestan province, western Iran, at latitude $48^{\circ} 33' 42.31''$ N and longitude $33^{\circ} 38' 1.31''$ E (Figure 1). Beiranshahr has a mountainous climate with cold and snowy winters and mild summers. The occupation of its people is mostly agriculture and animal husbandry. Soil moisture and thermal regimes are Xeric and Mesic, respectively. There is no evidence to suggest that the area lacks the necessary background conditions for rice cultivation. However, rice cultivation suddenly started on a large scale in this area in 2013. Therefore, we used Landsat

8 satellite images and Sentinel-1 radar images to monitor changes in the rice cultivation area. We first used Landsat 8 images to determine changes in the total crop cover in the area. We used the high accuracy of radar images to confirm the cultivated area in August 2021. Since the highest canopy cover for summer crops is in August, the images in this month were compared in different years.

Landsat 8 satellite images

Suitable images without a cloud cover of the Landsat 8 satellite were downloaded from the <https://earthexplorer.usgs.gov> website. The images from 2013 to 2021 belong to August. The characteristics of the images used in the research are shown in Table 1. In order to obtain multitemporal and multispectral reflection data on farmland and also to derive the time series of vegetation indices, which are calculated as a function of the red, green, blue, and infrared spectral bands, these satellite sensors can be used (Zhao *et al.*, 2021).

Images preprocessing

After downloading the images, a subset of images was taken according to the region boundary. Then the geometrical and georeferencing conditions of the images were checked. In this case, Landsat 8 images are reference images for geometric correction of other images and maps. For this reason, these images did not require geometric correction. A radiometric correction was used to reduce or eliminate two major types of atmospheric and sensor errors. Quick atmospheric correction (QAC) was used for atmospheric correction because its application speed is high compared to other atmospheric correction methods, and its absolute results are normal. It does not require the presence of other special bands for water absorption and aerosol dispersion.

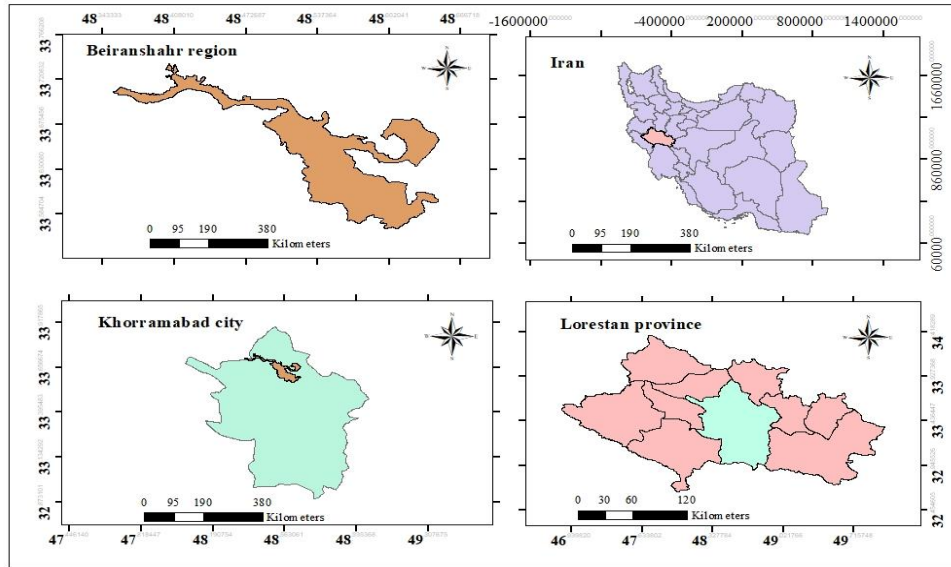


Fig 1. Location of study area

Table 1. The characteristics of the images used in the research

Row	Path	Date	Satellite	Sensor	Spatial resolution (m)	Number of bands
37	166	20130829	Landsat 8	OLI_TIRS	30	7
37	166	20140828	“	“	“	“
37	166	20150819	“	“	“	“
37	166	20160805	“	“	“	“
37	166	20170808	“	“	“	“
37	166	20180811	“	“	“	“
37	166	20190814	“	“	“	“
37	166	20200816	“	“	“	“
37	166	20210819	“	“	“	“

NDVI calculation

In this step, to convert the radiance values recorded by the sensor into the surface reflectance, all values that are smaller than zero are multiplied by zero, then values that are greater than ten thousand (10000) are set equal to one, and finally, all values that are greater than zero and smaller than one are multiplied by the 1/10000 ratio. In this way, all values are in the range of zero and one, according to Equation 1:

$$\text{Float} ((\text{MS} \leq 0) \times 0 + (\text{MS} \geq 10000) \times 1 + (\text{MS} > 0 \text{ and } \text{MS} < 10000) \times \text{float} (\text{MS} / 10000 / 0)) \quad (1)$$

Where the MS values are the multispectral bands of the Landsat 8 OLI sensor. Then the normalized difference vegetation index (NDVI) is calculated from Equation 2:

$$\text{NDVI} = (\text{NIR} - \text{Red}) / (\text{NIR} + \text{Red}) \quad (2)$$

Where, NIR and red are the near-infrared and red bands of Landsat 8, respectively. The numerical value of this index is between +1 and -1, and it has been proven that the closer this index is to +1, the higher the amount of vegetation (Yaghoobzadeh, 2015).

After preparing the NDVI maps, the studied area was classified into two classes: land with vegetation and land without vegetation (harvested area in August). In this research, NDVI values less than 0.2 belong to the class of land without vegetation, and more than that belongs to the vegetation class.

In the next step, the raster maps of NDVI were converted into vectors, and the

vegetation area in hectares was obtained using the pixel size of the images. Finally, the change in vegetation area with time was plotted graphically.

Sentinel-1 radar images

In order to accurately identify crop areas, a vegetation map of the area was prepared using radar images. Suitable

radar images of the Sentinel-1 satellite were downloaded from the <https://scihub.copernicus.eu> website. The radar images were from 2021 and the months of July, August, and September. Radiometric and geometric corrections and other processes were done on the images according to the diagram below:

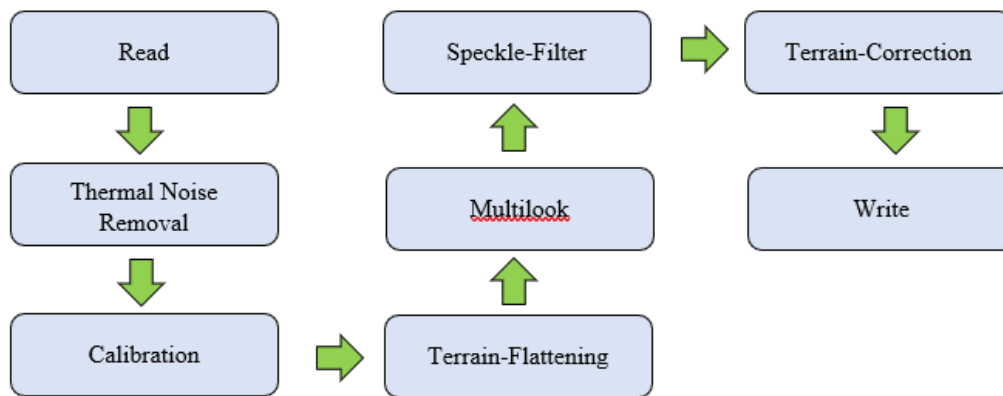


Fig 2. Processing steps performed on Sentinel 1 radar images

After performing the abovementioned processes, a suitable RGB image was created. Then sampling was done in different classes of land. The final land cover map was prepared using a random forest algorithm.

Validation and accuracy assessment

The error matrix was used to evaluate the accuracy of the classified map obtained from the radar images. Kappa coefficient, overall accuracy, producer accuracy, user accuracy, commission and omission parameters were used to evaluate the results. The overall accuracy is obtained from the ratio of the number of correctly classified pixels to the total number of classified pixels in all classes. Which can be calculated from the following relationship:

$$OA = \frac{1}{N} \sum P_{ii} \quad (3)$$

Where OA is overall accuracy, is the sum

of elements of the principal diameter of the error matrix, and N is the total number of training pixels.

Due to the defects in the overall accuracy of executive tasks, the kappa coefficient is also used to determine the classification accuracy. Because of this index, incorrectly classified pixels are also considered. The Kappa coefficient is calculated according to the following relationship:

$$Kappa = \frac{p_o - p_c}{1 - p_c} \quad (4)$$

Where p_o is the correct observation and p_c is the expected agreement. Producer accuracy indicates the probability that the producer has assigned a pixel to a certain class if its true class is known, and in the error matrix, it is the ratio of correct pixels to the total number of pixels in a column.

The user accuracy is the probability of classifying a certain class in the map

according to the same class in the ground, and in the error matrix, it is the ratio of correct pixels to the total number of pixels in a row.

The error of commission is a percentage of pixels that do not belong to the desired class, but are placed in that class, and the error of omission is the percentage of pixels that actually belong to the desired class, but are mistakenly placed in another class (Lennon, 2006).

Mann-Kendall test for trend and Sen's slope estimation

In order to estimate the trend in the time series of area change in the studied region, the Mann-Kendall test was used and the nonparametric Sen's method was used to determine the slope of a linear trend.

When the data values x_i of a time series can be assumed to obey the model below, the Mann-Kendall test is applicable:

$$x_i = f(t_i) + \varepsilon_i \quad (5)$$

Where $f(t)$ is a continuous monotonic increasing or decreasing function of time and the residuals ε_i can be assumed to be from the same distribution with a zero mean. It is therefore assumed that the variance of the distribution is constant over time.

We want to test the null hypothesis of no trend, H_0 , i.e., the observations x_i are randomly ordered in time, against the alternative hypothesis, H_1 , where there is an increasing or decreasing monotonic trend. For time series with less than 10 data points, the S test is used, and for time series with 10 or more data points the normal approximation is used. The S test was used in this study because our data was less than 10 points. The Mann-Kendall test statistic S is calculated using the following formula:

$$S = \sum_{k=1}^{n-1} \sum_{j=k+1}^n \text{sgn}(x_j - x_k) \quad (6)$$

Where x_j and x_k are the annual values in years j and k , $j > k$, respectively, and

$$\text{sgn}(x_j - x_k) = \begin{cases} 1 & \text{if } x_j - x_k > 0 \\ 0 & \text{if } x_j - x_k = 0 \\ -1 & \text{if } x_j - x_k < 0 \end{cases} \quad (7)$$

If n is 9 or less, the absolute value of S is compared directly to the theoretical distribution of S derived by Mann and Kendall (Gilbert, 1987). The two-tailed test is used for four different significance levels α : 0.1, 0.05, 0.01 and 0.001. At a certain probability level, H_0 is rejected in favor of H_1 if the absolute value of S equals or exceeds a specified value $S\alpha/2$, where $S\alpha/2$ is the smallest S that has a probability less than $\alpha/2$ to appear in the absence of a trend. A positive (negative) value of S indicates an upward (downward) trend.

Sen's method

To estimate the true slope of an existing trend (as change per year), Sen's nonparametric method is used. Sen's method can be used in cases where the trend can be assumed to be linear. This means that $f(t)$ in equation (1) is equal to:

$$f(t) = Qt + B \quad (8)$$

Where Q is the slope and B is a constant. To get the slope estimate Q in the equation above, the slopes of all data value pairs must be calculated.

$$Q_i = \frac{x_j - x_k}{j - k} \quad (9)$$

Where $j > k$.

If there are n values x_j in the time series, we get as many as $N = n(n-1)/2$ slope estimates Q_i . Sen's estimator of slope is the median of these N values of Q_i . The N values of Q_i are ranked from the smallest

to the largest and Sen's estimator is

$$Q = Q_{\lfloor \frac{N+1}{2} \rfloor} \text{ if } N \text{ is odd} \quad (10)$$

$$Q = \frac{1}{2} \left(Q_{\lfloor \frac{N}{2} \rfloor} + Q_{\lfloor \frac{N+2}{2} \rfloor} \right) \text{ if } N \text{ is even} \quad (11)$$

A $100(1-\alpha)\%$ two-sided confidence interval about the slope estimate is obtained by the nonparametric technique based on the normal distribution. The method is valid for n as small as 10 unless there are many ties (Salmi *et al.*, 2002).

Groundwater changes

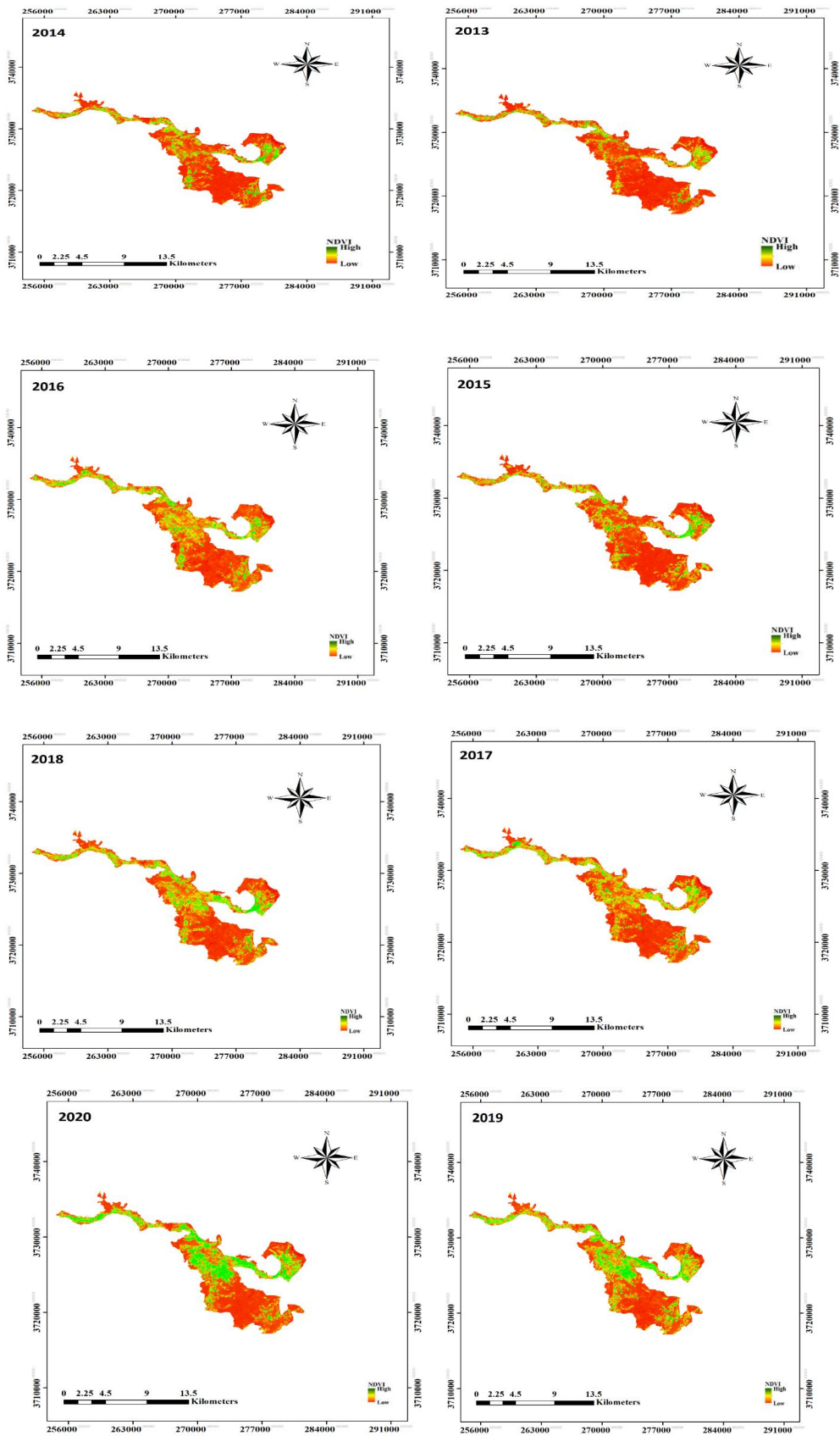
Using the groundwater data given by Lorestan Regional Water Company, a water table level change map was created. The data included the water depth of the wells in the region during 2005 to 2021. The water table map was obtained by using the IDW algorithm. In order to create the maps, ArcGIS 10.8.2, ENVI 5.3, SNAP 7.0, and Excel 2021 were used.

Results and Discussion

The crop cover changes in the main part of the study area are shown in Figure 3. The crop cover for rice has increased significantly since 2013. In the past, in the summer season, especially in August, the crop cover area was reduced after harvesting the spring crops. But with the extension of rice cultivation in the region, this trend has reversed, and the crop cover in the region has increased in the summer. The reason for the increase in rice cultivation in the region is the high price of this product on the market; this issue has caused the cultivation of other products to be abandoned. In the past, only some summer crops, such as cucumbers and fodder crops, have been cultivated in a limited area. The small amount of vegetation in 2013 is mainly related to these crops. But in 2021, most of the vegetation

will be related to rice cultivation (Figure 3). Based on NDVI images, the area under cultivation of summer crops has increased in recent years. These changes are mainly in the northwestern and central parts of the region. Because they are located upstream of the river, their access to water takes priority. In addition, the field conditions for farming in these areas are better. The changes in 2020 and 2021 are such that the area of fallow land is almost zero. In 2021, all arable land was used for rice cultivation. Since agricultural lands are bounded by the mountains from the south and part of the west, the land under rice cultivation could not be expanded. The largest expansion of cultivated rice land in the center of this region occurred due to its flatness. In Figure 4, cultivation changes in the center of this region during the years 2013 to 2021 are shown.

To get more detailed information, the cultivated area in August 2021 was also determined with radar images. To avoid repeating the results, only the map for 2021 is shown (Figure 5). According to Table 2, the area of vegetation in this map was 4113 hectares, which is almost close to the area calculated from the NDVI map of 2021. The validation results of this map are shown in Table 3. According to the Kappa coefficient and overall accuracy, with values of 72% and 82%, respectively, this map has good validity. Extracting the same results for the rest of the year showed the amount of vegetation has increased from 2564 hectares in 2013 to 4771 hectares in 2021, which is almost 1.8 times (Figure 6). The net water requirement of rice is about 10,000 cubic meters during the growing season in this area (Ghorbani Vaghei *et al.*, 2021). This amount is about twice as much as other summer crops in this region. However, the water loss



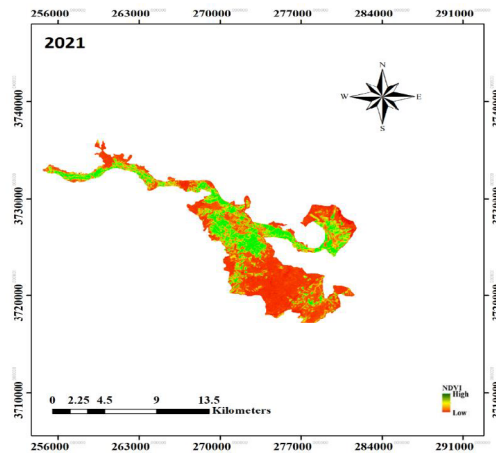


Fig 3. NDVI changes in the Beiranshahr region from 2013 to 2021 in August

is high due to the soil texture, seepage from the rice basins, and the irrigation method. This issue increases the gross water requirement for rice by about 1.5 times. For this reason, one hectare of rice consumes about three times as much water as other summer crops. In addition, due to the changes in rice cultivation area, water consumption has increased by more than 33 million cubic meters in 2021 compared to 2013. This condition is more critical due

to the fallowness of rice cultivated land in the past. Indeed, considering that the Beiranshahr region is located in a semi-arid climate, the increase in rice cultivation in the region can cause great damage to water resources.

For more certainty, the cultivated area in August 2021 was also determined with radar images. To avoid repeating the results, only the map for 2021 is shown (Fig. 5).

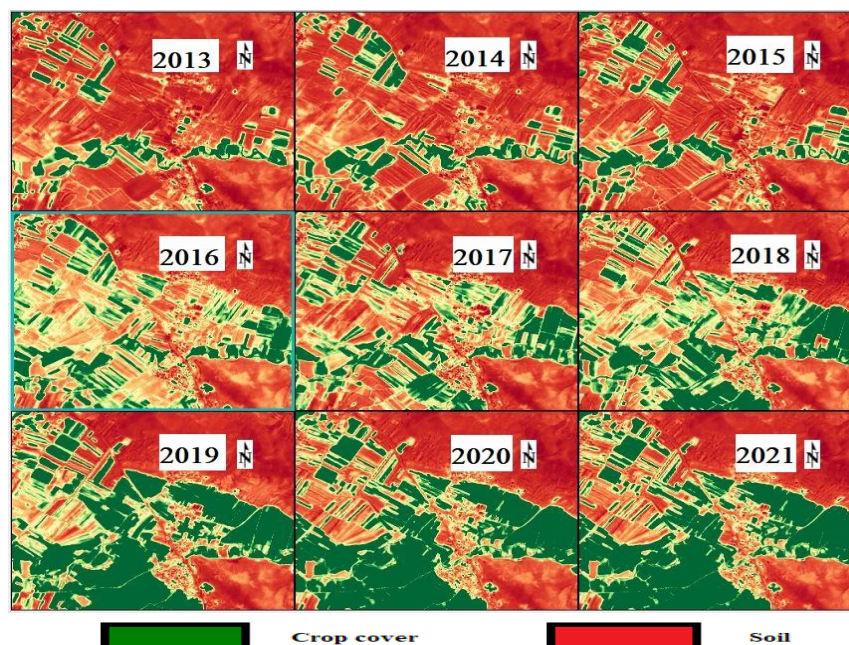


Fig 4. Vegetation changes trend in a part of the region in August from 2013 to 2021

According to Table 2, the area of vegetation in this map was 4113 hectares, which is almost close to the area calculated from the

NDVI map of 2021.

The validation results of this map are shown in Table 3.

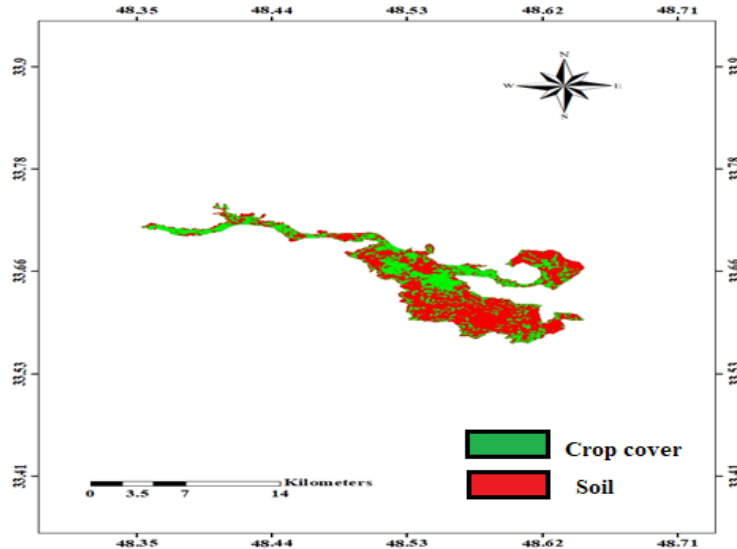


Fig 5. Map produced using Sentinel 1 radar images

Table 2. The area of rice fields according to the map extracted from Sentinel 1 radar images

Total area (hectare)	10466.48
Rice cultivation area (hectare)	4113.33

Table 3. Accuracy coefficients of the classified map using Sentinel -1 radar images

Class	Producer accuracy	User accuracy	Omission	Commission	Kappa	Overall accuracy
Mountainous area	93	96	6.67	3	0.72	82
Other crops	67	74	33.3	25.9		
Rice	85	77	15	22.7		

Table 4. The calculation of the Mann-Kendall test for data time serie

Name	area
Years	2013 - 2021
n	9
Test S	27
Signific.	**
Q	2.30E+02
B	3.14E+03

This map has good accuracy, according to the Kappa coefficient and overall accuracy of 72% and 82% respectively.

Extracting the same results, for the other years, showed the amount of vegetation has increased from 2564 hectares in 2013

to 4771 hectares in 2021, which is almost 1.8 times.

The calculation of the Mann-Kendall test for trend and the nonparametric Sen's method for magnitude of the trend are presented in Table 4 and Figure 6.

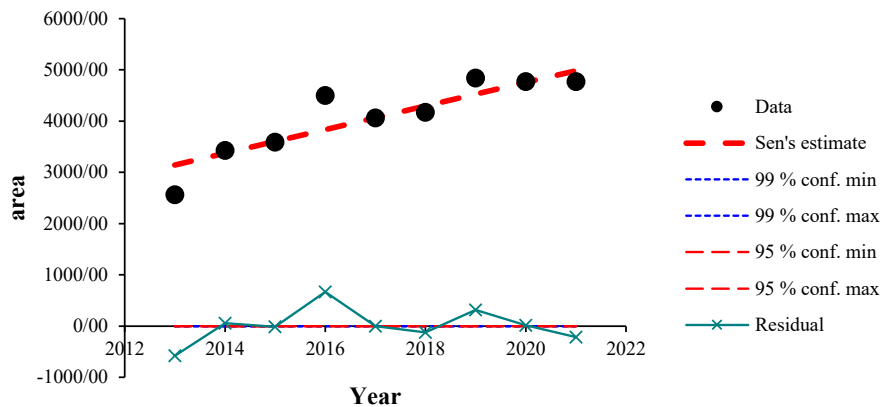


Fig 6. Trend statistics of vegetation area in Beiranshahr region in August from 2013 to 2021

As can be seen from Table 4, the S test is significant at the 0.01 level of significance statistically, and a positive increasing trend exists in the data series. The trend seems to be monotonic and thus the Mann-Kendall test is suitable. In table 4, Q and B are the slope and constant of the estimated equation for the illustrated line in Figure 6. Kamkar *et al.*, (2019) detected the rice and soybean grown fields and their related cultivation areas using Sentinel-2 satellite images in summer cropping patterns to analyze temporal changes in their cultivation area in Golestan province, Iran. They concluded that the soybean cultivation areas which is an alternative plant for rice in summer cropping, has decreased compared to past years and rice cultivation has increased.

Zhang *et al.* (2017) showed that acreage derived from the MODIScrop maps was generally consistent with that reported in the FAO data (a relative error of <4.1% for rice and <6.1% for maize, and <9.0% for soybean except for in 2004, 2008, and 2009) and the maps derived from the LScrop (a relative error of about 5% in 2013, and 7% in 2008 and 2014).

The net water requirement of rice is about

10,000 cubic meters during the growing season (Ghorbani Vaghei *et al.*, 2021). This amount is about twice as much as other summer crops in this region. Although the water loss is high due to the soil texture, seepage from the rice basins, and the irrigation method, This issue increases the gross water requirement for the rice by about 1.5 times. For this reason, one hectare of rice consumes about three times as much water as other summer crops. In addition, due to the changes in rice cultivation area, water consumption has increased by more than 33 million cubic meters in 2021 compared to 2013. This condition is more critical due to the fallowness of rice cultivated land in the past. Indeed, considering that the Beiranshahr region is located in a semi-arid climate, the increasing rice cultivation in the region can cause great damage to water resources. The map of the increase in the depth of water table level in the region is shown in Figure 7.

According to the map, the reservoir's depth has increased by 1 to 10 meters over the last ten years. The changes in water table depth in the central areas, which have the largest area under rice cultivation, are

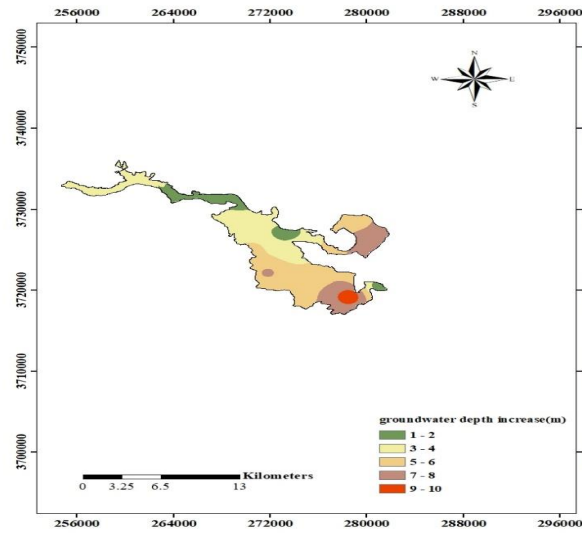


Fig 7. changes of water table depth during 2013 to 2021 in Beiranshar region, Iran



Fig 8. the status of the river in 2013 (up) and the holes dug in 2021 (down)

between 3 and 6 meters. The map marks two areas with lower water level changes, between one and two meters, in green. The permanent river in this region experiences a low flow in the summer due to a decrease in rainfall and a lack of snow reserves in the upstream mountains. The image related to this river in 2021 is shown in Figure 8. With the occurrence of drought in the region in recent years, the farmers dug the riverbed to get water. Figure 8 shows a photo of the holes drilled by farmers in the river bed.

Although these problems are related to climate change and recent droughts, the increase in rice cultivation cannot be ignored. Some researchers relate the problems of water resources in Iran only to drought, climate change and structural factors (Mardani et al., 2016; Zarepour Moshizi *et al.*, 2022), but social problems such as inflation and income reduction, which lead to encouraging farmers to grow rice, are mostly ignored. Most of the world's people, especially in the MENA region, will experience a severe water crisis by 2050. For this reason, most Iranian researchers stated that Iran would face a worrying prospect if they did not set the correct management and suitable domestic and international policies for the future (Rezayan and Rezayan, 2016). However, it is possible to prevent the increase in the cultivation of crops with high water consumption, such as rice, by solving social problems in areas where there was no history of rice cultivation until a decade ago. This will help save water resources and manage them better.

Most people in the world, especially in Africa and the Middle East, will experience severe water crises by 2050. Iran will face the worrying prospect that if it does not set the correct management and suitable domestic and international policies for

the future (Rezayan and Rezayan, 2016), Drying lakes and rivers demonstrate the critical level of water situation in Iran that is escalated by frequent droughts and overuse of surface and groundwater, so that this country is facing water bankruptcy where water demand exceeds the natural water supply (Madani et al., 2016).

Conclusion

Paddy rice distribution maps are of great importance for assessing and understanding water use at regional, national, and global scales. The results of this research showed that the area under rice cultivation in the Biranshahr region has increased significantly from 2013 to 2021. In general, increasing the planting of water-consuming crops such as rice in arid and semi-arid regions can endanger the water resources of the region, and in the long term, the region will face serious challenges. Therefore, it is recommended to limit the cultivation of rice in the region and cultivate crops with less water consumption instead. The development of pressurized irrigation systems in the region can help save water consumption. Local farmers neglect the water shortage and its future problems due to a lack of awareness; therefore, it is the responsibility of the government to inform the local farmers and conserve the groundwater resources.

References

- Anonymous. (2018). Statistical Center of Iran, available at www.amar.org.ir/english.
- Anonymous. (2021). Statistical Center of Iran, available at www.amar.org.ir/english.
- FAO. (2017). FAOSTAT. Statistical Databases. Food and Agriculture Organization of the United Nations. [http:// www.fao.org](http://www.fao.org).
- Ghorbani Vaghei, H., Sabouri, H., & Taliei, F. (2021). A new method for provid-

- ing water requirement of rice culture based on near-saturated soil matric potential, *Water and Irrigation Management*, 11(3), 421-432. DOI: 10.22059/JWIM.2021.319595.864 [In Persian].
- Gilbert, R.O. (1987). *Statistical methods for environmental pollution monitoring*. Van Nostrand Reinhold, New York.
- IPBES. (2019). *Global assessment report on biodiversity and ecosystem services of the Intergovernmental Science-Policy Platform on Biodiversity and Ecosystem Services*. E. S. Brondizio, J. Settele, S. Díaz, and H. T. Ngo (editors). IPBES secretariat, Bonn, Germany. <https://doi.org/10.5281/zenodo.3831673>.
- Kamkar, B., Dashtimarvili, M., & Kazemi Posht Msary, H. (2019). Detection of rice and soybean grown fields and their related cultivation area using Sentinel-2 satellite images in summer cropping patterns to analyze temporal changes in their cultivation area (Case study: four watershed basins of Golestan Province). *Journal of Water and Soil Conservation*, 26(1), 151-167. Doi: 10.22069/jwsc.2019.15246.3044 [In Persian].
- Lennon, R. (2006). *Remote sensing digital image analysis: An introduction*. United States: Esa/Esrin, 4th Edition, Chapter 1, Springer, Germany, Berlin, Heidelberg.
- Madani, K., AghaKouchak, A., & Mirchi, A. (2016). Iran's Socio-economic Drought: Challenges of a Water-Bankrupt Nation. *The International Society for Iranian Studies*, 49(6), 997-1016.
- Mansaray, L.R., Huang, W., Zhang, D., Huang, J., & Li, J. (2017). Mapping Rice Fields in Urban Shanghai, Southeast China, Using Sentinel-1A and Landsat 8 Datasets. *Remote Sensing*, 9(3), 257. <https://doi.org/10.3390/rs9030257>.
- Mousavi, S. R., Sarmadian, F., Omid, M., & Bogaert, P. (2022). Three-dimensional mapping of soil organic carbon using soil and environmental covariates in an arid and semi-arid region of Iran, *Measurement*, 201, 111706. <https://doi.org/10.1016/j.measurement.2022.111706>
- Nicholson, Ch, F., Stephens, E. C., Kopainsky, B., Jones, A. D., Parsons, D., & Garrett, J. (2021). Food security outcomes in agricultural systems models: Current status and recommended improvements, *Agricultural Systems*, 188, 103028. <https://doi.org/10.1016/j.agsy.2020.103028>
- Pourgholam, M. & Rahimzadegan, M. (2017). Identification of the area under cultivation of saffron using landsat 8 temporal satellite images (case study: Torbat Heydarieh). *Journal of Remote Sensing and Geographic Information System in Natural Resources*, 7(4), 97-115. https://girs.bushehr.iau.ir/article_528884.html?lang=en [In Persian].
- Renza, D., Martinez, E., Molina, I., & Ballesteros, D.M. (2017). Unsupervised change detection in a particular vegetation land cover type using spectral angle mapper, *Advances in Space Research*, 59(8), 2019-2031. <https://doi.org/10.1016/j.asr.2017.01.027>
- Rezayan, A., & Rezayan A.H. (2016). Future studies of water crisis in Iran based on processing scenario. *Iranian Journal of Ecohydrology*, 3(1), 1-11. DOI: 10.22059/IJE.2016.59185 [In Persian].
- Riahi, V., Zeaiean Firouzabadi, P., Azizpour, F., & Darouei, P. (2019). Identification and investigation of the area under cultivation in Lenjanat using Landsat 8 satellite images. *Journal of Applied researches in Geographical Sciences*, 19(52), 147-169. DOI: 10.29252/jgs.19.52.147 [In Persian].

- Sadoghi, H., Rajaei, T., & Rouhani, N. (2021). Identification and Investigation of Changes in Area of Hoseynabade Mishmast Village Using Satellite Images. *Journal of Water and Soil Science*, 24(4), 239-254. DOI: 10.47176/jwss.24.4.42521 [In Persian].
- Salmi, T., Määttä, A., Anttila, P., Ruoho-Airola, T. & Amnell, T. (2002). Detecting trends of annual values of atmospheric pollutants by the mann-kendall test and sen's slope estimates -the excel template application makesens. Finnish Meteorological Institute. *Publications on Air Quality*. FIN-00101 Helsinki, Finland.
- Talema, T., & Hailu, B.T. (2020). Mapping rice crop using sentinels (1 SAR and 2 MSI) images in tropical area: A case study in Fogera wereda, Ethiopia, *Remote Sensing Applications, Society and Environment*, 18,100290. <https://doi.org/10.1016/j.rsase.2020.100290>.
- Weiss, M., Jacob, F., & Duveiller, G. (2020). Remote sensing for agricultural applications: A meta-review. *Remote Sensing of Environment*, 236, 111402. <https://doi.org/10.1016/j.rse.2019.111402>
- Yaghoobzadeh, M., Ahmadee, M., Boroomand Nasab, S., & Haghayeghi Maghamam, S.A. (2017), Impact of Climate Change on Changing Trend of Evapotranspiration during the Growth Period of Irrigated and Rainfed Field Crops by AOGCM Models, *Iranian Journal of Water Research in Agriculture (Formerly Soil and Water Sciences)*, 30(4), 511-523. <https://doi.org/10.22092/jwra.2017.109013> [In Persian].
- Yaghoobzadeh, M., Ahmadee, M., Seyyed Kaboli, H., Zamani, Gh. R., & Amirabadi-zadeh, M. (2017), The evaluation of effect of climate change agricultural drought using ETDI and SPI indexes, *Journal of Water and Soil Conservation*, 24(4), 43-61. DOI: 10.22069/JWFSt.2017.12202.2671 [In Persian].
- Yaghoobzadeh, M. (2015). The simulation of evapotranspiration and moisture soil for agricultural drought evaluation in the base line and future by using remote sensing, Ph. D. dissertation, Shahid Chamran University of Ahvaz, Ahvaz. [In Persian].
- Zarepour Moshizi, M., Yousefi, A., Mozafar Amini, A., & Shojaei, P. (2022). Rural vulnerability to water scarcity in Iran: an integrative methodology for evaluating exposure, sensitivity and adaptive capacity, *Geo Journal*. <https://doi.org/10.1007/s10708-022-10726-0>
- Zhang, H., Li, Q., Liu, J., Shang, J., Du, X., Zhao, L., Wang, N., & Dong, T. (2017). Crop classification and acreage estimation in North Korea using phenology features. *GIS science and Remote Sensing*. 54(3). 381-406. doi.org/10.1080/15481603.2016.1276255
- Zhao, R., Li, Y., & Ma, M. (2021). Mapping Paddy Rice with Satellite Remote Sensing: A Review. *Sustainability*, 13, 503. <https://doi.org/10.3390/su13020503>



Measuring Discharge in a Shallow River in an Arid Area solely using an Unmanned Aerial Vehicle

Farhad Akbarpour^{1*}, Mohammad Adel Khorasani Nejad², Shervin Shahriari³, Mostafa Rahmanshahi⁴

1. River Conservation Engineer, Tehran Regional Water Company, Tehran, Iran.
2. PhD candidate, Islamic Azad University, Science and Research Branch, Tehran, Iran.
3. PhD graduate, Institute of Hydraulic Engineering and Water Resources Management, Graz University of Technology, Austria.
4. Postdoctoral fellow, Hong Kong Polytechnic University, Hong Kong.

* corresponding author: farhad.akbarpoor@gmail.com

Keywords:

Discharge, LSPIV, UAVs, Bathymetry, Large Eddy PIV.

Abstract

Unmanned Aerial Vehicles (UAVs) have recently been applied for river flow measurement. In this research, UAV images were first used to acquire surface velocity fields of a small river in an arid area in Iran based on the principles of Large Scale Particle Image Velocimetry (LSPIV). Subsequently, Large Eddy PIV method was applied on the instantaneous velocity data to obtain turbulent kinetic energy dissipation rates along a selected cross section of the experimented river. In addition, a UAV image was captured and processed to gain the bed material grain size distribution and consequently the Manning roughness coefficient. The resulted gradation curve matched the graph given by sieve analysis with an accuracy of nearly 7.8 percent. Moreover, an equation combining the acquired surface velocity, dissipation rates and Manning coefficient was used to estimate the river bathymetry. Although, the evaluated bathymetry does not fit the surveyed cross section very well, the average predicted depth matches the measured mean depth with a high precision. Finally, the river flow rate calculated using the information solely resulted from UAV images fitted the measured discharge with an accuracy of 5 percent proving the described framework to be a very effective method for primary river flow evaluation especially when supplementary depth measurement is not feasible.

Received:

02 March 2024

Revised:

28 April 2024

Accepted:

11 May 2024

How to cite this article:

Akbarpour, F., Khorasani Nejad, M.A., Shahriari, Sh., & Rahmanshahi, M. (2024). Measuring Discharge in a Shallow River in an Arid Area solely using an Unmanned Aerial Vehicle. *Journal of Drought and Climate change Research (JDCR)*, 2(6), 93-104. [10.22077/jdcr.2024.7376.1061](https://doi.org/10.22077/jdcr.2024.7376.1061)



Introduction

Flow discharge is a very important feature of rivers in arid areas for water resources management and allocation and also for designing flood control schemes in the case of extreme hydrological events. Especially, under drought conditions it is crucial to measure water flowing in rivers as accurate as possible. Most stream gages currently being operated in Iran are based on stage-discharge method which is of course of major deficiencies. The rating curves are mainly drawn based on measurements conducted under low flow conditions and extrapolated for higher amounts of discharge. Thus, discharge records for flood events are normally subject to significant errors. Therefore, in the situation of water scarcity where annual average precipitation in Tehran Province hardly reaches 300 millimeters, seeking alternative approaches with higher accuracies deems essential for sustainable management of available water resources. Meanwhile, image-based velocity measurement methods also referred to as near field remote sensing techniques have recently been widely utilized by water professionals.

Large Scale Particle Image Velocimetry (LSPIV) is among the most frequently used imagery methods applied under different conditions from very low flow to flood events. The method firstly suggested and experimented by Fujita et al, 1998 in Japan is built essentially upon particle pattern recognition formed on flow surface in consecutive images under natural light exposures. The principles of LSPIV are similar to the conventional PIV excluding the necessity of laser application for flow visualization while larger flow fields even up to hundreds of meters might be measured.

In addition to flow measurement, LSPIV

has also been used to investigate time-averaged surface flow patterns (Bieri et al., 2009 Kantoush et al., 2011; Sutarto, 2015), turbulence features on the free surface (Orlins and Gulliver, 2000; Albayrak and Lemmin, 2007; Fox and Patrick, 2008) and the effect of free surface turbulence on the air- water gas transfer (Mc Kenna and Mc Gillis, 2004).

For flow discharge measurement in waterways using image-based techniques, two supplementary data sets are necessary to acquire. Firstly, the mean velocity at the surface obtained through processing the recorded images ought to be converted to depth-averaged velocity. This is usually achieved by multiplying the surface velocity by a constant coefficient (the velocity index or coefficient) which is well established to be equal to 0.85. However, it is to be borne in mind that the value of 0.85 is proposed for deep hydraulically smooth channels where it is possible to assume a logarithmic velocity profile (Welber et al., 2016). In some studies, LSPIV has been used to measure surface velocity to investigate the velocity index (Polatel, 2006; Welber et al., 2016; Novak et al., 2017). Several researchers have found different values for this index. For instance, Weitbrecht et al (2002) obtained 0.805 for a smooth bed. Lee & Julien (2006) obtained values 0.61 and 0.79 for a gravel bed river and clay bed canal, respectively. Novak et al (2017) found values between 0.73 and 0.89 for a horizontal glass bed flume and values 0.72 to 0.85 for a concrete flume with a slope of 0.001 where in both cases VI increases with depth. Huang et al (2018) found 0.737 for the gravel bed Yufeng Creek. Akbarpour et al (2020) obtained values 0.61 to 0.78 for steep slopes (2, 6 and 10 percent) of a flume roughened with identical glass spheres ideally representing gravel bed rivers.

The variations in the velocity index might be attributed to the parameters such as bed roughness, relative submergence or aspect ratio and flow regime (Polatel, 2006). Akbarpour et al (2020) also showed that the index is increased as the bed gradient increases and proposed an equation relating the index to the relative roughness and the slope. Johnson and Cowen (2017) in a different approach expressed the possibility of evaluating the velocity index by estimating the shear velocity from the turbulence spatial spectra and the recorded surface velocity and consequently predicting the velocity power-law exponent. Gunawan et al (2012) proved that the coefficient also varies in the transverse direction along the cross section due to the variations in the cross sectional shape of the reach, local vegetation and stage.

In addition to the velocity index, channel bathymetry or depth should also be known when measuring river flow rate using LSPIV. Johnson and Cowen (2016) suggested that through measuring surface turbulence metrics and more specifically integral length scales it is feasible to estimate the flow depth. Jin and Liao (2019) applied LSPIV to evaluate statistics of surface turbulence of a natural river and correlated the flow depth with the turbulent kinetic energy dissipation rate of the flow surface. They suggested that the water depth along the cross section might be estimated using the river Manning's n and the dissipation rate obtained from processing the sequence of surface images. On the other hand, image processing techniques have been utilized throughout the recent years to determine grain size distribution of river bed material (Butler et al., 2001; Graham et al., 2005; Buscombe et al., 2010; Spada et al., 2018). Moreover, some researchers have applied Unmanned

Aerial Vehicles as platforms for cameras to be mounted on for the same purpose (Vázquez-Tarrío et al., 2017; Lang et al., 2020).

Recently efforts have been made to explore the applicability of airborne velocimetry methods to measure stream flow discharge without any supplementary bathymetry measurements. Detert et al (2017) introducing applications of airborne image velocimetry (AIV) used an off-the-shelf action camera mounted to a lowcost quadcopter to determine a small rivers' surface velocity field, bathymetry, and its flow discharge. They applied particle image velocimetry to compute flow velocities. In order to remotely determine the river bathymetry they used structure from motion (SfM) and MultiView Stereo (MVS) techniques applied to the UAV images. Kinzel and Legleiter (2019) measured the surface velocity field and bathymetry of a river employing two small Unmanned Aerial Systems (sUAS) equipped with a thermal infrared camera and a polarizing lidar, respectively. Eltner et al (2020) introduced a remote sensing workflow for automatic flow velocity calculation and discharge estimation using the depth-averaged velocity obtained from application of PTV and the wetted cross section derived from SfM and multi-media photogrammetry applied to UAV imagery. In this paper a UAV was employed to measure surface velocity of a shallow river flowing in an arid region located in the south of Tehran the capital city of Iran. The results show that through the analysis of the acquired images based on Large Scale Particle Image Velocimetry principles an accurate surface velocity field was obtained. In addition, the airborne device was used to acquire few images from the dry river bank adjacent to the wetted section. Image processing techniques

were later used to determine the bed grain size distribution and subsequently the Manning's n . Moreover, Large Eddy PIV method was used to calculate turbulence dissipation rate on flow surface. Finally, a simple method was proposed to estimate the river bathymetry enabling the calculation of river discharge. The results show that the employed framework yields acceptable values for the river flow rate under the experimented conditions.

Material and Methods

1. Study Area

This study was conducted in a rather straight short reach of the river Kan located in the south of Tehran Province, Iran at $51^{\circ} 19' 04''$ E and $35^{\circ} 32' 58''$ N (Figure 1). The field measurement was carried out on May 28, 2020 when the river flow rate according to the current meter measurement was equal to $2.82 \text{ m}^3/\text{s}$. The site consists of a

transect (shown with red dashed line in Figure 1) where the bathymetry of the river channel was manually surveyed by a wading meter at a 0.5-m interval. The channel top width at the time of survey was 9.1 m at the selected transect. Bed materials are primarily composed of gravel without the presence of large boulders.

2. LSPIV measurements

The measurement device was a DJI Phantom 4 Pro which has a camera capable of shooting 4k video at 60 fps and capturing 20 megapixel stills on board. In our experiment the camera recorded videos in a resolution of 1920×1080 at 30 fps. The drone is equipped with a stabilizing gimbal to diminish camera movements to an acceptable level for image processing. The camera was held at a nadir position as much as possible throughout the image capturing period.



Fig 1. Location and an aerial image of the study area. The blue circles and the red dashed line on the right hand image show location of the GCPs and the surveyed cross section.

The airborne image data were captured at a flying height of about 20 meters. Video sequences were converted into individual frames prior to the image

processing. Since the camera was kept quite stable during the measurement campaign image co-registration to remove the camera movements was not necessary.

Four ground control points (GCPs) were distributed uniformly on both riversides whose coordinates were required during the image processing. The geocoordinates were recorded by a Garmin eTrex which was used three times for each GCP to improve its accuracy. However, final accuracy of the GCPs' positions is estimated to be $\pm 2-3$ m which is quite poor but sufficient for the current purpose. It is also advised to use tracer particles in LSPIV for the image processing step. The tracers need to be somewhat lighter than water to be floating on the flow surface while not too light to represent the flow behavior passively. In this study pieces of walnut wood with a specific density of 0.7 and an average size of 3×3 cm and thickness of about 1 cm were manually distributed on the water surface to act as the flow tracers. However there are evidences that natural tracing might also work under some circumstances. For unseeded applications, natural tracers such as foams, bubbles or superficial reflection patterns due to surface deformations might be used for PIV processing (Jin and Liao, 2019; Bentazzo et al., 2017). In this research, the MATLAB toolbox PIVlab was used to process the images (Thielicke and Stamius, 2014). PIVlab and most PIV software packages are based on cross correlation algorithm where the images are first divided into a number of interrogation areas (IA). Since this algorithm is in fact based on the recognition of the patterns formed by the tracer particles in each IA, for each of the two consecutive images, the correlation coefficient of each IA in the first image with the adjacent IAs in a certain area in the second image is calculated for pattern recognition. Then the IA with the largest value of the correlation coefficient is determined as the destination of the tracer particles displacement. Having the

direction and value of the displacement within the time dt , the velocity vector is obtained for the desired IA. This process continues until the velocity vector calculation for all IAs in the image is performed and thus the velocity field for each two consecutive images is achieved. In this study, the video recording was performed for a duration of 60 seconds at the rate of 30 fps and in total 1800 images were acquired. Before starting the main stage of image processing the region of interest (ROI) was cropped from the original images by masking the unwanted parts on either sides of the river. Then the raw images were converted to grayscale, contrast-limited adaptive histogram equalization (CLAHE) was used to enhance the images contrast, and a high-pass filtering was applied. According to the physical dimensions of the measurement plane the size of each pixel would be equal to 16.5 mm. In the next step, the images were calibrated using the GCPs' recorded coordinates and then the image evaluation settings were introduced. In this study, multi-pass cross correlation method via Fast Fourier Transform (FFT) was used where initially the image evaluation starts with a large IA (128×128 pixels) and the results are used for smaller IAs (eventually 16×16 pixels) and velocity vectors are obtained for each IA. Finally, in post processing bad vectors are omitted by defining the minimum and maximum acceptable velocity values and the velocity fields are calculated.

3. Flow depth estimation from surface velocity fluctuations and Manning coefficient

Jin and Liao (2019) assumed that Law-of-Wall equation for the vertical profile of the dissipation rate can be extended to the free surface, combined it with Manning-Strickler equation and proposed the

following equation for water depth estimation in rivers involving the turbulent surface velocity measurement and the Manning's roughness coefficient, n :

$$H = \frac{K^2 U_s^2 n^2 g}{(k \varepsilon_s)^{2/3}} \quad (1)$$

Where for the estimation of depth (H), having the surface velocity (U_s) and surface dissipation rate (ε_s) is necessary and g is gravitational accretion and k is von Karman constant equal to 0.41. The velocity index (K) was taken equal to the conventional 0.85 value since we do not have any preceding knowledge of the water depth to benefit from the existing relationships.

3.1. Remote estimation of the Manning's n

In order to evaluate the Manning's n we captured a supplementary image from the left bank side of the studied river using the aforementioned drone from a point 5 meters above the surface. A square wooden frame (40 by 40 cm) was placed over the selected area to ensure the possibility of scale definition. FHWA Hydraulic Toolbox was used to extract bed gradation information from the digital image. The workflow utilized by the program and the captured digital image are shown in Figure 2. As it could be seen in the figure, Grain size distribution will be the outcome of the program. Having the bed material gradation information and using one of the existing empirical equations the Manning coefficient could be estimated from the bed grain size already estimated. In this paper, since we would intend to propose a method to evaluate the flow rate without direct depth measurement and considering the fact that the experimented reach is quite straight without any vegetation roughness, Strickler (1923) formula was used to convert grain size to roughness coefficient as follows:

$$n = 0.015 D_{50}^{1/6} \quad (2)$$

1.1.

3.2. Surface turbulence dissipation rate approximation using Large Eddy PIV method

Sheng et al (2000) proposed Large Eddy PIV inspired by the concept of Large Eddy Simulation (LES). Since in PIV measurements image correlation is applied on finite grid sizes, it is similar to LES filtering where the instantaneous velocity is decomposed into a resolved velocity \bar{U}_i , and an unresolved velocity u_i :

$$u_i = \bar{U}_i + \tilde{u}_i \quad (3)$$

The turbulence dissipation rate can be estimated as follows:

$$\varepsilon \approx -2 \langle \tau_{ij} \bar{S}_{ij} \rangle \quad (4)$$

Where $\langle \rangle$ denotes ensemble averaging and \bar{S}_{ij} is the strain rate tensor defined as:

$$\bar{S}_{ij} = \frac{1}{2} \left(\frac{\partial \bar{U}_j}{\partial x_i} + \frac{\partial \bar{U}_i}{\partial x_j} \right) \quad (5)$$

And τ_{ij} is the stress tensor often obtained using Smagorinski model: $\tau_{ij} = -C_s^2 \Delta^2 |\bar{S}| \bar{S}_{ij}$ where Δ is the interrogation area size in PIV and C_s is Smagorinski constant equal to 0.17. In this paper this method is used to approximate surface turbulence dissipation rate ε_s .

Results and Discussion

1. Surface velocity field

The two dimensional time-averaged surface velocity field of the experimented river reach is depicted in Figure 3.

As it could be observed the mean surface velocity is higher tending to the left hand side of the channel which is quite sensible because the corresponding depth at that part is larger in comparison to other regions. The velocity gradient on the left

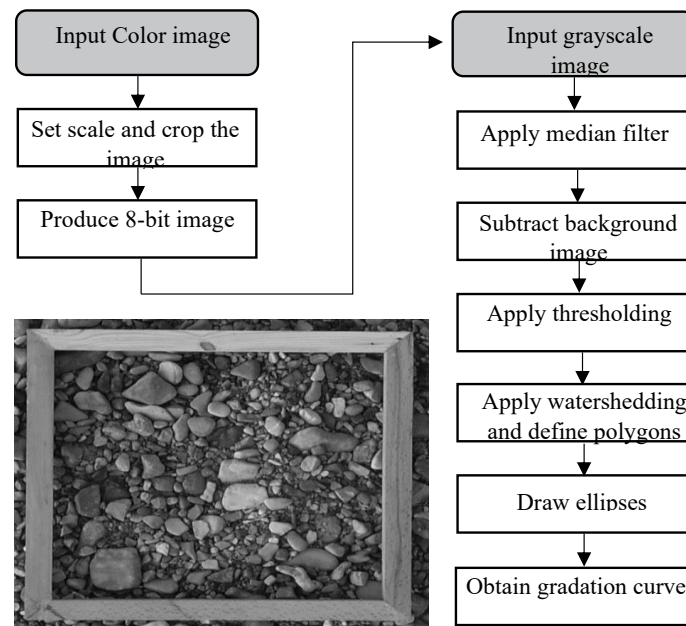


Fig 2- The underlying workflow used to estimate bed gradation from the digital image (a), the image captured at 5-meter height on the left bank of the river reach (b).

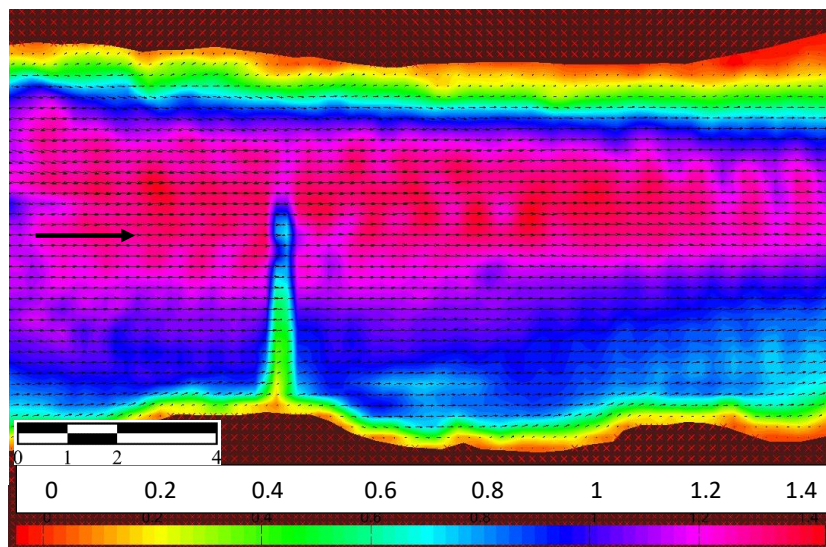


Fig 3- 2D surface velocity field of the experimented river reach.

bank is more gradual because of its gentle slope while on the right bank we observe a sharper gradient due to the abrupt slope of the river edge. The position of the wading meter is also detected in the image processing as a narrow bar with a much smaller velocity appearing on the velocity

field.

The lateral variation of the surface velocity against the depth-averaged velocity measured by the current meter is depicted in Figure 4. It is obvious that on the right hand side of the cross section the surface and depth-averaged velocities agree very

well. However, in the left hand side the depth-averaged velocity has an abrupt increase at $y=0.2$ which is not detected accordingly by LSPIV. The reason might be inappropriate distribution of seeding particles or unwanted light reflections at that area.

2. Manning roughness coefficient

As explained in section (2-3-1) image processing was applied to approximate river bed gradation. In order to be able to compare the results, a sample sediment

patch was taken from the same place as the imaged area. Figure 5 shows the gradation graphs obtained from sieve analysis and image processing. The results agree very well with the measured gradation data with a RMSE equal to 7.8 %. The calculated median grain size (D_{50}) obtained through the image analysis equals 24.9 mm and according to equation (2) the Manning roughness coefficient is estimated to be 0.025.

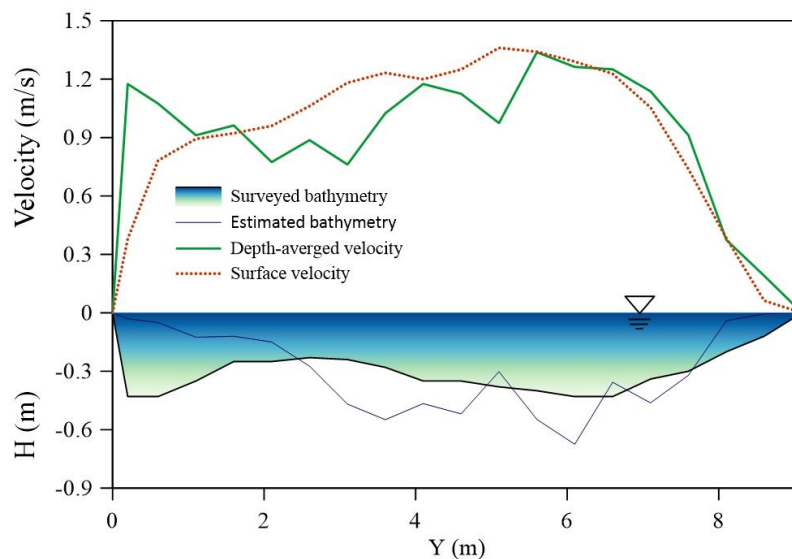


Fig 4. Surface velocity (LSPIV) versus depth-averaged velocity (current meter) and also comparison of the estimated bathymetry using equation 1 against the surveyed cross section.

3. River bathymetry and discharge

Following equation (1) and taking Manning's n equal to 0.025 as obtained from image processing techniques and inserting the surface turbulence dissipation rates calculated from Large Eddy PIV method, the values of flow depth across the selected cross section were calculated as shown in Figure 4. Except from the near end of the section the general trend of the estimated depth variation agrees to some extent with the measured bathymetry. However, the estimated bathymetry shows more fluctuations and with the exception of the first two meters mostly higher

depth values. The average depth of the section resulted from equation (1) is 0.27 m while the average depth according to the surveyed data is 0.288 m showing an error of nearly 6 percent. Thus, the applied method in this paper proves to be quite adequate to roughly estimate the mean water depth. Whilst, to be able to depend on the bathymetry obtained from the method more investigations ought to be carried out.

Moreover, the river discharge was calculated using the velocity-area method as follows with the measured surface velocity gained from LSPIV multiplied by

$K=0.85$ and the water depth distribution estimated by equation (6):

$$Q = \int_0^w KU_s(y)H(y)dy \quad (6)$$

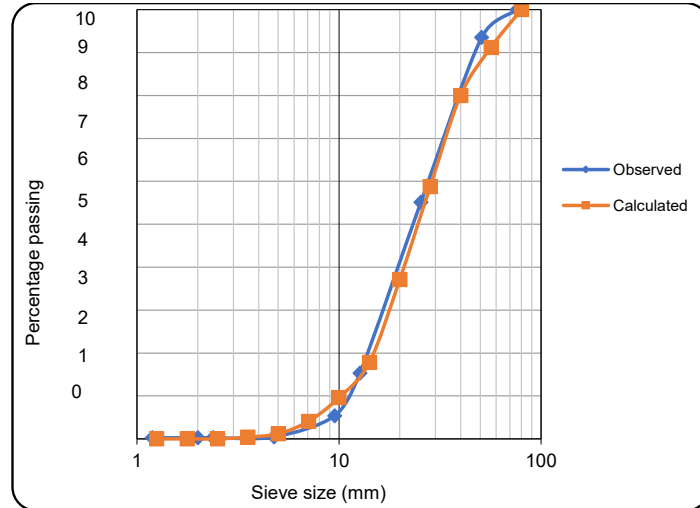


Fig 5. Evaluated (image processing) versus measured (sieve analysis) bed sediment gradation curves.

The calculated flow rate based on equation (6) equals $2.67 \text{ m}^3/\text{s}$ which is approximately 5 percent lower than the measured discharge of $2.82 \text{ m}^3/\text{s}$ using the current meter. Therefore, the proposed method which only relies on the data acquired from a UAV including surface velocity and subsequently surface turbulence dissipation rate distributions and also bed material gradation obtained through image processing techniques shows a great potential to be applied for primary river discharge estimations especially once it is not feasible to wade the river bathymetry.

Conclusions

A UAV was used in this paper to estimate both mean velocity and water depth distribution (bathymetry) in a small shallow river in an arid area in Iran solely by imaging the free surface. According to the surface velocity distribution obtained from the application of LSPIV method, the surface velocity in the left half (with reference to the flow direction) of the observed river reach is quite higher than

that of the right half. The trend recorded by the current meter also shows that the depth-averaged velocities are larger in the left half confirming the results of the surface velocity measurement. With the exception of the first one meter and the last two meters of the cross section, for the majority of the section width the depth-averaged velocity is lower than the surface velocity which is consistent with the previous findings indicating dip phenomenon.

Bed grain size distribution was also approximated using image processing techniques. The estimated gradation graph shows a very good agreement with the measured curve with a RMSE of 7.8 percent. Subsequently, the Manning roughness coefficient was calculated from the calculated median grain size (D_{50}) using Strickler formula showing a value equal to 0.025 which is around 16 percent lower than the calculated 0.029 from the measured data based on Manning equation. Hence, using the gradation acquired from drone imagery in a gravel bed river without major large roughness elements and

vegetation yielded an acceptable Manning coefficient.

The application of equation (1) proposed by Jin & Liao to estimate lateral water depth distribution using the Manning coefficient obtained through image processing and surface turbulence dissipation rate distribution calculated from Large Eddy PIV did not result in an identical bathymetry with the surveyed cross section. However, the resulted average depth is really close to the mean surveyed depth with a 6 percent error.

The discharge calculated from the introduced methodology agreed very well with the measured value with a distinction of approximately 5 percent. Therefore, it is possible to take advantage of the proposed methodology to estimate velocity, depth and consequently discharge using solely a UAV with an acceptable precision without any supplementary measurement for bathymetry under similar conditions to the experimented river reach.

Finally, in order to enhance the proposed framework, more laboratory and field experiments should be conducted in the future to explore correlations between flow depth and turbulence metrics including integral length scales and surface dissipation rate of turbulent kinetic energy.

Acknowledgements

The authors would like to thank the kind support of Roodkhiz Water and Environment Company for providing the UAV and their participation in river flow measurement.

References

Akbarpour, F., Fathi-Moghadam, M., & Schneider, J. (2020). Application of LSPIV to measure supercritical flow in steep channels with low relative submergence. *Flow Measurement and Instrumentation*, 72,

101718. <https://doi.org/10.1016/j.flow-measinst.2020.101718>.

Albayrak, I., & Lemmin, U. (2007). Large scale PIV-measurements on the water surface of turbulent open channel flow. *18^{ème} Congrès Français de Mécanique*, August 27-31., Grenoble, France. <https://hal.science/hal-03358595>.

Benetazzo, A., Gamba, M., & Barbariol, F. (2017). Unseeded large scale PIV measurements corrected for the capillary-gravity wave dynamics. *Rendiconti Lincei*, 28(2), 393-404. <https://doi.org/10.1007/s12210-017-0606-2>

Bieri, M., Jenzer, J., Kantoush, S.A., & Boillat, J. L. (2009). Large scale particle image velocimetry applications for complex free surface flows in river and dam engineering. *33rd IAHR Congress Proc.* British Columbia, Vancouver, 604-611.

Buscombe, D., Rubin, D.M., & Warrick, J.A. (2010). A universal approximation of grain size from images of noncohesive sediment. *Journal of Geophysical Research: Earth Surface*, 115(F2). <https://doi.org/10.1029/2009JF001477>.

Butler, J.B., Lane, S.N., & Chandler, J.H. (2001). Automated extraction of grain-size data from gravel surfaces using digital image processing. *Journal of hydraulic research*, 39(5), 519-529. <https://doi.org/10.1080/00221686.2001.9628276>

Detert, M., Johnson, E.D., & Weitbrecht, V. (2017). Proof-of-concept for low-cost and non-contact synoptic airborne river flow measurements. *International Journal of Remote Sensing*, 38(8-10), 2780-2807. <https://doi.org/10.1080/01431161.2017.1294782>

Eltner, A., Sardemann, H., & Grundmann, J. (2020). Flow velocity and discharge measurement in rivers using terrestrial and un-

- manned-aerial-vehicle imagery. *Hydrology and Earth System Sciences*, 24(3), 1429-1445. <https://doi.org/10.5194/hess-24-1429-2020>
- Fox, J.F & Patrick, A. (2008). Large-scale eddies measured with large scale particle image velocimetry. *Flow Measurement and Instrumentation* (19), 283–291. <https://doi.org/10.1016/j.flowmeasinst.2008.01.003>.
- Fujita, I., Muste, M., & Kruger, A. (1998). Large-scale particle image velocimetry for flow analysis in hydraulic engineering applications, *Journal of Hydraulic Research*, 36(3), 397-414. <https://doi.org/10.1080/00221689809498626>.
- Graham, D.J., Rice, S.P., & Reid, I. (2005). A transferable method for the automated grain sizing of river gravels. *Water Resources Research*, 41(7). <https://doi.org/10.1029/2004WR003868>.
- Gunawan, B., Sun, X., Sterling, M., Shiono, K., Tsubaki, R., Rameshwaran, P., Knight, D.W., Chandler, J.H., Tang, X., & Fujita, I. (2012). The application of LSPIV to a small irregular river for inbank and overbank flows. *Flow Measurement and Instrumentation*, 24, 1-12. <https://doi.org/10.1016/j.flowmeasinst.2012.02.001>.
- Huang, W.C., Young, C.C., & Liu, W.C. (2018). Application of an automated discharge imaging system and LSPIV during typhoon events in Taiwan. *Water*, 10(3), 280. DOI:10.20944/preprints201802.0089.v1
- Jin, T., & Liao, Q. (2019). Application of large scale PIV in river surface turbulence measurements and water depth estimation. *Flow Measurement and Instrumentation*, 67, 142-152. <https://doi.org/10.1016/j.flowmeasinst.2019.03.001>.
- Johnson, E.D., & Cowen, E.A. (2016). Remote monitoring of volumetric discharge employing bathymetry determined from surface turbulence metrics. *Water Resources Research*, 52(3), 2178-2193. <https://doi.org/10.1002/2015WR017736>
- Johnson, E.D., & Cowen, E.A. (2017). Remote determination of the velocity index and mean stream wise velocity profiles. *Water Resources Research*, 53(9), 7521-7535. <https://doi.org/10.1002/2017WR020504>
- Kantoush, S.A., Schleiss, A.J., Sumi, T., & Murasaki, M. (2011). LSPIV implementation for environmental flow in various laboratory and field cases. *Journal of Hydro-environment Research*, (5), 263-276. <https://doi.org/10.1016/j.jher.2011.07.002>
- Kinzel, P.J., & Legleiter, C.J. (2019). sUAS-based remote sensing of river discharge using thermal particle image velocimetry and bathymetric lidar. *Remote Sensing*, 11(19), 2317. <https://doi.org/10.3390/rs11192317>
- Lang, N., Irniger, A., Rozniak, A., Hunziker, R., Wegner, J.D., & Schindler, K. (2021). GRAINet: Mapping grain size distributions in river beds from UAV images with convolutional neural networks. *Hydrology and Earth System Sciences Discussions*, 25(5), 2567-2597. <https://doi.org/10.5194/hess-25-2567-2021>
- Lee, J. S., & Julien, P. Y. (2006). Electromagnetic wave surface velocimetry, *J. Hydraul. Eng.*, 132(2), 146-153. DOI: 10.1061/(ASCE)0733-9429(2006)132:2(146)
- McKenna, S.P., & McGillis, W.R. (2004). The role of free-surface turbulence and surfactants in air–water gas transfer. *International Journal of Heat and Mass Transfer*, 47(3), 539-553. <https://doi.org/10.1016/j.ijheatmasstransfer.2003.06.001>
- Novak, G., Rak, G., Prešeren, T., & Bajcar, T. (2017). Non-intrusive measurements of

- shallow water discharge. *Flow Measurement and Instrumentation* (56), 14–17.
- Orlins, J.J., & Gulliver, J.S. (2000). Measurements of free surface turbulence. *Fourth International Symposium on Gas Transfer at Water Surfaces*, June 5-8., Miami Beach, Florida, the USA, 1-7.
- Polatel, C. (2006). *Signature of the roughness and the flow regime on the free surface*. Ph.D. thesis, Univ. of Iowa, Iowa City.
- Sheng, J., Meng, H., & Fox, R.O. (2000). A large eddy PIV method for turbulence dissipation rate estimation. *Chemical engineering science*, 55(20), 4423-4434. [https://doi.org/10.1016/S0009-2509\(00\)00039-7](https://doi.org/10.1016/S0009-2509(00)00039-7)
- Spada, D., Molinari, P., Bertoldi, W., Vitti, A., & Zolezzi, G. (2018). Multi-temporal image analysis for fluvial morphological characterization with application to Albanian Rivers. *ISPRS International Journal of Geo-Information*, 7(8), 314. <https://doi.org/10.3390/ijgi7080314>
- Sutarto, T.E. (2015). Application of large scale particle image velocimetry (LSPIV) to identify flow pattern in a channel. *Procedia Engineering* (125), 213 – 219. <https://doi.org/10.1016/j.proeng.2015.11.031>
- Vázquez-Tarrío, D., Borgniet, L., Liébault, F., & Recking, A. (2017). Using UAS optical imagery and SfM photogrammetry to characterize the surface grain size of gravel bars in a braided river (Vénéon River, French Alps). *Geomorphology*, 285, 94-105. <https://doi.org/10.1016/j.geomorph.2017.01.039>
- Thielicke, W., & Stamhuis, E.J. (2014). PIV-lab- Time-Resolved Rigital Particle Image Velocimetry Tool for MATLAB.
- Weitbrecht, V., Kühn, G., & Jirka, G.H. (2002). Large scale PIV-measurements at the surface of shallow water flows, *Flow Meas. Instrum.* (13), 237–245. [https://doi.org/10.1016/S0955-5986\(02\)00059-6](https://doi.org/10.1016/S0955-5986(02)00059-6)
- Welber, M., Le Coz, J., Laronne, J.B., Zolezzi, G., Zamler, D., Dramais, G., Hauet, A., & Salvaro, M. (2016). Field assessment of noncontact stream gauging using portable surface velocity radars (SVR). *Water Resour. Res.* (52), 1108–1126. <https://doi.org/10.1002/2015WR017906>



Spatial Analysis of Flood Risk in Tabas Watershed Using Satellite Images and Geographic Information System

Mahdi Kaffash¹, Elham Yousefi^{2*}, Mohsen Shariati³

1. MSc in Land Use Planning, Faculty of Environment, University of Birjand, Birjand, Iran.

2. Assistant Professor, Department of Environment, Faculty of Natural Resources and Environment, University of Birjand, Birjand, Iran.

3. MSc in Environmental Planning, University of Tehran, Tehran, Iran.

*Corresponding author email: e_yusefi_31@birjand.ac.ir

Keywords:

Zoning, Hierarchical method, Tabas, Fuzzy.

Abstract

Among the natural phenomena, flood can be the biggest cause of damage, which always endangers the lives and properties of people. One of the management measures that can play a significant role in reducing damages is flood risk zoning. In this research, flood risk zoning has been done in the Tabas watershed. In general, the steps and this research were done in four stages. The effective criteria for creating the risk of flooding were identified, and the relevant layers were prepared. In the next step, mapping and standardization were done using fuzzy membership functions, then weighting of parameters was done using the hierarchical method, and finally overlapping of the layers was done using fuzzy operators. The criteria of distance from the river, slope, land use, rainfall, soil, digital elevation model and normalized difference vegetation index were respectively assigned the highest weight. Also, all fuzzy superposition operators (OR, AND, SUM, Product and Gamma) have been used for flood risk zoning. Among these operators, the 0.9 gamma operator shows the best and most reasonable result, so this map was chosen as the final flood risk zoning. In the final map, the total area of high-risk areas is 15432.13 ha. According to the final map obtained, areas with very high flood risk are located in the eastern part of the studied area. Areas with low risk are mostly located in the plains, valleys and depressions with less slope. The method used in this study can be used in other studies, such as zoning of earthquake risk potential, development zoning and spatial analysis of disease distribution.

Received:

05 April 2024

Revised:

01 June 2024

Accepted:

01 June 2024

How to cite this article:

Kaffash, M., Yousefi, E., & Shariati, M. (2024). Spatial Analysis of Flood Risk in Tabas Watershed Using Satellite Images and Geographic Information System. *Journal of Drought and Climate Change Research (JDCR)*, 2(6), 105-118. [10.22077/jdcr.2024.7489.1066](https://doi.org/10.22077/jdcr.2024.7489.1066)



Introduction

Floods are natural disasters that, according to the United Nations Development Program, rank high in terms of loss of life and property (Beheshti et al., 2009). Floods can cause severe economic damage and pose a threat to human life worldwide (Ouma and Tateishi, 2014). Among natural phenomena, floods can be the primary cause of damage, consistently endangering the lives, properties, and assets of countless people. Iran, due to its Mediterranean climate, ranks 7th globally in terms of flooding and suffers significant damages in this regard every year. Mitigating the effects of this crisis necessitates the integration of various data, such as topography, roads, buildings, and urban facilities. The research highlights the importance of studying urban floods as a vital component of urban watershed management programs. Flood zoning in urban areas is crucial for evaluating and identifying areas prone to flooding and potential damage, as well as for identifying safe routes for relief and resettlement of people. Utilizing models related to flood effects and considering the economic implications of flood damages is paramount in flood zoning in urban areas. Hence, studying floods in urban areas and preparing a risk zoning map is essential for reducing damages caused by urban floods and assisting managers in formulating better management plans. This phenomenon can be studied through flood zoning in cities, where areas prone to flooding are identified, and flood control measures are implemented accordingly. Additionally, safe routes for relief and secure settlements for affected populations have been established. Several natural factors can disrupt the balance of river flow, turning it into a destructive force. These include vegetation destruction, land conversion, rainfall intensity, as well

as the degree of soil saturation, slope, and permeability of the basin. Flood risk analysis is required as a major challenge in urban areas compared to rural areas due to its greater complexity. Flood risk analysis often overlooks social and environmental impacts, focusing solely on quantifying economic damages (Kubal et al., 2009). Identifying flood-prone areas is a crucial step in managing flood impacts and classifying affected regions (Patil et al., 2008). This information guides decisions regarding land use, including the future development of cities and villages, with the aim of mitigating flood damages to some extent (Saeedi and Asiaei, 2021). There are a lot of vague ideas, variables, and systems in the real world, but fuzzy logic theory helps us think about them mathematically. It also gives us a way to make decisions and reason in uncertain situations (Zadeh, 1998). Community membership and complementary sharing, multiplication, addition, and gamma are fundamental aspects of this integration model. The hierarchical analysis process is also utilized as a decision system for multiple criteria location-based on expert knowledge, as presented by Thomas Al Saati (1990). In this method, the effective factors causing flood risk are first identified through a literature review and qualitative methods examining the characteristics of the study area.

Various factors, such as DEM, slope, distance from the river, NDVI, land use, soil, and rainfall, can affect flood risk zoning. In this regard, Rashetnia (2021) investigated flood vulnerability assessment using fuzzy rule-based indicators in Melbourne, Australia. The results of this study indicated that the distance of the river and the site of rainfall are the most significant variables in causing floods in this city. Schumann (2021) conducted

a study on modeling river floods using remote sensing in Brazil. The findings of various studies and investigations revealed that variables such as distance from the river, topography, and precipitation have the greatest impact on the occurrence of floods in Brazil (Schumann, 2021). Mishra et al. (2020) evaluated flood risk in the Kosi district of India and found that this area is one of the most flood-prone regions in India and requires proper planning. Among domestic studies, we can also refer to the research by Eslaminezhad et al. (2022), Khorshidi et al. (2021), and Solaimani and Darvishi (2020). Therefore, with the growth and development of new technologies, spatial flood risk analysis methods require a more practical tool. This tool should not only provide users with more mathematical models and facilities for accurately explaining flood flow, but also offer systems with geographic information capabilities. These systems provide users with significant abilities

to analyze the risk of flooding. The flood risk-zoning map can serve as an effective tool for planning the future development path of the city. It can also help identify areas where the development of flood evacuation and drainage infrastructure is necessary. Thus, in this research, a flood risk zoning map has been prepared for the Tabas catchment area.

Material and Methods

Study Area

Tabas is one of the study areas within the Lut Desert watershed, in South Khorasan Province, Iran. The total area of the Tabas study area is 12,484.85 square kilometers, comprising 4,566.73 square kilometers of plains and 7,918.13 square kilometers of highlands. Additionally, there are two alluvial aquifers in this study area, with extents of 859.81 and 389.74 square kilometers, respectively. Figure 1 below illustrates the geographical location of the study area in South Khorasan Province, Iran.

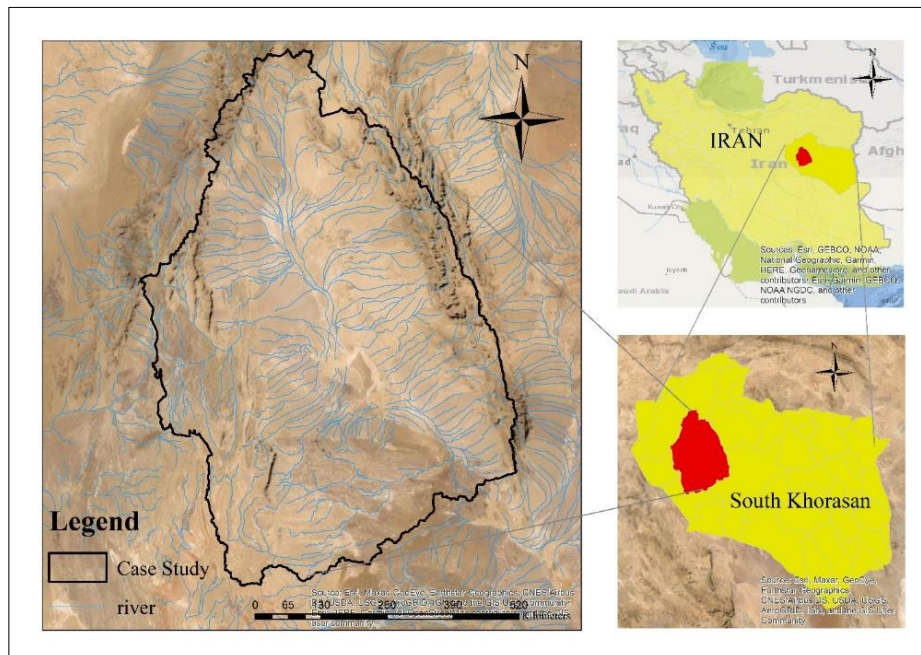


Fig 1. Geographical location of the study area.

As one of the most dangerous natural disasters that has big effects on cities, urban floods are studied in this study. To find good ways to deal with the risk of flooding and keep people safe, the Tabas watershed is used for spatial analysis of flood risk using fuzzy logic based on GIS, AHP, and spatial analysis. In this study, land use and land cover, elevation, slope, distance from the river, soil, and rainfall are considered important factors in zoning the flood phenomenon in the Tabas watershed. To compile some of the information used in this study, such as vegetation data, satellite images, including those from the Landsat 8 satellite, have been employed. An aerial image from the summer of 2022 was prepared and enhanced using ENVI 5.6.1 software and the NDVI index was subsequently extracted. The data of distance from the river, rainfall or land use were obtained from the maps received from the relevant organizations. The raster layers land use and soil were polygonal in nature and were rasterized using the feature to raster tool. The rasterization of the other layers was carried out using the Euclidean distance, interpolation, and kernel density tools. The raster maps were colored from blue to red to differentiate the values of raster cells. In this regard, the color red (in raster layers except soil, land use, NDVI, and rainfall) represents higher values. The general stages of this research include information gathering, rasterization, standardization using fuzzy membership functions, weighting using the hierarchical method, and overlaying layers using fuzzy operators. To fuzzily classify the layers, it was necessary to have a raster structure from the input information. Thus, in this research, all the information layers (excluding DEM and slope) were prepared using various tools in Arcmap 10.8.1, including a raster calculator, feature

to raster, and interpolation. Here is an explanation of the types of fuzzy operators used in this research:

We define the operator of fuzzy and value as the following equation:

$$a. W_{Combination} = MIN(W_A, W_B, W_C, \dots) \quad (1)$$

where W_B , W_A and W_C represent the fuzzy membership values of factors B, A and C in a specific situation. The effect of this operator is that the output map is controlled by the smallest fuzzy membership value that occurs at each position. fuzzy OR value is defined as the following relation:

$$b. W_{Combination} = MAX(W_A, W_B, W_C, \dots) \quad (2)$$

The effect of this operator is that the output map is controlled by the largest fuzzy membership value that occurs at each position. Product operator is defined as the following relation.

$$c. W_{Combination} = \prod_{i=1}^n W_i \quad (3)$$

In this method, n fuzzification controlling factors are combined, and we represent the weight of each layer. The values of fuzzy membership with this operator tend to be very small, in other words, the output value of each position is always smaller or equal to the smallest value of fuzzy membership in the corresponding positions of the input maps. Therefore, the above operator has a reduction effect. In this method, unlike fuzzy AND and OR, all membership values of the input maps affect the output map.

d- SUM operator

This operator is defined as the following relation.

$$d. W_{Combination} = 1 - \left(\prod_{i=1}^n (1 - W_i) \right) \quad (4)$$

By using this fuzzy operator, the fuzzy membership value of the output map in each position is always greater than or equal to the largest fuzzy membership value in the corresponding positions of the input maps. Therefore, the super operator has an increasing effect.

$$e. \mu_{Combination} = (Fuzzy\ Algebraic\ Sum)^\delta * (Fuzzy\ Algebraic\ Product)^{1-\delta} \quad (5)$$

In this regard, the value of γ is determined between zero and one. If we want the algebraic sum method (SUM) to be more important, the value of γ is chosen close to one, if we want the algebraic multiplication method (PRODUCT) to be more important, the value of γ is chosen close to zero. The correct and conscious choice of γ produces values in the output that have a flexible adaptation between the decreasing and increasing tendencies of the two fuzzy operators of algebraic multiplication and algebraic addition (Eastman, 2012). Consequently, Qanavati et al. (2012) employ the gamma operator to modify the algebraic multiplication and algebraic addition operators.

Today, there are different methods for zoning and flood risk estimation, For example, the use of the Google Earth Engine platform has found many applications and has provided fast and reliable results to researchers (Bagheri *et al.*, 2022).

Results and Discussion

Mapping Results

Figure (2) depicts the raster layers related to seven measures: DEM, slope, distance from the river, NDVI, land use, soil, and rainfall. Among these layers, NDVI exhibits an inverse relationship with flood risk, while rainfall, DEM, slope, and distance from the river show a direct relationship with the risk of flooding (Ogato et al., 2020). After rasterizing the

E- GAMMA operator

This method is a combination of algebraic multiplication and algebraic addition techniques. In this method, factors with different weights are combined according to the following relationship:

criteria, we standardized the rasterized layers using different fuzzy membership functions.

The results of standardization:

In the measurement of traits, a diverse range of scales is used, necessitating the conversion of values in different layers of the map into comparable units and proportions to each other. This process creates standard and comparable maps. One standardization method is the fuzzy method, in which the fuzzification operation assigns an appropriate degree to each input using the respective membership functions (Zadeh, 1965). There is no specific algorithm for obtaining the membership function; however, experience, innovation, and even the application of expert opinion can be effective in forming and defining it. At this stage, raster layers of each of the factors affecting flood risk in Tabas plain converted into fuzzy layers using linear, sigmoid, and user-defined membership functions in ARC MAP 10.8.1 software (Table 1).

The standardized layers have values between zero and one, wherein higher values indicate a higher favorability for flood risk (Figure 3). In this context, the rainfall criterion, as well as the digital elevation model of DEM and slope in the eastern part of Tabas plain exhibit the highest favorability in relation to the risk of flooding. In terms of the distance layer from the river and the soil, the predominant land

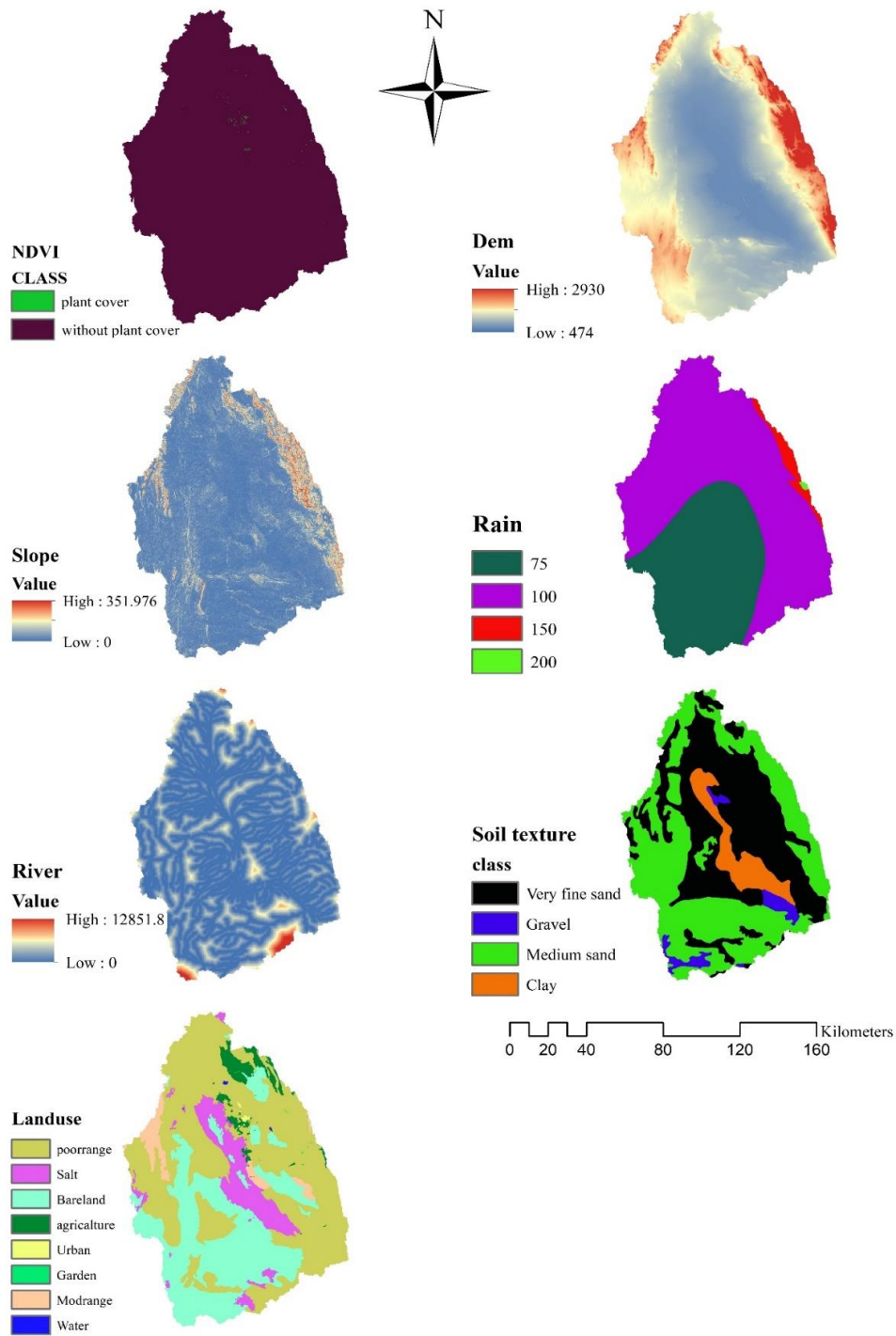


Fig 2. Raster maps of selected criteria for flood risk zoning in the study border related to 7 criteria of DEM, slope, distance from the river, NDVI, land use, soil and rainfall

Table 1. Standardization of criteria based on fuzzy membership functions

Control Points				Fuzzy Membership Function	Factor
a=0		b=1		User defined	NDVI
Poor Pasture (0.7), Salt (1), Barren Land (0.8), Agriculture (0.3), Urban (0.9), Garden (0.1), Medium Pasture (0.2), Water (1)				User defined	Land Use
a=1000		b=2500		Sigmoid (Increasing)	Dem
a=0		b=30		Linear (Increasing)	Slope
a=500		b=3000		Linear (Decreasing)	River
75mm=0.25	100mm=0.5	150mm=0.75	200mm=1	User defined	Rain
Sand (0), Clay (1), Medium Sand (0.33), Very Fine Sand (0.66)				User defined	Soil Pattern

use along the study boundary demonstrates a high level of favorability compared to the risk of flooding.

The use of hierarchical fuzzy method has been used in many environmental studies such as Rezaei & Roshani (2024) to prioritize parameters and prepare risk zoning maps. In this study, given that each criterion contributes differently to flooding, we utilized hierarchical analysis for weighting, ensuring that each phase layer carries its own unique value and importance. Experts and specialists assigned these values based on their judgments for the seven criteria. The AHP method comprises three main stages (Saaty, 2008). First, we analyze the decision-making problem in a hierarchical structure, determining the goal, criteria, and sub-criteria. Pairwise comparisons, the subsequent step in AHP, determine the weights for different criteria. Expert judgment guides the evaluation of paired comparisons, establishing the weight of a particular criterion by ranking its importance and suitability. The final step entails checking the consistency ratio. This ratio indicates whether the comparisons are stable or not. We can rely on the AHP results, including the calculated weights, if the consistency ratio is less than 0.1, indicating the stability of the created matrix. Table (2) presents the final weights assigned to each of the selected criteria in this analysis. The table assigns the highest

weights to the criteria of distance from the river, slope, land use, precipitation, soil, DEM, and NDVI, respectively.

The results of stacking layers using fuzzy operators:

In the fuzzy method, classes and spatial units with degrees of membership between zero and one can be defined for each raster layer. Subsequently, each fuzzy layer is combined using fuzzy operators. These operators include fuzzy union (OR), fuzzy intersection (AND), fuzzy algebraic addition (SUM), algebraic multiplication (Product), and fuzzy gamma operator (Gamma). In this study, all fuzzy overlay operators have been utilized for flood risk zoning. During the overlay of fuzzified layers, the fuzzy intersection operator calculates the minimum values in the set of layer values in the output layer.

In this research, fuzzification was performed using ARC GIS software and the Fuzzy Overlay tool available in the Spatial Analysis toolbox. By utilizing this tool, all standardized and weighted layers were overlaid sequentially with all operators. It's important to note that during overlay, all raster layers must have the same correct cell size and coordinate system. Figure (4) displays the final layers resulting from overlay with five fuzzy operators; red-colored areas indicate high flood risk areas, while blue spots represent low flood risk areas.

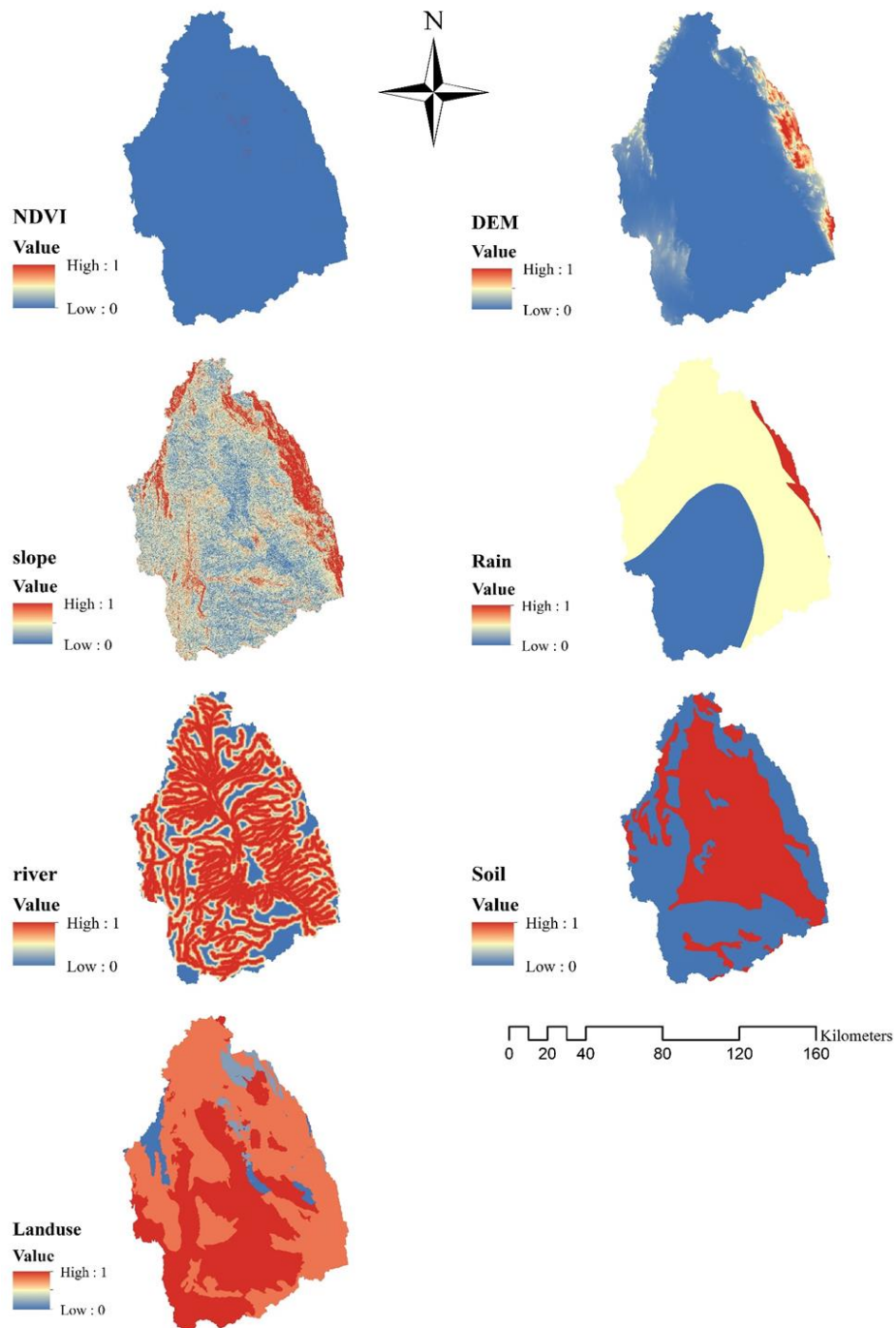


Fig3. Fuzzy maps of the raster layer for zoning the risk of flooding in the study border related to 7 parameters of DEM, slope, distance from the river, NDVI, land use, soil and rainfall

Table 2. Importance of weights of criteria and sub-criteria.

criteria	W1	sub-criteria	W2	Final weight
Hydroclimate	0.441	distance from the river	0.666	0.2734
		Precipitation	0.333	0.1368
topography	0.261	DEM	0.333	0.0858
		Slope	0.666	0.1719
Land type	0.327	land use	0.475	0.1553
		Soil	0.415	0.1357
		NDVI	0.109	0.356

In this research, flood risk zoning in the Tabas watershed was established based on the combination of fuzzy layers weighted with different fuzzy operators (Figure 4). According to the resulting maps, except for the OR and SUM operators, which exhibit illogical results, the rest of the operators, with slight differences, indicate the highest flood risk in the eastern part of the study area near the Tabas plain. Among these operators, the 0.9 gamma operator demonstrates the most accurate and logical result according to reality (Figure 5). Because, this map showed a more realistic result, some methods responded pessimistically and showed areas less than reality, such as Product, AND and Gamma 0.1 operators, and some operators showed much more areas, such as OR and SUM operators. In fact, this validation was done by comparing the output maps with the flood events that happened, and for this, the expert opinions of the employees of the Water and Sewerage Department as well as hydrometric data were used.

In Figure 5, the total area of high-risk areas is 15,432, 1324 ha, indicated by pixels with a value above 0.1, represented by red and orange spots. Areas with moderate risk (0.05 to 0.1) cover 97,205, 1958 ha of the Tabas Plain. The largest area corresponds

to values less than 0.05, covering 926,531, 8431 ha, denoted by blue and safe spots on the map. As depicted in Figure (4), most residential areas along the study border are located in areas with low to medium flood risk.

In a study by Khorshidi et al. (2021) on prioritizing flood potential in watersheds lacking statistics using the AHP-VIKOR method in the Haji Bakhtiari watershed of Ilam province, the results indicated that the area index has the greatest effect, while the index of medium slope has the least effect on flood risk in the studied area. Similarly, in the study by Saeedi and Asiaei (2021) on flood risk zoning in Sabzevar city using fuzzy logic, slope and precipitation were identified as the most effective variables, with vegetation having the least effect in the region. Also, in relation to flood control, flood control by prioritizing flooding in sub-basins and by implementing managements to improve the coverage of pastures and build watershed structures in the river basin reduced the amount of flood discharge and prevented sudden damages (Chazgi et al., 2024).

Conclusion

In this research, flood risk zoning has been done in the Tabas watershed. Based on

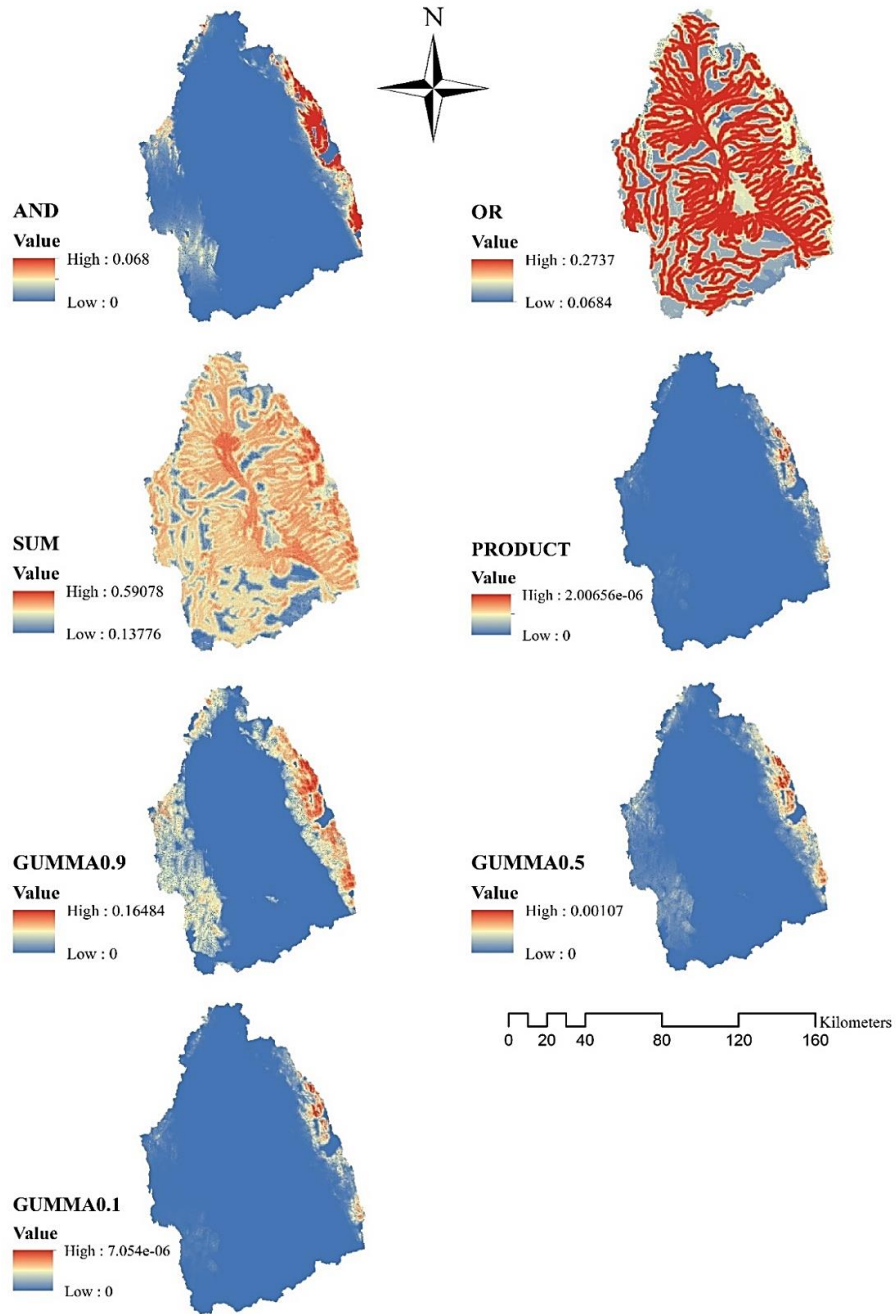


Fig4. Maps resulting from superimposing weighted fuzzy layers using fuzzy operators AND, OR, SUM, Product, Gamma0.9, Gamma0.5, Gamma0.1

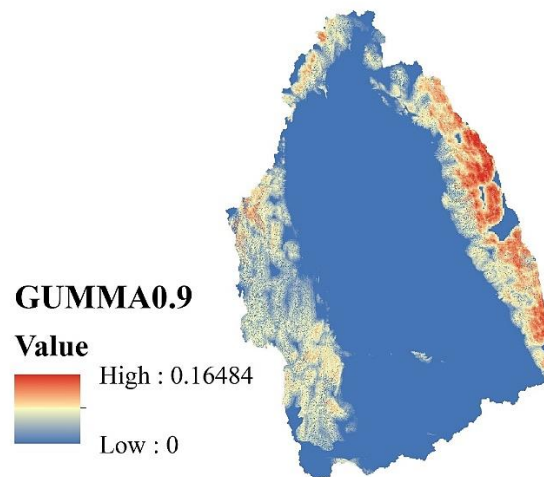


Fig5. The final map of Tabas plain flood zoning using the Gamma 0.9 operator

the range of values for each zone and the ground reality map, the Gamma operator 0.9 was chosen for the final flood risk zone. Furthermore, in this research, the prioritization and importance of different criteria in causing the flood phenomenon in the Tabas watershed were determined as follows: the criteria of distance from the river, slope, land use, rainfall, soil, DEM, and NDVI were respectively assigned the highest weights. The distance from the river, being the most influential among the variables, designates more pixels as flood risk areas than other variables. Conversely, the NDVI and DEM layers, which have fewer pixels indicating high flood risk (red color), are predominantly located in the eastern areas of the study border.

These findings align with the current research's results, recommending the distribution of land uses, specifically industrial, residential, and commercial ones, according to the flood risk potential zoning map this study generated. In potentially hazardous areas, we recommend measures like revitalizing vegetation, conducting watershed studies in basin

DEM, monitoring land use changes in the upper reaches of the basin, and converting some rained and agricultural lands into gardens. Finally, it is suggested to utilize other multi-criteria methods (such as TOPSIS, etc.) to validate the flood risk potential in this area and compare their results with the findings of this research.

Reference

- Bagheri, M. H., Farzaneh, M., & Rayegani, B. (2022). Development of Remote Sensing-Based Flood Estimation Methodology in Google Earth Engine. *Environment and Interdisciplinary Development*, 7(76), 12-26. <https://doi.org/10.22034/envj.2022.154826>
- Beheshti Rad, M., Faiznia, S., Selajqa, A., & Ahmadi, H. (2009). Investigating the efficiency of landslide risk zoning model, confidence factor (CF) A case study of Moalem Kalaye watershed. *Natural Geography*, 2(5), 19-28. [In Persian].
- Chehzi, J., & Hamedi, E. (2023). Flood Prioritization of Sarbaz River Sub-Basins Using SWAT Model. *Journal of Drought*

- and *Climate change Research*, 1(3), 73-86. doi: 10.22077/jdcr.2023.6478.1026.
- Eslaminezhad, S.A., Eftekhari, M., Akbari, M., Haji Elyasi, A., & Farhadian, H. (2022). Predicting flood prone areas using advanced machine learning models (Birjand plain), *Journal of Water and Irrigation Management*, 11(4), 885-904. 10.22059/jwim.2022.332875.934 [In Persian].
- Eastman, J. R. (2012). *IDRISI Selva manual*. Clark University. Sitio web: www.Clarklabs.org.
- Khorshidi, Sh., Rostami, N., & Salehpourjam, A. (2021). Prioritizing flood producing potential in ungauged watersheds using the AHP-VIKOR method (Case study: Haji-Bakhtiar Watershed, Ilam), *Environmental Erosion Researches*, 11(2), 66-92. 20.1001.1.22517812.1400.11.2.4.4 [In Persian].
- Kubal, C., Haase, D., Meyer, V., & Scheuer, S. (2009). Integrated urban flood risk assessment—adapting a multicriteria approach to a city. *Natural hazards and Earth System Sciences*, 9(6), 1881-1895. <https://doi.org/10.5194/nhess-9-1881-2009>.
- Mishra, K., & Sinha, R. (2020). Flood risk assessment in the Kosi megafan using multi-criteria decision analysis: A hydro-geomorphic approach. *Geomorphology*, 350, 106861. <https://doi.org/10.1016/j.geomorph.2019.106861>
- Ogato, G. S., Bantider, A., Abebe, K., & Geneletti, D. (2020). Geographic information system (GIS)-Based multicriteria analysis of flooding hazard and risk in Ambo Town and its watershed, West shoa zone, oromia regional State, Ethiopia. *Journal of Hydrology: Regional Studies*, 27, 100659. <https://doi.org/10.1016/j.ejrh.2019.100659>
- Qanavati, E., Karam, A., & Agha Alikhani, M. (2012). Flood risk zonation in the Farahzad basin (Tehran) using Fuzzy model. *Journal of Geography and Environmental Planning Consecutive*, 48(4). 20.1001.1.20085362.1391.23.4.8.2
- Ouma, Y. O., & Tateishi, R. (2014). Urban flood vulnerability and risk mapping using integrated multi-parametric AHP and GIS: methodological overview and case study assessment. *Water*, 6(6), 1515-1545. <https://doi.org/10.3390/w6061515>.
- Patil, J. P., Sarangi, A., Singh, O. P., Singh, A.K., & Ahmad, T. (2008). Development of a GIS interface for estimation of runoff from watersheds. *Water Resources Management*, 22(9), 1221-1239. <https://doi.org/10.1007/s11269-007-9222-8>
- Rezaei, A. R., & Roshani, A. (2024). Prioritization of Factors Affecting Drought using the Fuzzy Analytic Hierarchy Process Method (Study Case: Torbat Heydarieh City). *Journal of Drought and Climate change Research*, 2(1), 77-92. doi: 10.22077/jdcr.2024.7255.1057
- Rashetnia, S., & Jahanbani, H. (2021). Flood vulnerability assessment using a fuzzy rule-based index in Melbourne, Australia. *Sustainable Water Resources Management*, 7(2), 1-13. <https://doi.org/10.1007/s40899-021-00489-w>.
- Saaty, T. L. (1990). How to make a decision: the analytic hierarchy process. *European Journal of Operational Research*, 48(1), 9-26. [https://doi.org/10.1016/0377-2217\(90\)90057-I](https://doi.org/10.1016/0377-2217(90)90057-I).
- Saaty, T. L. (2008). Decision making with the analytic hierarchy process. *International Journal of Services Sciences*, 1(1), 83-98. <https://doi.org/10.1504/IJSSCI.2008.017590>.
- Saeedi, S., & Asiaei, M. (2021). Flood risk zoning

in Sabzevar city using fuzzy logic, *Journal of Urban and Regional Development Planning*, 5(15), 27-49. <https://doi.org/10.30473/grup.2024.55316.2554> [In Persian].

Schumann, G. J. (2021). Earth Observation for Flood Applications: Progress and Perspectives. *Earth Observation for Flood Applications*, 3-6. <https://doi.org/10.1016/B978-0-12-819412-6.00001-8>.

Solaimani, K., & Darvishi, Sh. (2020). Zoning and monitoring of spring 2019 Flood hazard in Khuzestan using Landsat-8 data, *Iranian Journal of Eco Hydrology*, 7(3), 647-662. [10.22059/ije.2020.302703.1333](https://doi.org/10.22059/ije.2020.302703.1333) [In Persian].

Zadeh, L. A. (1965). *Fuzzy sets. Information and control*, 8(3), 338-353. [https://doi.org/10.1016/S0019-9958\(65\)90241-X](https://doi.org/10.1016/S0019-9958(65)90241-X).

Zadeh, L.A. (1988). Fuzzy logic. *Computer*, 21(4), 83-93. <https://doi.org/10.1109/2.53>



Application of Time Series Method and Artificial Neural Networks in Drought Simulation (Case study: Bojnourd city)

Mohtaram Mohamadyariyan^{1*}, Ebrahim Amiri²

1. Department of Geography Education, Farhangian University, Tehran, Iran.

2. Department of Geography Education, Farhangian University, Tehran, Iran.

*Corresponding Author: m_65yaran@yahoo.com

Keywords:

Bojnourd, Box Jenkins, Minitab,
Post release networks, SPI.

Abstract:

Drought is a climatic phenomenon that is considered part of a region's climate. It has a hidden nature whose duration of occurrence is long, and its effects appear in a non-structural way. As a result, its damages gradually appear in various sectors such as agriculture, social, economic, environmental, and so on. In this research, an artificial neural network was used as a powerful tool in simulating the drought of Bojnourd city. For this purpose, the statistical data of precipitation, relative humidity, and temperature from 1997 to 2014 constituted the basis of the research. SPI drought index was used as sample output. Specifically, 70% of the data were considered as training data and 30% as testing data. The networks used were of backpropagation type and radial basis function with error backpropagation algorithm plus Levenberg–Marquardt learning method. Box Jenkins method from MINITAB software and BPI to BP24 models from MATLAB software were employed in drought simulation. The value of the correlation coefficient for the training phase (R) was 0.95, while for the test phase it was 0.81, showing the lowest error in the test phase. Meanwhile, the results of the training phase were close to each other in most of the models. Among the selected models of the post-release network, the BP19 model was selected as the selected example. The RMSE determination coefficient was estimated with a value of 0.16 for the training stage and MAE (mean absolute error) was estimated as 0.0071.

Received:

08 August 2024

Revised:

22 August 2024

Accepted:

29 August 2024

How to cite this article:

Mohamadyariyan, M., & Amiri, E. (2024). Application of Time Series Method and Artificial Neural Networks in Drought Simulation (Case study: Bojnourd city). *Journal of Drought and Climate change Research (JDCR)*, 2(6), 119-134. [10.22077/jdcr.2024.8014.1074](https://doi.org/10.22077/jdcr.2024.8014.1074)



Introduction

Droughts are recurring natural hazards that result from abnormally low rainfall, and if such conditions persist for long periods, they may spread to other components of the water cycle, such as soil, streams, and aquifers (Meng Dai et al., 2020). Drought is a phenomenon that has different meanings from different perspectives. So far, there have been many definitions of drought, but each of these definitions has taken into account a specific point of view. Accordingly, the lack of a comprehensive and accurate definition of drought and its different meanings from different points of view have hindered the understanding of the concept of drought. Since drought has a direct and indirect effect on all aspects of life and different parts of society, especially the change of the natural environment, the lack of understanding of its meaning causes doubt and recession in various economic, managerial, and policy-making sectors. Compared to other forms of natural disasters, drought is considered one of the most unknown and costly natural disasters (Hong et al., 2019). Finally, from the point of view of climatology, if the amount of rainfall falls to less than 60% of its annual normal in a period of more than two years in 50% of the region, there will be a drought and the economic-social effects will be widespread. All regions of the world may be affected by drought from time to time, but this situation is more observed in regions that are irregularly and randomly affected by climate systems (Raziei et al., 2012: 307). Knowing about the occurrence of drought in the future can be very useful to prevent or reduce the harmful effects of its occurrence. Thus, so far, there have been various methods related to drought prediction. Studies suggest that in most cases, statistical models are used to predict different types of drought, and these

models are designed based on time series models. Regression and autoregression methods are types of time series models that are used in forecasts. These models are types of linear models in which the data are assumed to be fixed and have limited capabilities in dealing with non-linear and non-statistical data. According to what has been said, non-statistical and non-linear models are necessary in predictions. In recent decades, the use of artificial neural network technique among the types of non-linear models has shown brilliant results in predicting problems related to water engineering and hydrology. Today, one of the efficient methods that are widely used in air and water science is the artificial neural network (ANN). According to researchers, the main reason for its increasing acceptance and usage is its high power and speed in simulating the processes that need to be properly understood, which does not exist or checking them with other available methods is very difficult and time-consuming. In general, it can be expected that the artificial neural network model would be a strong model with high capability that can be viewed with a positive perspective in predicting climate-hydrological issues, especially since this network is able to extract the law governing data, even confusing data (Dehghani and Ahmadi, 2017). Neural networks are a kind of simplistic modeling of real neural systems that are widely used in solving various problems in science. The field of these networks is very wide, spanning from classification applications to applications such as interpolation, estimation, detection, etc. Perhaps the most important advantage of these networks is their notable ability in addition to their ease of use (Sayadi, 2007).

The first attempts at simulation using a logic model were made in the early

1940s by Warren McCullock and Walter Pitts, which is the building block of most artificial neural networks today. He approached the issue by creating a computational model for neural networks. The use of artificial neural networks for monitoring droughts, water resources management, and hydrology topics has started since the first decades of the 20th century. In water resources management, according to the nonlinear management of phenomena, artificial neural networks have shown the greatest ability in modeling and forecasting time series in hydrology and water resources engineering (Mishra & Desai, 2005). This method, which is one of the efficient and useful methods in climate science, has been an artificial neural network, which, according to researchers, whose main reason of popularity and acceptance is its high power and speed in simulating processes that require proper understanding, which does not exist, or it is very difficult and time-consuming to check them with the existing methods (Dehbozorgi et al.). DiKshit et al. (2022) used artificial neural network in predicting droughts in the 21st century. They found that by using a complex input, artificial intelligence-based solutions that are used to predict the drought of water and meteorological variables are promising, especially in complex geographical scenarios. Future research needs to focus on interpretable models, use deep learning architectures for long-term forecasting, and employ neural networks to predict different drought characteristics, such as drought propagation and sudden droughts. They also presented the most widely used neural network approaches in spatial drought forecasting, which serves as a foundation for future research in drought forecasting studies. Fan et al. (2021) evaluate the climate change

effects on temperature, precipitation, and evapotranspiration in eastern Iran using CMPI5. The results revealed that the GFDLCM2, MPI, and IPSL models were more accurate in terms of precipitation, while the GISS E2 and GFDLCM2 models were the suitable option for predicting the maximum and minimum temperatures and evapotranspiration. Considering the evaluated parameters, minimum temperature, maximum temperature and evapotranspiration had approximately constant trends and were accompanied by a slight increase and decrease for the next two decades. However, for precipitation, large fluctuations were predicted for the next period. Further, in the study years for the four parameters in all simulated models, the RCP 8.5 scenario estimated a higher value than the RCP 4.5 scenario. Wabel et al. (2023) investigated the application of hybrid artificial neural network techniques for drought prediction in the semi-arid region of India. In this research, four ANN models have been developed, which include a normal ANN model and three hybrid ANN models: A: Wavelet-based ANN (WANN), B: Bootstrap-based ANN (BANN), and C: Wavelet-basedANN.Bootstrap(WBANN). They used the standardized precipitation evaporation and transpiration index (SPEI), which is one of the best drought indices identified for the studied area, as a variable for predicting drought. In their research, three drought indices, including SPEI-3, SPEI-6, and SPEI-12 represented drought conditions respectively. "Short-term", "medium-term" and "long-term" were used for a forecast period of one month to three months. The results of their research revealed that the bootstrap-based model offered the best performance for analyzing the uncertainty associated with different drought predictions. Among the

developed models for drought forecasting for the period of 1 to 3 months, WANN and WBANN models outperformed simple ANN and BANN models for 3-SPEI-, 6-SPEI- and 12-SPEI- up to 3 months. Helmi & Shahidi (2023) employed SPI and SPEI to evaluate the effect of drought on the quality of surface water resources in the Kashafrud River). The results of their research showed that the average concentration of cations and anions in Olang Asadi station had an increase of about 5 times compared to Golmkan station. Finally, they concluded that with decline in rainfall, increase in temperature and drought, the water quality has decreased, especially in the downstream stations.

Evkaya & Kurans (2020) dealt with drought forecasting using neural network approaches with transformed time series data. The main goal of this research was to study drought forecasts for a meteorological station located in Marmara region. For this purpose, the widely used univariate drought index, the standard precipitation index for Bursa station, has been calculated. Thereafter, both the historical information retrieved from the time series data and its wavelet transformation were considered for examining automatic nonlinear models and automatic nonlinear regression with external input (NARX) and neural network (NN) type. According to a set of GOF¹ tests, the prediction performance of models with different numbers of hidden neurons was compared. Finally, the results of this study showed that with the transformation of wavelets (NARX-NN), the prediction capacity of the drought index increased. Amiri et al., (2024) tried to evaluate different drought indices to find the most applicable index in Aleshtar Plain. According to the results, the CZI index

1. Goodness-of-Fit

outperformed other indices by correctly estimating one out of four cases. They also investigated Spearman's correlation between precipitation parameters and drought indices. The results showed a significant correlation between all indices at all stations except for MCZI, which had a poor performance. Finally, considering the total scores, the CZI index, which obtained 21 points out of the total tests, was selected as the superior index for the region. The SPI and ZSI indices also yielded satisfactory and accurate results in this area.

Mishra et al. (2018) developed and analyzed artificial neural network models to forecast rainfall using time series data. In this study, they used the artificial neural network (ANN) technique to develop one-month and two-month prediction models for rainfall forecasting using monthly rainfall data from North India. In this model, feed forward neural network (FFNN) was used via back propagation algorithm and Levenberg–Marquardt training function. The performance of both models was evaluated based on regression analysis, mean square error (MSE), and magnitude of relative error (MRE). The proposed ANN model revealed promising results for forecasting and showed that the one-month forecasting model predicted better than the two-month forecasting model. This research also provided some future directions for precipitation forecasting and time series data analysis. Esfandiyari et al. (2016) used artificial neural network to predict drought in Isfahan. The results of their research revealed that among the different artificial neural network models, the perceptron network was able to predict SPI values in the future with a high correlation in most stations. Among the used stations, the Kohpayeh station indicated the best performance with the

highest correlation coefficient equal to 0.96 and with the average performance error equal to 0.04. Ziyar station with a correlation of 0.86 and an average error of 0.087 presented a lower performance than other stations.

Sharifipour et al. (2021) examined four artificial intelligence methods for drought prediction. The results of their study showed that all networks had the ability to predict drought, based on the evaluation criterion of the macro, fl-deep learning network in the time scale of 1 month with 22.71% was the most inefficient method while decision tree with 64.65% was the most efficient method. However, with the increase of the time scale, the deep learning network improved its performance, so that in the time scale of 24 months with 65.35%, the best performance was related to the deep learning network followed by the support vector machine network with 57.40%. Salehi (2016) presented an algorithm to capture the uncertainty of artificial neural network model in drought prediction. The final results showed that although the ANFIS model presented a lower R² value than the ANN model, it had less uncertainty than the ANN model, thus demonstrating the superiority of the ANFIS model over the ANN model. Dastorani et al. (2008) investigated the use of artificial neural network models in drought simulation and prediction. In this research, various artificial neural network structures were used in this respect, in which various meteorological parameters were employed as model inputs. The amount of rainfall as the main effective factor in drought for the next year was as the output of the models. The results showed that the dynamic structures of neural networks had a better performance in this field and especially TLRN networks provided the best results.

Golabi et al. (2013) examined the performance of artificial neural network and time series in modeling standard precipitation drought index (case study: selected stations of Khuzestan province). They reported that time series models outperformed artificial neural networks in predicting standard precipitation index values in all studied time periods. Also, multi-layered perceptron artificial neural networks showed a better performance than radial basis function artificial neural networks in all periods, and predicted the standard precipitation index better. Sadeghiyan et al. (2019) evaluated the performance of time series models, neural network, and neural-fuzzy inference system in meteorological drought prediction (case study: Semnan synoptic station). In this research, using time series methods, artificial neural network (ANN) and adaptive neural fuzzy inference system (ANFIS), they tried to provide suitable models for predicting the drought of Semnan city. In these modeling, monthly average data including rainfall, temperature, maximum and minimum temperature, relative humidity, maximum and minimum relative humidity, and SPI drought index were used during the statistical period of 1966 to 2013. Based on the results, SPI and its previous values outperformed precipitation. By examining all models, ARIMA model 6 (1,0,1)(0,0,1) with proper fitting of SPI data with the lowest root mean square error (RMSE) value equal to 0.442 in the training phase and 0.521 in the test phase as well as the most appropriate correlation coefficient (R) equal to 0.889 in the training phase and 0.846 in the test phase was selected as the best model. Using this model, SPI values were predicted for the next 12 time steps. ARIMA was followed by ANFIS model with RMSE = 0.513 MAE = 0.377 and

correlation coefficient (R) equal to 0.861 in the training phase and RMSE = 0.518 = MAE = 0.41 and R = 0.841 in the test phase and ANN with values of 534 RMSE = 0.393 MAE and R = 0.85 in the training phase and RMSE = 0.532 MAE = 0.402 and R = 0.837 in the test phase.

Future studies need to focus on interpretable models, use deep learning architectures for long-term forecasting, and employ neural networks to predict various drought characteristics such as drought propagation and sudden droughts (Dikshit et al., 2022). Khoshgoftar et al. (2018) compared ARIMA and neural network methods in drought modeling and monitoring using remote sensing time series data (case study: Arak city). The results of their research indicated that TVX, NDVI, and SPI indicators can be used to predict the drought situation in the studied area. Najafi et al. (2021) predicted drought using artificial neural network and SPI index. In this research, the drought situation from 2020 to 2024 for the city of Kermanshah was determined by predicting precipitation amounts through artificial neural network, which was employed to predict each year from the data of the last five years, as well as calculating the SPI drought index on an annual scale. Mirdar Soltani et al. (2019) used the artificial neural network and regression method in the modeling of precipitation time series. In this research, the prediction of the annual rainfall time series of Nigeria was done using the artificial intelligence method. In this context, feedforward artificial neural network method was utilized for modeling and finally the results were compared with linear regression. The results revealed that the neural network method had a far better performance than linear regression. Yonesi et al. (2017) predicted drought using the combined wavelet-artificial neural network

model and ARIMA time series model. In this research, artificial neural networks of multilayer perceptron (MLP) and radial basis function (RBF) of ARIMA time series, as well as artificial neural networks - wavelet of multilayer perceptron (WA-MLP) and radial basis function (WA-RBF) were used for prediction. In this regard, the rainfall data of Bedistan station with a statistical period of 44 years in the Shore catchment area were applied. The humidity condition was calculated using the standardized precipitation index (SPI) in the three-month period. To estimate the value of SPI in each time period, the corresponding values in previous times were employed. The results showed that the WA-MLP model predicted SPI values and short-term drought conditions with higher accuracy ($R^2=0.87$). Mohamadyarian et al. (2013) utilized the SPI index to zoning droughts in northeastern Iran. This study revealed that in recent years, the recurrence and persistence of this phenomenon has increased in all three provinces of North, Razavi, and South Khorasan. According to the results of the research, the most severe drought has occurred in the stations of Golmkan, Ghoochan, and Sabzevar, while the most moderate drought has been found in the station Golmakan, Torbetjam and Bojnourd floods.

Material and Methods

Study Area

As the capital of North Khorasan province (area of 35 km²), Bojnourd city, with an area of 579,959 hectares covers about 20% of the total area of the province. This city is located in the northeast of Iran at 57 degrees and 20 minutes of geographic longitude and 37 degrees and 28 minutes of geographic latitude, in the south of the Kopeh Dagh mountain range and the east of the Aaladagh Mountain range. It

is also located in the north of the Alborz Mountain. The altitude of Bojnourd is 1070 meters above sea level. According to the climate classification of the Köppen, the climate of the city is dry and semi-arid, and the maximum temperature in summer (August) reaches 40 degrees Celsius while the lowest temperature during the months of January and February reaches -15 degrees Celsius. Bojnourd city shares border with Republic of Turkmenistan from the north, Esfaryen city from the south, Shirvan city from the east, and Ashkhaneh and Jajarm cities from the west. Due to its mountainous nature, Bojnourd city is a favorable area for floods and destructions, especially with regard to the destruction of forests and pastures in the city, as well as

illegal cultivation and excessive livestock grazing in the slopes and steep areas of this region; favorable conditions have been found for massive landslides and ditch erosions. Atrak river is the most important the river of the city. In terms of underground water sources, Bojnourd city has a large number of springs, deep and semi-deep wells, and aqueducts, so that about 90% of the city's water consumption is supplied from underground water. Finally, since the water resources of the city are often in the form of temporary springs, hand wells as well as temporary and permanent rivers, the lack of necessary credits for storing temporary and permanent river water is the main problem of the city regarding water resources and soil erosion.



Fig 1. Geographical location of the study area

Methodology

This research has used the monthly statistics of climatic elements such as precipitation, relative humidity, temperature together with climatic indicators affecting drought from 1977 to 2018. In the neural network, 70% of the data were used for training (269 months from January 1, 1977 to the end of December 2008) and 30% of the data (from January 1, 2009 to the end of December 2014) for testing the models. The seals from 2020 to 2030 were predicted by the Box Jenkins model and simulated. The data used in the present study were standardized and then applied to the neural network model with a 70:30 combination

(70% of data for training and 30% of data for testing). The reason for using relative humidity and temperature data is that during the occurrence of drought, the normal state of these data has undergone changes so that the lack of humidity due to the decline in the entry of moist air masses affects the relative humidity and causes its reduction. Temperature fluctuations are also influential and increase it. This is because the presence of humidity in the region is a good guarantee for reducing the range of temperature changes while its lack causes the range of temperature fluctuations to increase. In this research, nineteen climate indices with a time delay

of one to three months along with monthly data of relative humidity and average monthly temperature with a delay of one to three months were used to predict and simulate drought. Standard precipitation index (SPI) has been used as the output of the models.

Standard precipitation index

This index was presented in 1993 by McKee and his colleagues. This index is obtained based on the difference of precipitation from the average for a certain time scale and then dividing it by the standard deviation, where the only effective factor in its calculation is the rainfall element. This index can be calculated in time scales of 3, 6, 12, 24, and 48 months. Another feature of the standardized precipitation index is that based on this index, in addition to calculating the severity of the drought its duration can also be determined. The standardized precipitation index is based on the probability of precipitation for each time period. Indeed, it is very important for the purpose of early warning and monitoring the severity of drought. This index is designed to quantify the lack of precipitation in multiple time periods (Bazarafshan, 2018). Experience has shown that the gamma distribution is a suitable distribution to fit on rainfall data; if it is assumed that the rainfall in a region follows the gamma distribution and χ is the rainfall values, the two-parameter probability density function of gamma is defined as follows: (Jahangiri et al. 2014)

$$f(x) = \frac{1}{\beta^\alpha \Gamma(\alpha)} x^{\alpha-1} e^{-\frac{x}{\beta}} \quad x > 0 \quad (1)$$

In Equation 1, α is the shape parameter, β denotes the distribution scale parameter, and $\Gamma(\alpha)$ represents the gamma function, which are defined as follows:

$$\int_0^\infty \gamma^{\alpha-1} e^{-\gamma} d\gamma = (\alpha) \Gamma \quad (2)$$

The optimal β and α coefficients are also calculated through the following relations:

$$\hat{\alpha} = \frac{1}{4A} \left[1 + \sqrt{1 + \frac{4A}{3}} \right] \quad (3)$$

$$A = \ln(\bar{x}) - \frac{\sum \ln(x)}{n} \quad (4)$$

$$\hat{\beta} = \frac{\bar{x}}{\hat{\alpha}} \quad (5)$$

In order to calculate A, it should be noted that the parameter n is the number of rainfall observations. Gamma cumulative probability distribution is used to calculate the SPI index, whose relationship is as follows:

$$f(x) \frac{1}{\Gamma \hat{\alpha}} \int_0^\infty t^{\hat{\alpha}-1} e^{-t} dt \quad t = x/\hat{\beta} \quad (6)$$

Since the logarithm value of zero is not defined in the above relation and the rainfall distribution may have zero values, thus in this situation cumulative probability is calculated from Equation 7.

$$H(x) = q + (1 - q)F(x) \quad (7)$$

In this relationship, the probability of rain q is zero. To calculate q, one can use the California equation (Equation 8).

$$q = \frac{m}{n} \quad (8)$$

In this relationship, m denotes the number of zero data in the time series and n represents the total number of rainfall data. The next step in SPI calculation is to transfer the cumulative probability H(x) obtained from the cumulative gamma distribution to the normal distribution. It is a cumulative standard with a mean of zero and a standard deviation of one. Indeed, the standardized precipitation index is a variable of the standard normal distribution function, whose cumulative probability value is equal to the cumulative probability value of the considered variable in the gamma distribution. Drought is severe when the SPI index is -1 or lower, and if

it becomes positive, the drought event will end. The duration of the drought period is determined by the beginning and end of negative SPI figures, and the cumulative values of SPI also show the magnitude and intensity of the drought period (Ensafi

Moghadam, 2016). The classification of SPI index varies from Very severe drought to Moderate drought. Table 1 reports the classification of drought intensity based on the standard precipitation index.

Table 1. Classification of drought severity using the index (SPI) (Kamali & Nikzad, 1999).

SPI	Index value
>2	Excessive humidity
1.50 : 1.99	Very humid
1 : 1.49	Moderate humidity
-1 : 1	Normal
-1 : -1.49	Moderate drought
-1.5 : -1.99	severe drought
< -2	Very severe drought

Artificial Neural Network

Artificial neural networks, or neural networks (NNs) in simpler terms, are predictive methods based on simple mathematical models of the human brain. These methods enable the investigation of complex nonlinear relationships between the response variable and its predictors. In recent years, growing interest has been engendered for theoretical development of model-free intelligent dynamic systems. Artificial neural networks consist of several interconnected layers of neurons. Neurons are processing units that work in parallel in one layer. Each network consists of an input and output layer and possibly several intermediate hidden layers. When each neuron receives the input vector X from the previous neurons, it converts it to the y point with a matrix as well as functional operation and transmits the output to the next neurons. In this process, W and β are predetermined weight vectors and f is the transfer function:

$$y = f(w \cdot x - \beta) = f\left(\sum w_i x_i - \beta\right) \quad (9)$$

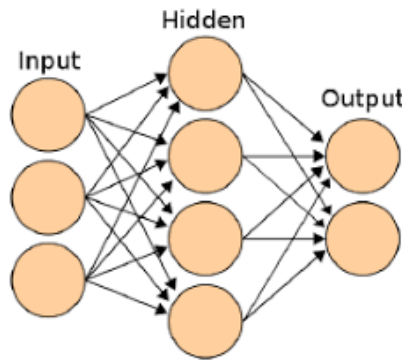
This process reaches the final stage in the output layer whereby the optimal weights of the network are determined and fixed.

Such a network, in which the messages pass only the input and output path to the front, is called a forward network. The method of determining the correct values of weights is called learning algorithm. The most popular learning algorithm is called error back propagation (BP)¹ in which, corresponding to the input matrix, the target matrix is also defined for the network; the learning process continues until the mean square of the error of the network reaches the lowest possible value. In addition to the input and output layers, such networks have also at least one hidden layer. The number of layers, the number of neurons in each layer, the weight matrix of each layer, the transfer functions as well as the learning algorithm are the determining elements in the design of a neural network. Neural networks, which are part of these dynamic systems, transfer the law hidden behind the data to the network structure by processing experimental data. These networks learn general rules based on calculations on numerical data (Menhaj, 2007). The structure of these networks follows biological neural networks, in which the way of communication between

1. Back-Propagation

its components is determined by adjusting the weights. After training the network, applying a specific input leads to receiving a specific response (Kia, 2007). The elements of the neural network are the input vector, weights, stimulus, and output functions. The basis of the neural network is indeed the simulation of thinking and processing the actions of the human brain, which is formed by modeling the cells of the community of neurons, where each neuron consists of three parts: framework, dendrite, and axon.

The learning function of the Marquardt-Levenberg algorithm and the driving function of the hidden layer is hyperbolic tangent, and the driving function of the output layer is linear. To train the network, the Marquardt-Levenberg algorithm, which follows the error back propagation rule, has been used. This co-algorithm is one of the standard numerical optimization tactics that tries to reduce calculations by not calculating the Hessian matrix. The Hessian matrix is calculated as follows:



Fi 2. A neural network with four inputs and a hidden layer consisting of three hidden neurons

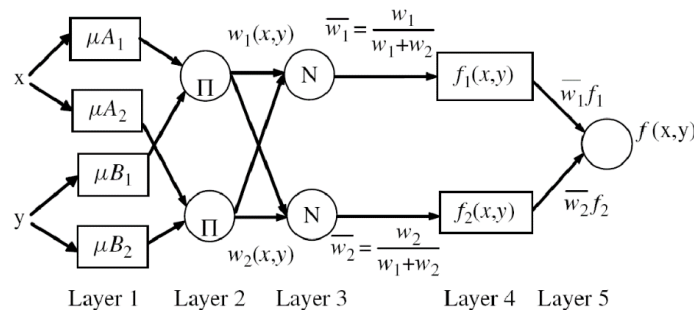


Fig 3. An example of a three-layer feed-forward network with an error back propagation training algorithm

Box Jenkins Model

Among the forecasting methods, the one-variable method is the Box-Jenkins model. This method basically involves fitting an ARIMA model to the data. In this method, after determining the order of differentiation as well as the order of each of the AR and MA processes, the parameters of the model are specified.

The suitability of the model is checked by analyzing the residuals of the fitted model. If the model is correctly identified, the residuals should have the properties of independent normal random variables with zero mean and constant variance. For the prediction, first the time series of the data is drawn. A trending series is a non-stationary series, where stationarity can

be checked by drawing autocorrelation diagram (ACF). A correlation chart in which r values do not approach zero at a reasonable rate indicates instability. If the values of r decline relatively quickly, the series will be stationary. However, if the values of the autocorrelation function slowly tend to zero, it confirms the instability of the corresponding series. Indeed, we need to calculate the sample autocorrelation function for the stationary time series. Therefore, any trend should be removed before calculating ACF.

Also, before any transformation in order to make the average of the series reliable, we should ensure reliability of its variance. The most important tool for variance analysis is the power transformation introduced by Box and Cox (1964). If, by drawing the Box-Cox diagram, the number one is within the 95% confidence limit, it can be accepted as an acceptable value of the transformation parameter. Therefore, data conversion can be omitted. The most important transformations are variance stabilizers and differential transformations. For the series to be stationary in the mean, it is necessary to convert it into a stationary series by performing appropriate transformations. In order to identify the model, it is necessary to draw the graph of the partial autocorrelation function of the stationary series and identify the orders of q plus p in the ARIMA model. In the next step, we fit this model to the data to predict the values. As a reminder, fitting means estimating the unknown parameters of the model. Finally, the suitability of the model is examined by analyzing the residuals of the fitted model.

Results and Discussion

The effective variables in monthly drought include temperature, relative humidity, and remote connection indices in the order of

application in networks. Models 1 to 9 are simulated with climate index only. The model includes 10 to 24 climatic indicators along with the relative average and average monthly temperature of Bojnourd. The use of climate indicators alone would lower the accuracy of the neural network model, while the variables of relative humidity and temperature would enhance the accuracy of the models for monthly drought prediction. In the neural network model, first, only climatic indicators were used using the step-by-step regression method, and nine variables were selected by the regression model; models one to nine were implemented based on these inputs. Due to the low accuracy of the models, once again the variables affecting drought were identified from the climatic indices and monthly data of the synoptic station of Bojnourd, which include models 10 to 24. After developing the mass of models, 24 models from the post-release network were selected as suitable models (Table 2). Among the selected models, the BP19 model with 6 inputs and 1 hidden layer of 25 neurons was selected as the optimal model. The mentioned model had the highest correlation coefficient (R) value of 0.99 for the training phase as well as the highest correlation coefficient (R) value of 0.68 for the test phase, which caused the minimum error in the test phase. Meanwhile, the results of the test phase were close to each other in most of the models. RMSE in this model was estimated at 0.16 and MAE equal to 0.0071 in the training phase, while RMSE in this model was estimated at 0.59 and MAE equal to 0.759 in the testing phase.

Since the main aim of time series analysis is to identify and separate the effective factors in the past in order to predict and plan the future, thus, this analysis is related to data that are not independent and

Table 2. Specifications of the selected model in the neural network model in the monthly time frame

Test stage			Training stage			Specifications of selected models			
MAE	RMSE	R	MAE	RMSE	R	number of neurons	number of hidden layers	number of inputs	Model
0.0703	1.22	0.64	0.0083	0.21	0/96	20	1	8	BP01
0.0759	1.00	0.68	0.0037	0.20	0.98	25	1	8	BP02
0.1023	0.81	0.65	0.0077	0.17	0.95	20	1	8	BP03
0.0760	0.85	0.57	0.0135	0.08	0.98	30	2	8	BP04
0.0844	0.79	0.54	0.0196	0.22	0.99	15	2	7	BP05
0.1138	0.95	0.55	0.2225	0.13	0.95	25	2	7	BP06
0.0895	0.85	0.60	0.1400	0.18	0.96	30	3	7	BP07
0.0795	1.09	0.63	0.1492	0.09	0.99	20	3	9	BP08
0.0742	0.89	0.57	0.1731	0.22	0.95	25	3	9	BP09
0.1084	0.83	0.61	0.0902	0.23	0.96	15	2	9	BP10
0.1138	0.75	0.55	0.1204	0.11	0.98	20	2	10	BP11
0.1061	0.87	0.63	0.1292	0.22	0.95	30	4	10	BP12
0.1023	0.88	0.57	0.9860	0.08	0.99	20	4	5	BP13
0.0760	1.22	0.54	0.9668	0.17	0.96	15	3	5	BP14
0.8064	1.28	0.60	0.9868	0.14	0.98	25	3	5	BP15
0.0855	0.69	0.60	0.9880	0.09	0.99	10	2	6	BP16
0.0869	0.72	0.64	0.0083	0.22	0.99	15	2	6	BP17
0.0940	0.76	0.55	0.0067	0.12	0.95	20	2	6	BP18
0.0759	0.59	0.68	0.0071	0.16	0.99	25	1	6	BP19
0.0996	1.09	0.57	0.2226	0.17	0.96	15	1	5	BP20
0.0732	0.83	0.54	0.2213	0.18	0.98	10	4	5	BP21
0.0853	0.88	0.63	0.0603	0.12	0.94	15	4	5	BP22
0.0108	0.81	0.55	0.2646	0.15	0.95	25	4	5	BP23
0.1176	0.82	0.54	0.2213	0.17	0.99	30	4	5	BP24

are connected sequentially. Accordingly, to study the area in question, in the first stage, statistical information on the precipitation element has been collected at the selected station. To analyze the time series of seasonal rainfall, the inter-seasonal difference orders (d) of Bojnourd station were investigated. The results revealed that the seasonal rainfall time series of Bojnourd did not have any trend (random or non-random) and this trend was constant. In other words, over the last 30 years, there has been no evidence

of a significant decrease or increase in seasonal rainfall at Bojnourd station. This does not indicate the temporal invariance of rainfall and its uniformity every year. Correlations in which the values cut off relatively quickly or decline relatively quickly indicate stationarity. If a time series has seasonal changes, its correlation graph also shows fluctuations. According to Figure 5 of the annual precipitation of Bojnourd station between the seals of 1977 and 2014, a descending trend can be observed in precipitation.

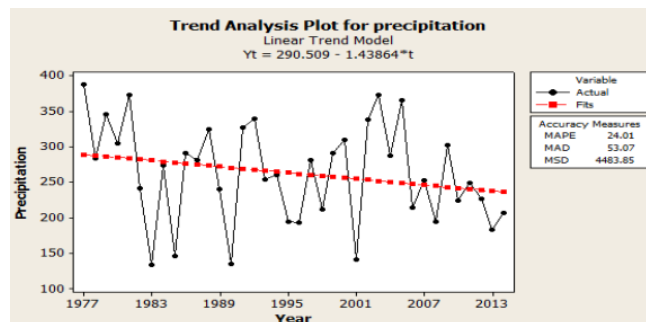


Fig 4. Bojnourd annual rainfall time series

Conclusion

Based on the results of autoregression orders and seasonal and inter-seasonal moving average results from the fitted models, the dependence of seasonal and inter-seasonal rainfall of Bojnourd station was investigated. In the study of the seasonal pattern, it was determined that Bojnourd station follows the seasonal pattern. In Bojnourd's seasonal autoregression, direct dependence of the rainfall of each season on the rainfall of the same season was found in 1 to 2 years before it. Also, the random fluctuation of seasonal rains 1 to 2 years ago had an indirect effect. In general, the timely prediction results indicated the effectiveness of the mentioned model in water resources management. Undoubtedly, what is meant by the word forecast in the hydrological studies of Mod is to present the values that have the highest probability of occurrence according to the historical time series, and it is not intended to provide exact values for future rainfall. This is because due to extreme temporal and spatial variability of climate parameters, this claim simply means a lack of correct understanding of the complex cycle of climate and its governing conditions. In any case, the researchers' studies indicate that the values obtained from these studies, despite the uncertainties governing them, have been very influential on the more efficient management of water resources. Therefore, the mentioned method can be used to know the amount of rainfall and the probability of drought in the coming years.

Drought is one of the natural phenomena that occurs in all climatic regimes and geographical regions, but its effects and frequency are abundant in arid and semi-arid regimes. The most important direct effect of drought is on the water resources of each region. Due to the ability

of artificial neural networks (ANN) in predicting natural events, the use of this method for prediction and simulation has grown widely. In this research, the drought of Bojnourd city was predicted by the post-release network in a monthly period, and the results of the regression model were also mentioned to show the performance of the network and comparison. The accuracy and correctness of the predicted model was determined using evaluation methods such as correlation coefficient, absolute average of deviations, square of absolute average of deviations and percentage of absolute average of errors, where finally the best method was selected. Using the selected model, the amount of precipitation in 1991 and 1992 was predicted. According to the amount of errors, the neural model provided better results for prediction and simulation. Among the selected models of the post-release network, the BP19 model was selected as the selected model. The prediction data of the regression model was estimated using the ENTER method. RMSE in the model was estimated with a value of 0.16 for the training stage and the mean absolute error (MAE) was estimated at 0.0071. According to the research conducted worldwide, the Standardized Evaporation and Transpiration Index (SPEI), which is one of the best drought indicators identified for the studied area, was used as a variable to predict drought. The performance of both models was evaluated based on regression analysis, mean absolute error (MAE), and root-mean-square error (RMSE). Finally, the neural network method offered a far better performance than linear regression.

References

- Amiri, A., Baharvand, S., Rad, M. (2024). Evaluation of different drought indices to find the most Applicable Index (Case Study:

- Aleshtar Plain). *Journal of Drought and Climate change Research*, 1(4), 71-86. Doi: 10.22077/jdcr.2023.6775.1043. [In Persian].
- Bazarafshan, J. (2008). Comparative study of some meteorological drought indicators in some climatic samples of Iran. Master's thesis, Faculty of Natural Resources, University of Tehran. [In Persian].
- Box, G. E., & Cox, D. R. (1964). An analysis of transformations. *Journal of the Royal Statistical Society Series B: Statistical Methodology*, 26(2), 211-243.
- Dastorani, M. T., Afkhami, H., Maleki Nejad, H., & Mobin, M. H. (2009). Studying the application of artificial neural network models in drought simulation and forecasting, the second national conference on the effects of drought and its management strategies, Isfahan. <https://civilica.com/doc/67349>. [In Persian].
- Deh Bozorgi, M. R., Malekian, A., & Ehsani, A. H. (2014). Evaluation of the performance of artificial neural network in forecasting meteorological drought in north-west Iran, *Applied Research Journal of Geographical Sciences*, 15(36), 139-156. Doi: 20.1001.1.22287736.1394.15.36.8.4
- Dehghani, A. A., & Ahmadi, R. (2008). Watershed estimation of watersheds without statistics using artificial neural network, the first international water conference, Zabol University. <https://civilica.com/doc/64342>. [In Persian].
- Dikshit, A., Pradhan, B., & Santosh, M. (2022). Artificial neural networks in drought prediction in the 21st century—A scientometric analysis, *Applied Soft Computing*, 114, 108080. Doi: <https://doi.org/10.1016/j.asoc.2021.108080>.
- Ensafi Moghadam, T. (2007). Evaluation of several indicators of climatic drought and determination of the most appropriate index in the Salt Lake basin. *Iranian Journal of Range and Desert Research*. 14(2), 271-288. https://ijrdr.areeo.ac.ir/article_105638.html. [In Persian].
- Evkaya, Ozan & Kurnaz, F. S. (2020). Forecasting drought using neural network approaches with transformed time series data. *Journal of Applied Statistics*. 48, 1-16. Doi: 10.1080/02664763.2020.1867829.
- Esfandiyari, M., Malekinejad, H., Hakimzadeh, M. A., & Afkhami, H. (2016). Application of artificial neural network model in drought prediction of Isfahan province, *Watershed Promotion and Development Journal*, 5(16), 25-34. https://www.wmji.ir/article_696843_1091f8df7dc97_eb66b-066cabd459629a.pdf. [In Persian].
- Fan, G., Sarabandi, A., & Yaghoobzadeh, M. (2021). Evaluating the climate change effects on temperature, precipitation and evapotranspiration in eastern Iran using CMPI5, *Water Supply*, 21 (8), 4316-4327. Doi: <https://doi.org/10.2166/ws.2021.179>
- Golabi, M., Radmanesh, F. & Akhund Ali, A. M. (2013). Investigation of the performance of artificial neural network and time series in modeling standard rainfall drought index (case study: selected stations of Khuzestan province), *Journal of Arid Biome*, 3(1), 82-87. [In Persian].
- Helmi, M., & Shahidi, A. (2023). The using of SPI and SPEI indices in evaluating the effect of drought on quality of surface water resources (Case study: Kashafrud river). *Journal of Drought and Climate change Research*, 1(1), 83-96. Doi: 10.22077/jdcr.2023.6023.1008. [In Persian].
- Jahangiri, M. H., Khoshmashraban, M., & Yousefi, H. (2014). Monitoring and forecasting the drought condition using Standard Rainfall Index (SPI) and Multilayer Perceptron Neural Network (Case

- Study: Tehran and Alborz Provinces.) *Ecohydrology Journal*, 2(4), 417-428. Doi:10.22059/ije.2015.58068. [In Persian].
- Kamali, Gh., & Nikzad, M., (1999), Meteorological indicators in agricultural drought, *Nivar Journal*, 9-19. [In Persian].
- Khoshgoftar, M. M., Akhundzadeh Hanzaei, M., & Khosravi, I. (2018). Comparison of ARIMA and neural network methods in drought modeling and monitoring using remote sensing time series data (case study: Arak city), *Sepehr Geographical Information Journal*, 109, Doi: <https://doi.org/10.22131/sepehr.2019.35646>. [In Persian].
- Kia, M. (2007), *Neural Network in Matlab*, Publications of Kian Sabz Computer Publishing Cooperative, Persian Gulf, Zaniz. ISBN: 978-600-6021-41-6.
- Menhaj, M. B. (2007). *Basics of Neural Networks - Computational Intelligence*, Volume I, Fifth Edition, Amirkabir University of Technology Publications. ISBN: 978-964-463-087-3
- Meng, D., Shengzhi, H., Qiang, H., Guoyong, L., Yi Guo, L., Wang, W.F., P, Li., & Xudong Z. (2020). Assessing agricultural drought risk and its dynamic evolution characteristics, *Agricultural Water Management* 10600 ,231 ., <https://doi.org/10.1016/j.agwat.2020.106003>.
- Mohamadyariyan, M., Mofidi, A., & Mokaram, L. (2013). Using the SPI index in zoning droughts and disasters Northeast Iran with AHP method In the G environment, National conference „Challenges of adaptation to climate change and solutions to reduce its adverse effects, North University.
- Mirdar Soltani, A. H., Heydari, Kh., Safar & Alizadeh, A. H. (2019). The use of neural network and regression methods in rainfall time series modeling, the 6th International Conference on Mechanics, Construction, Industries and Civil Engineering. [In Persian].
- Mishra, N., Soni, H., Sharma, S., & Upadhyay, A. (2018). Development and Analysis of Artificial Neural Network Models for Rainfall Prediction by Using Time-Series Data. *International Journal of Intelligent Systems and Applications*. Doi: 10.16-23. 10.5815/ijisa.2018.01.03.
- Mishra, A.K., & Desai, V.R. (2005). Drought Forecasting Using Stochastic Models, *Stochastic Environmental Research and Risk Assessment (SERRA)*, 19(5), 326-339. Doi: 10.1007/s00477-005-0238-4.
- McKee, T. B., Doesken, N. J., & Kleist, J. (1993). The relationship of drought frequency and duration to time scales. Preprints, Eighth Conference on Applied Climatology. Anaheim, California.
- Najafi, M. S., Qaini Hesarouieh, M., & Fedai Kermani, E. (2021). Drought prediction using artificial neural network and SPI index, 8th National Conference on Sustainable Development in Civil Engineering, Tehran, <https://civilica.com/doc/1240078>. [In Persian].
- Sadeghiyan, M., Kerami, H., & Mousavi, S. F. (2019). Performance evaluation of time series models, neural network and neural-fuzzy inference system in meteorological drought forecasting (case study: Semnan synoptic station), *Journal of Irrigation Engineering Sciences*, 43(2), 1-18. Doi: 10.22055/jise.2017.17729.1283. [In Persian].
- Sharifipour, L., Qanei Bafghi, M. J., Kothari, M. R., & Sharifipour, S. (2021). Comparing the efficiency of four artificial intelligence methods in drought prediction, *Journal of Spatial Analysis of Environ-*

- mental Hazards*, 8th year, 30, 139-156. Doi: 10.52547/jsaeh.8.3.139. [In Persian].
- Salehi., H. (2016). Presenting an algorithm to achieve the uncertainty of the artificial neural network model in drought forecasting, master's thesis, Shahrood University of Technology. [In Persian].
- Sayadi, O. (2007). Introduction to Artificial Neural Networks, Laboratory of Vital Signals and Medical Images Processing, Faculty of Electrical Engineering, Sharif University of Technology. [In Persian].
- Wabel, P., Jha, M. K., Adamala, S., Tiwari, M. K., & Biswal, S. (2023). Application of Hybrid ANN Techniques for Drought Forecasting in the Semi-Arid Region of India. *Environmental monitoring and assessment*. 24,195 (9). Doi: 10.1007/s10661-023-11631-w. PMID: 37615733.
- Yonesi, M., Shahraki, N., Marofi, S., & Nozari, H. (2017). Drought forecasting using the integrated model of artificial neural network-wavelet and ARIMA time series model, *Journal of Irrigation Science and Engineering*, 41(2), 167-181. Doi: 20.10 01.1.25885952.1397.41.2.12.0. [In Persian].

Journal of Drought and Climate change Research

JDCR

September, 2024, Vol. 2, No.6



- Evaluation of Drought in Gandaki River Basin, Nepal** 1
Aayush Bhattarai, Sachin Timilsina, Santosh Ayer, Gayatri Paudel, Menuka Maharjan
- A Biophysical Approach to Assess the Risks Associated with Climate Change for Spatial Analysis of Agricultural Drought Vulnerability** 27
Mohammadreza Farzaneh, Masoumeh Fakhri, Iman Fazeli-Farsani, Maryam Najafi-Biragani, Mohammad Abdolhosseini
- Assessment of Water, Food, and Energy Efficiency Indicators with a Nexus Approach and Sustainable Agricultural Management** 57
Seyyed Ali Moasheri, Saman Javadi, Mahmoud Mashal, Behzad Azadegan, Hamid Kardan Moghadam
- Monitoring Changes in Rice Cultivation Area Using Multi-Temporal Satellite Images (Case Study: Beiranshahr Region, Iran)** 77
Samad Abdi, Mohsen Ahmadede, Rabee Rustum, Anahid Salmanpour
- Measuring Discharge in a Shallow River in an Arid Area solely using an Unmanned Aerial Vehicle** 93
Farhad Akbarpour, Mohammad Adel Khorasani Nejad, Shervin Shahriari, Mostafa Rahmanshahi
- Spatial Analysis of Flood Risk in Tabas Watershed Using Satellite Images and Geographic Information System** 105
Mahdi Kaffash, Elham Yousefi, Mohsen Shariati
- Application of Time Series Method and Artificial Neural Networks in Drought Simulation (Case study: Bojnourd city)** 119
Mohtaram Mohamadyariyan, Ebrahim Amiri